

Phenomenology of semileptonic B -meson decays with form factors from lattice QCD

Daping Du,^{1,*} A.X. El-Khadra,² Steven Gottlieb,³ A.S. Kronfeld,^{4,5}
J. Laiho,¹ E. Lunghi,^{3,†} R.S. Van de Water,^{4,‡} and Ran Zhou^{4,§}

(Fermilab Lattice and MILC Collaborations)

¹*Department of Physics, Syracuse University, Syracuse, New York, 13244, USA*

²*Department of Physics, University of Illinois, Urbana, Illinois, 61801, USA*

³*Department of Physics, Indiana University,
Bloomington, Indiana, 47405, USA*

⁴*Theoretical Physics Department, Fermi National
Accelerator Laboratory, Batavia, Illinois, 60510, USA*

⁵*Institute for Advanced Study, Technische Universität München, 85748 Garching, Germany*

(Dated: March 6, 2022)

Abstract

We study the exclusive semileptonic B -meson decays $B \rightarrow K(\pi)\ell^+\ell^-$, $B \rightarrow K(\pi)\nu\bar{\nu}$, and $B \rightarrow \pi\tau\nu$, computing observables in the Standard model using the recent lattice-QCD results for the underlying form factors from the Fermilab Lattice and MILC Collaborations. These processes provide theoretically clean windows into physics beyond the Standard Model because the hadronic uncertainties are now under good control for suitably binned observables. For example, the resulting partially integrated branching fractions for $B \rightarrow \pi\mu^+\mu^-$ and $B \rightarrow K\mu^+\mu^-$ outside the charmonium resonance region are $1\text{--}2\sigma$ higher than the LHCb Collaboration's recent measurements, where the theoretical and experimental errors are commensurate. The combined tension is 1.7σ . Combining the Standard-Model rates with LHCb's measurements yields values for the Cabibbo-Kobayashi-Maskawa (CKM) matrix elements $|V_{td}| = 7.45(69) \times 10^{-3}$, $|V_{ts}| = 35.7(1.5) \times 10^{-3}$, and $|V_{td}/V_{ts}| = 0.201(20)$, which are compatible with the values obtained from neutral $B_{(s)}$ -meson oscillations and have competitive uncertainties. Alternatively, taking the CKM matrix elements from unitarity, we constrain new-physics contributions at the electroweak scale. The constraints on the Wilson coefficients $\text{Re}(C_9)$ and $\text{Re}(C_{10})$ from $B \rightarrow \pi\mu^+\mu^-$ and $B \rightarrow K\mu^+\mu^-$ are competitive with those from $B \rightarrow K^*\mu^+\mu^-$, and display a 2.0σ tension with the Standard Model. Our predictions for $B \rightarrow K(\pi)\nu\bar{\nu}$ and $B \rightarrow \pi\tau\nu$ are close to the current experimental limits.

PACS numbers: 13.20.He, 12.15.Mm, 12.15.Hh, 12.38.Gc

* dadu@syr.edu

† elunghi@indiana.edu

‡ ruthv@fnal.gov

§ zhouran@fnal.gov

I. INTRODUCTION AND MOTIVATION

The experimental high-energy physics community is searching for virtual effects of new heavy particles that would give rise to deviations from Standard-Model predictions via a broad range of precision measurements [1]. Because the masses and couplings of the new particles are not known *a priori*, indirect searches are being pursued in many areas of particle physics, including the charged-lepton sector [2], the Higgs sector [3], and the quark-flavor sector [4]. Within heavy-quark physics, B -meson semileptonic decays provide numerous observables such as decay rates, angular distributions, and asymmetries that are expected to be sensitive to different new-physics scenarios. For example, the rare decays $B \rightarrow K\ell^+\ell^-$, $B \rightarrow K\nu\bar{\nu}$, $B \rightarrow \pi\ell^+\ell^-$, and $B \rightarrow \pi\nu\bar{\nu}$ proceed via $b \rightarrow s$ and $b \rightarrow d$ flavor-changing neutral currents (FCNCs) and are sensitive to the effects of new heavy particles that can arise in a wide range of models. These include supersymmetry [5–8], leptoquarks [9–11], and a fourth generation [12]; models with flavor-changing Z' gauge bosons [13–20]; and models with extended [5, 21–25] or composite [10] Higgs sectors. Decays to τ -lepton final states such as $B \rightarrow \pi\tau\nu$ are especially sensitive to charged scalars that couple preferentially to heavier particles [26–31], such as those that occur in two-Higgs-doublet models. Tree-level CKM-favored $b \rightarrow u$ charged-current processes can be modified due to the presence of new right-handed currents [32–34]. If deviations from the Standard Model are observed in B -meson semileptonic decays, correlations between measurements can provide information on the underlying masses and couplings of the new-physics scenario that is realized in Nature. (See, *e.g.*, Refs. [35, 36] for recent reviews.)

Several tensions between theory and experiment have recently been observed in B -meson semileptonic decays. The BaBar experiment found excesses in both $R(D) \equiv \mathcal{B}(B \rightarrow D\tau\nu)/\mathcal{B}(B \rightarrow D\ell\nu)$ and $R(D^*) \equiv \mathcal{B}(B \rightarrow D^*\tau\nu)/\mathcal{B}(B \rightarrow D^*\ell\nu)$ with a combined significance of 3.4σ [37, 38]. These results were subsequently confirmed by Belle [39] and LHCb [40], albeit with somewhat lower significance; a recent HFAG average of these measurements quotes a combined significance of 3.9σ [41]. The LHCb experiment recently reported a measurement of the ratio of $B^+ \rightarrow K^+\mu^+\mu^-$ over $B^+ \rightarrow K^+e^+e^-$ branching fractions (denoted $R_{K^+}^{\mu e}$ below) in the range $1 \text{ GeV}^2 \leq q^2 \leq 6 \text{ GeV}^2$ that is 2.6σ lower than Standard-Model expectations [42]. The Standard-Model predictions for the $B \rightarrow K^{(*)}\mu^+\mu^-$ differential decay rates are slightly, but systematically, higher than experimental measurements by LHCb [43–45]. Discrepancies of 2 – 3σ between theory and experiment have also been observed for several $B \rightarrow K^*\ell\ell$ angular observables [46, 47]. The long-standing $\approx 3\sigma$ tensions between determinations of the CKM matrix elements $|V_{ub}|$ and $|V_{cb}|$ obtained from inclusive and exclusive tree-level semileptonic B -meson decays were recently confirmed with a new high-precision lattice-QCD calculation of the $B \rightarrow \pi\ell\nu$ form factors [48], the first unquenched lattice-QCD calculations of the $B \rightarrow D\ell\nu$ form factors at nonzero recoil [49, 50], and the first unquenched lattice-QCD calculation of the ratio of $\Lambda_b \rightarrow p\ell\nu$ to $\Lambda_b \rightarrow \Lambda_c\ell\nu$ form factors [51].¹

Experimental progress on B -meson semileptonic decays has also been, and will continue to be, significant. The LHCb experiment recently announced the first measurement of the $B^+ \rightarrow \pi^+\mu^+\mu^-$ differential decay rate [55], as well as for the ratio of $B^+ \rightarrow \pi^+\mu^+\mu^-$ to $B^+ \rightarrow K^+\mu^+\mu^-$ rates. This enables a more stringent test of the Standard Model via comparison of the shape to the theoretical prediction. The Belle experiment recently presented

¹ Note, however, that the Belle experiment’s preliminary measurement of the $B \rightarrow D\ell\nu$ differential decay rate [52], when combined with lattice-QCD form-factor calculations [49, 50], yields a value of $|V_{cb}|$ [53] that is in better agreement with the inclusive determination [54].

an upper limit on the total rate for $B^0 \rightarrow \pi^- \tau \nu$ decay [56] from their first search for this process that is less than an order of magnitude above that of the Standard-Model prediction. The upcoming Belle II experiment expects to observe $B \rightarrow \pi \tau \nu$ and other heretofore unseen processes such as $B^0 \rightarrow \pi^0 \nu \bar{\nu}$ [57]. (The charged counterpart $B^+ \rightarrow \pi^+ \nu \bar{\nu}$ is part of the analysis chain $B^+ \rightarrow \tau^+ \nu$, $\tau^+ \rightarrow \pi^+ \bar{\nu}$ [58–61].) Given the several observed tensions in semileptonic B -meson decays enumerated above and the recent and anticipated improvement in experimental measurements, it is important and timely to critically examine the assumptions entering the Standard-Model predictions for semileptonic B -decay observables and to provide reliable estimates of the theoretical uncertainties.

The Fermilab Lattice and MILC Collaborations (Fermilab/MILC) recently completed calculations of the form factors for $B \rightarrow K$ [62] and $B \rightarrow \pi$ [48, 63] transitions with lattice QCD using ensembles of gauge configurations with three dynamical quark flavors. For $B \rightarrow K$, the errors are commensurate with earlier lattice-QCD results [64]. For $B \rightarrow \pi$, the results of Refs. [48, 63] are the most precise form factors to date, with errors less than half the size of previous ones [65, 66]. Reference [48] also contains a joint fit of lattice-QCD form factors with experimental measurements of the differential decay rate from BaBar and Belle [67–70] to obtain the most precise exclusive determination to date of the CKM matrix element $|V_{ub}| = 3.72(16) \times 10^{-3}$. This fit also improves the determination of the vector and scalar form factors f_+ and f_0 , compared to those from lattice-QCD alone, provided that new physics does not contribute significantly to tree-level $B \rightarrow \pi \ell \nu$ ($\ell = e, \mu$) transitions.

Given the landscape of quark-flavor physics described above, it is timely to use the form factors from Refs. [48, 62, 63] to obtain Standard-Model predictions for various B -meson semileptonic-decay observables. (For brevity, the rest of this paper refers to these results as the “Fermilab/MILC form factors.”) The new *ab initio* QCD information on the hadronic matrix elements allows us to obtain theoretical predictions of the observables with fewer assumptions than previously possible. In this work, we consider the processes $B \rightarrow K \ell^+ \ell^-$, $B \rightarrow K \nu \bar{\nu}$, $B \rightarrow \pi \ell^+ \ell^-$, $B \rightarrow \pi \nu \bar{\nu}$, and $B \rightarrow \pi \tau \nu$. We present the following observables: differential decay rates, asymmetries, combinations of $B \rightarrow \pi$ and $B \rightarrow K$ observables, and lepton-universality-violating ratios. For partially integrated quantities, we include the correlations between bins of momentum transfer q^2 . Where possible, we make comparisons with existing experimental measurements. We also combine our predictions for the $B \rightarrow K(\pi) \ell^+ \ell^-$ Standard-Model rates with the most recent experimental measurements to constrain the associated combinations of CKM matrix elements $|V_{tb} V_{td}^*|$, $|V_{tb} V_{ts}^*|$, and $|V_{td}/V_{ts}|$. For the $B \rightarrow \pi$ vector and scalar form factors, we use the more precise Standard-Model determinations, which use experimental shape information from $B \rightarrow \pi \ell \nu$ decay.

We do not consider $B \rightarrow K^*$ processes in this paper, although there is extensive experimental and theoretical work. Lattice-QCD calculations of the hadronic form factors are available [44, 71], albeit without complete accounting for the $K^* \rightarrow K \pi$ decay [72]. The phenomenology of these processes [73–79] often assumes various relations deduced from flavor symmetries. Here we use the $B \rightarrow K$ and $B \rightarrow \pi$ form factors obtained directly from lattice QCD [48, 62, 63] to test some of the symmetry relations employed in the literature.

The semileptonic form factors suffice to parametrize the factorizable hadronic contributions to $B \rightarrow \pi$ and $B \rightarrow K$ decays in all extensions of the Standard Model. New heavy particles above the electroweak scale only modify the short-distance Wilson coefficients of the effective Hamiltonian [80–83]. Here we use the Fermilab/MILC form factors to obtain model-independent constraints on the Wilson coefficients for the effective operators that govern $b \rightarrow d(s)$ FCNC transitions. To facilitate the use of these form factors for additional

phenomenological studies, the original papers [48, 62, 63] provided complete parametrizations of the $B \rightarrow \pi$ and $B \rightarrow K$ form factors as coefficients of the z expansions and their correlations. To enable the combined analysis of both modes, this paper supplements that information by providing the correlations between the $B \rightarrow \pi$ and $B \rightarrow K$ form-factor coefficients.

This paper is organized as follows. We first provide an overview of the theoretical framework for the semileptonic decay processes studied in this work in Sec. II. Next, in Sec. III, we summarize the calculations behind the Fermilab/MILC $B \rightarrow \pi$ and $B \rightarrow K$ form factors [48, 62, 63], providing a table of correlations among all form factors. Here, we also use the form factors to directly test heavy-quark and SU(3) symmetry relations that have been used in previous Standard-Model predictions for rare semileptonic B -meson decay observables. In Sec. IV, we present our main results for Standard-Model predictions for $B \rightarrow \pi \ell^+ \ell^-$, $B \rightarrow K \ell^+ \ell^-$, $B \rightarrow K(\pi) \nu \bar{\nu}$, and $B \rightarrow \pi \tau \nu$ observables using the Fermilab/MILC form factors, discussing each process in a separate subsection. Then, in Sec. V we use our predictions for the partially integrated branching fractions together with experimental rate measurements to constrain the associated CKM matrix elements (Sec. VA) and relevant Wilson coefficients (Sec. VB). To aid the reader in digesting the information presented in Secs. IV and V, we summarize our main results in Sec. VI. Finally, we give an outlook for future improvements and concluding remarks in Sec. VII.

Three Appendices provide detailed, supplementary information. In Appendix A, we tabulate our numerical results for $B \rightarrow \pi \ell^+ \ell^-$ and $B \rightarrow K \ell^+ \ell^-$ observables in the Standard Model integrated over different q^2 intervals. We present the complete theoretical expressions for the $B \rightarrow K(\pi) \ell^+ \ell^-$ differential decay rates in the Standard Model, including nonfactorizable terms, in Appendix B. The numerical values of the parametric inputs used for our calculations are provided in Appendix C.

II. THEORETICAL BACKGROUND

Here we summarize the Standard-Model theory for the semileptonic decay processes considered in this work. First, Sec. IIA provides the standard definitions of the form factors. Next, in Sec. IIB, we discuss the theoretical framework for rare processes with a charged-lepton pair final state, $b \rightarrow q \ell \ell$ ($q = d, s$). Then we briefly summarize the formulae for rare decays with a neutrino pair final state $b \rightarrow q \nu \bar{\nu}$ ($q = d, s$) in Sec. IIC and for tree-level $b \rightarrow u \ell \nu_\ell$ semileptonic decays in Sec. IID. The latter two processes are theoretically much simpler, being mediated by a single operator in the electroweak effective Hamiltonian.

A. Form-factor definitions

The pseudoscalar-to-pseudoscalar transitions considered in this paper can be mediated by vector, scalar, and tensor currents. It is conventional to decompose the matrix elements into Lorentz-invariant forms built from the pseudoscalar- and B -meson momenta p_P and p_B , multiplied by form factors that depend on the Lorentz invariant q^2 , where $q = p_B - p_P$ is the momentum carried off by the leptons. For the vector current,

$$\langle P(p_P) | \bar{q} \gamma^\mu b | B(p_B) \rangle = f_+(q^2) \left[(p_B + p_P)^\mu - q^\mu \frac{M_B^2 - M_P^2}{q^2} \right] + f_0(q^2) q^\mu \frac{M_B^2 - M_P^2}{q^2}, \quad (2.1)$$

$$= f_+(q^2)(p_B + p_P)^\mu + f_-(q^2)(p_B - p_P)^\mu. \quad (2.2)$$

The form factors $f_+(q^2)$ and $f_0(q^2)$ couple to $J^P = 1^-$ and 0^+ , respectively, and therefore enter expressions for differential decay rates in a straightforward way. Because the terms proportional to $f_0(q^2)$ carry a factor of q^μ , their contributions to differential decay rates are weighted by the lepton mass, m_ℓ , and is therefore significant only in the case of τ -lepton final states. The form factor $f_-(q^2)$ is useful for a test of heavy-quark symmetry, discussed in Sec. III B. Partial conservation of the vector current implies that f_0 also parametrizes the matrix element of the scalar current:

$$\langle P(p_P) | \bar{q} b | B(p_B) \rangle = \frac{M_B^2 - M_P^2}{m_b - m_q} f_0(q^2). \quad (2.3)$$

Finally, the matrix element of the tensor current is

$$\langle P(p_P) | i \bar{q} \sigma^{\mu\nu} b | B(p_B) \rangle = \frac{2}{M_B + M_P} (p_B^\mu p_P^\nu - p_B^\nu p_P^\mu) f_T(q^2), \quad (2.4)$$

where $\sigma^{\mu\nu} = i[\gamma^\mu, \gamma^\nu]/2$.

These form factors suffice to parametrize the hadronic transition when the leptonic part of the reaction factorizes. Particularly important corrections arise in the penguin decays $B \rightarrow \pi \ell \ell$ and $B \rightarrow K \ell \ell$ studied in this work, as discussed in the next subsection and in Appendix B.

B. Rare $b \rightarrow q \ell \ell$ ($q = d, s$) decay processes

In this subsection, we first present the effective Hamiltonian for this case in Sec. II B 1, followed by a description of how we obtain the short-distance Wilson coefficients of the effective Hamiltonian at the relevant low scale in Sec. II B 2. To obtain physical observables, one also needs the on-shell $b \rightarrow d(s) \ell \ell$ matrix elements of the operators in the effective Hamiltonian. As discussed in Sec. II B 3, for decays into light charged leptons, $\ell = e, \mu$, it is necessary to treat the different kinematic regions within different frameworks. In Sec. II B 4 we present the general structure of the double differential decay rate. Details of the calculations at high and low q^2 are relegated to Appendix B.

1. Effective Hamiltonian

The starting point for the description of $b \rightarrow q \ell \ell$ ($q = d, s$) transitions is the effective Lagrangian [82]:

$$\begin{aligned} \mathcal{L}_{\text{eff}} = & + \frac{4G_F}{\sqrt{2}} V_{tq}^* V_{tb} \left[\sum_{i=1}^8 C_i(\mu) Q_i + \frac{\alpha_e(\mu)}{4\pi} \sum_{i=9}^{10} C_i(\mu) Q_i + \sum_{i=3}^6 C_{iQ}(\mu) Q_{iQ} + C_b(\mu) Q_b \right] \\ & + \frac{4G_F}{\sqrt{2}} V_{uq}^* V_{ub} \sum_{i=1}^2 C_i(\mu) [Q_i - Q_i^u] + \mathcal{L}_{\text{QCD} \times \text{QED}}. \end{aligned} \quad (2.5)$$

Throughout this paper, as in the literature, we refer to $\mathcal{H}_{\text{eff}} = -\mathcal{L}_{\text{eff}}$ as the (electroweak) effective Hamiltonian.

At leading order in the electroweak interaction, there are twelve independent operators, which we take to be

$$\begin{aligned}
Q_1^u &= (\bar{q}_L \gamma_\mu T^a u_L)(\bar{u}_L \gamma^\mu T^a b_L), \\
Q_2^u &= (\bar{q}_L \gamma_\mu u_L)(\bar{u}_L \gamma^\mu b_L), \\
Q_1 &= (\bar{q}_L \gamma_\mu T^a c_L)(\bar{c}_L \gamma^\mu T^a b_L), \\
Q_2 &= (\bar{q}_L \gamma_\mu c_L)(\bar{c}_L \gamma^\mu b_L), \\
Q_3 &= (\bar{q}_L \gamma_\mu b_L) \sum_{q'} (\bar{q}' \gamma^\mu q'), \\
Q_4 &= (\bar{q}_L \gamma_\mu T^a b_L) \sum_{q'} (\bar{q}' \gamma^\mu T^a q'), \\
Q_5 &= (\bar{q}_L \gamma_{\mu_1} \gamma_{\mu_2} \gamma_{\mu_3} b_L) \sum_{q'} (\bar{q}' \gamma^{\mu_1} \gamma^{\mu_2} \gamma^{\mu_3} q'), \\
Q_6 &= (\bar{q}_L \gamma_{\mu_1} \gamma_{\mu_2} \gamma_{\mu_3} T^a b_L) \sum_{q'} (\bar{q}' \gamma^{\mu_1} \gamma^{\mu_2} \gamma^{\mu_3} T^a q'), \\
Q_7 &= \frac{e}{16\pi^2} m_b (\bar{q}_L \sigma^{\mu\nu} b_R) F_{\mu\nu}, \\
Q_8 &= \frac{g}{16\pi^2} m_b (\bar{q}_L \sigma^{\mu\nu} T^a b_R) G_{\mu\nu}^a, \\
Q_9 &= (\bar{q}_L \gamma_\mu b_L) \sum_{\ell} (\bar{\ell} \gamma^\mu \ell), \\
Q_{10} &= (\bar{q}_L \gamma_\mu b_L) \sum_{\ell} (\bar{\ell} \gamma^\mu \gamma_5 \ell).
\end{aligned} \tag{2.6}$$

Because the top-quark mass is above the electroweak scale, only the five lightest quark flavors $q' = u, d, s, c, b$ are included in operators Q_3 through Q_6 . All three lepton flavors $\ell = e, \mu, \tau$ appear in operators Q_9 and Q_{10} .

Once QED corrections are considered, five more operators must be included, which we choose to be

$$\begin{aligned}
Q_{3Q} &= (\bar{q}_L \gamma_\mu b_L) \sum_{q'} e_{q'} (\bar{q}' \gamma^\mu q'), \\
Q_{4Q} &= (\bar{q}_L \gamma_\mu T^a b_L) \sum_{q'} e_{q'} (\bar{q}' \gamma^\mu T^a q'), \\
Q_{5Q} &= (\bar{q}_L \gamma_{\mu_1} \gamma_{\mu_2} \gamma_{\mu_3} b_L) \sum_{q'} e_{q'} (\bar{q}' \gamma^{\mu_1} \gamma^{\mu_2} \gamma^{\mu_3} q'), \\
Q_{6Q} &= (\bar{q}_L \gamma_{\mu_1} \gamma_{\mu_2} \gamma_{\mu_3} T^a b_L) \sum_{q'} e_{q'} (\bar{q}' \gamma^{\mu_1} \gamma^{\mu_2} \gamma^{\mu_3} T^a q'), \\
Q_b &= \frac{1}{12} [(\bar{q}_L \gamma_{\mu_1} \gamma_{\mu_2} \gamma_{\mu_3} b_L)(\bar{b} \gamma^{\mu_1} \gamma^{\mu_2} \gamma^{\mu_3} b) - 4(\bar{q}_L \gamma_\mu b_L)(\bar{b} \gamma^\mu b)].
\end{aligned} \tag{2.7}$$

where $e_{q'}$ are the electric charges of the corresponding quarks ($\frac{2}{3}$ or $-\frac{1}{3}$).

2. Wilson coefficients

In the calculation of any $b \rightarrow q$ ($q = d, s$) transition, large logarithms of the ratio $\mu_{\text{high}}/\mu_{\text{low}}$ arise, where $\mu_{\text{high}} \sim m_t, m_W, m_Z$ is a scale associated with virtual heavy-particle exchanges and $\mu_{\text{low}} \sim p_{\text{ext}} \sim m_b$ is a scale associated with the typical momenta of the final state on-shell particles.

The standard procedure to resum these large logarithms is based on the factorization of short- and long-distance physics, *i.e.*, writing $\ln(\mu_{\text{high}}/\mu_{\text{low}}) = \ln(\mu_{\text{high}}/\mu) + \ln(\mu/\mu_{\text{low}})$ and absorbing the first logarithm into the Wilson coefficients and the second into the matrix elements of the local operators. The independence of the overall amplitude on the factorization scale μ leads to renormalization group equations for the Wilson coefficients whose solution resums terms of the type $[\alpha_s^L \ln(\mu_{\text{high}}/\mu)]^n$ to all orders in perturbation theory. ($L = 0, 1$ are known as leading and next-to-leading log approximations.) The scale μ can then be chosen close to μ_{low} (typically $\mu \simeq m_b$), thus eliminating all large logarithms from the calculation of the amplitude. Any residual dependence on the scales μ_{high} and μ_{low} is taken as an uncertainty from missing higher order perturbative corrections. We follow the standard practice of varying these scales by a factor of two around some nominal central values, which we choose to be $\mu_{\text{high}} = 120$ GeV and $\mu_{\text{low}} = 5$ GeV.

The $b \rightarrow d(s)\ell\ell$ case is complicated by the fact that the Wilson coefficients for the leading semileptonic operators Q_9 and Q_{10} carry explicit factors of α_e , in addition to the common factor $4G_F/\sqrt{2}$. Moreover, the current-current operators Q_1 and Q_2 mix with the semileptonic operators at one loop in QED and at two loops in mixed QED-QCD. These complications can all be straightforwardly addressed in a double expansion in α_s and α_e/α_s . We refer the reader to Ref. [82] for a detailed account of this double expansion as well as a complete collection of all anomalous dimension matrices required for the running of the Wilson coefficients and of the QED and QCD couplings. In contrast to earlier analyses [84, 85], we do not include the gauge couplings in the normalization of Q_9 and Q_{10} , precisely to simplify the mixed QCD-QED renormalization group equations. Finally, note that the operator Q_b contributes to the transition amplitude only via mixing with the other operators.

3. Matrix elements

The calculation of exclusive $b \rightarrow s(d)\ell\ell$ matrix elements for the operators $Q_{7,9,10}$ is relatively simple. Because these operators contain an explicit photon or charged-lepton pair, the $B \rightarrow K(\pi)\ell\ell$ matrix element trivially factorizes in QCD into the product of a charged-lepton current and a form factor. The matrix element of Q_7 is proportional to the tensor form factor f_T , while those of $Q_{9,10}$ only get contributions from the vector-current operator because of parity conservation and the fact that the incoming and outgoing mesons are both pseudoscalars. The vector-current matrix element leads to the form factors f_+ and f_0 . Note that f_+ and f_0 , being matrix elements of a partially conserved vector current, do not renormalize and have no scale dependence. On the other hand, the μ dependence of f_T is canceled by that of the quark mass and the Wilson coefficient for Q_7 .

The calculation of $B \rightarrow P\ell\ell$ ($P = K, \pi$) matrix elements of operators that do not involve an explicit photon or charged-lepton pair is more complicated. Schematically,

$$\langle P\ell\ell|Q_i(y)|\bar{B}\rangle \sim (\bar{u}_\ell\gamma_\mu v_\ell) \int d^4x e^{iq\cdot(x-y)} \langle P|T J_{\text{em}}^\mu(x)Q_i(y)|\bar{B}\rangle, \quad (2.8)$$

where u_ℓ and v_ℓ are the lepton spinors and J_{em}^μ is the electromagnetic current. The matrix elements of the T -product include long-distance contributions that are difficult to calculate, even with lattice QCD. In certain kinematic regions, however, these complex matrix elements can be expressed in terms of simpler objects, namely the form factors defined in Sec. II A plus the light-cone distribution amplitudes, up to power corrections of order Λ_{QCD}/m_b .

Before discussing the effective theories used to simplify the matrix elements in Eq. (2.8), let us comment on the role of $c\bar{c}$ and $u\bar{u}$ states. The processes $B \rightarrow K(\pi)\ell\ell$ can proceed through the following intermediate resonances: $B \rightarrow K(\pi)\psi_{uu,cc} \rightarrow K(\pi)\ell\ell$ where $\psi_{uu} = \rho, \omega$ and $\psi_{cc} = \psi(1S, 2S, 3770, 4040, 4160, 4415)$. In the language of Eq. (2.8), contributions of intermediate ψ_{cc} and ψ_{uu} states stem from matrix elements involving the operators $Q_{1,2}$ and $Q_{1,2}^u$, respectively. The two lowest charmonium states have masses below the open charm threshold ($D\bar{D}$) and have very small widths, implying very strong violations of quark-hadron duality; consequently the regions including the $\psi(1S)$ and $\psi(2S)$ masses (also known as J/ψ and ψ') are routinely cut from theoretical and experimental analyses alike. Above the $\psi(2S)$, a resonance compatible with the $\psi(4160)$ has been observed in $B \rightarrow K\mu^+\mu^-$ decay [86]; the $\psi(3770)$ is also seen, but the signal for the $\psi(4040)$ and higher resonances is not significant. Because the four higher charmonium resonances are broad and spread throughout the high- q^2 region, in this region quark-hadron-duality violation is estimated to be small [77] for observables integrated over the full high- q^2 range. The kinematic region where the light resonances (ρ, ω, ϕ) contribute is typically not excluded from experimental analyses. Although their effects on branching fractions and other observables can be substantial, their contributions cannot be calculated in a fully model-independent manner. References [87, 88] estimate the size of nonlocal contributions to $B \rightarrow K(\pi)\ell\ell$ decays from the ρ and ω using hadronic dispersion relations [89]. They predict an enhancement of the $B^+ \rightarrow \pi^+\mu^+\mu^-$ differential branching fraction at low q^2 in good agreement with the q^2 spectrum measured by LHCb [55].

At high q^2 the final-state meson is nearly at rest, and the two leptons carry half the energy of the B meson each. As first discussed by Grinstein and Pirjol [73], the photon that produces them has $q^2 \sim M_B^2$ and the T -product in Eq. (2.8) can be evaluated using an operator product expansion (OPE) in $1/M_B$ [77, 78, 90, 91]. The resulting matrix elements can be parametrized in terms of the three form factors $f_{+,0,T}$. In the literature f_T is usually replaced by f_+ using heavy quark relations [73, 78, 92, 93], whereas in this paper we use the lattice-QCD results for f_T . Within this framework, the high- q^2 rate is described entirely in terms of the form factors $f_{+,0,T}$ up to corrections of order Λ/M_B . It is important to realize that the high- q^2 OPE requires $(x-y)^2 \sim 1/m_b^2$ implying that all matrix elements should be expanded in $1/q^2 \sim 1/m_b^2$. In Refs. [73, 90], the authors treat $m_c \ll m_b$ and expand $Q_{1,2}$ in powers of m_c^2/q^2 . Here we instead follow Ref. [77] by integrating out the charm quark at the m_b scale and including the full m_c dependence of the $Q_{1,2}$ matrix elements. This approach simplifies the operator basis without introducing any loss of accuracy. We include a 2% uncertainty to account for quark-hadron duality violations [77].

At low q^2 the two leptons are nearly collinear, and the daughter meson recoils with large energy $E_P \sim m_b/2$. In this kinematic configuration, three scales play an important role: the hard scale $\sim m_b^2$, the hard-collinear scale $\sim \Lambda_{\text{QCD}}m_b$ stemming from interactions of the energetic final state quarks with the light quarks and gluons in the B meson, and the purely nonperturbative scale $\sim \Lambda_{\text{QCD}}^2$. Note that the ratio of any two scales vanishes in the $m_b \rightarrow \infty$ limit. In the soft-collinear effective theory (SCET) [94–97], an expansion in Λ_{QCD}/m_b exploits this hierarchy such that all contributions stemming from physics above

Λ_{QCD} can be calculated in perturbative QCD. At leading power, the remaining nonperturbative objects are standard form factors and B , π and K mesons light-cone distribution amplitudes. SCET is therefore a double expansion in α_s and Λ_{QCD}/m_b . The application of soft-collinear factorization to exclusive $b \rightarrow s\ell\ell$ decays was pioneered in Refs. [98, 99] and subsequently employed in many phenomenological analyses; see, for instance, Refs. [83, 100].

The structure of the low- q^2 SCET expansion (also known as QCD factorization [94, 95]) for $B \rightarrow P\ell\ell$ ($P = K, \pi$) is (omitting prefactors)

$$C_i \langle P\ell\ell | Q_i | \bar{B} \rangle \sim C_i \left[(1 + \alpha_s) f_T + (1 + \alpha_s) f_+ + \phi_B \star T \star \phi_P \right], \quad i = 1, \dots, 6, \quad (2.9)$$

$$C_7 \langle P\ell\ell | Q_7 | \bar{B} \rangle \sim C_7 f_T, \quad (2.10)$$

$$C_8 \langle P\ell\ell | Q_8 | \bar{B} \rangle \sim C_8 \left[\alpha_s f_T + \alpha_s f_+ + \phi_B \star T \star \phi_P \right], \quad (2.11)$$

$$C_9 \langle P\ell\ell | Q_9 | \bar{B} \rangle \sim C_9 f_+, \quad (2.12)$$

$$C_{10} \langle P\ell\ell | Q_{10} | \bar{B} \rangle \sim C_{10} f_+, \quad (2.13)$$

where the coefficients of f_+ and f_T originate from hard interactions, and $\phi_B \star T \star \phi_P$ denotes a convolution of a short-distance kernel T , originating from hard-collinear interactions, with the B -meson and final-state meson light-cone distribution amplitudes ϕ_B and ϕ_P , respectively. As explained in detail in Appendix B, it is customary to collect all terms proportional to the form factors and introduce effective Wilson coefficients C_7^{eff} and C_9^{eff} . The structure of the whole amplitude is then

$$A(B \rightarrow P\ell\ell) \sim C_7^{\text{eff}} f_T + (C_9^{\text{eff}} + C_{10}) f_+ + \phi_B \star T \star \phi_P. \quad (2.14)$$

Further, some terms in $\langle Q_3 \rangle$ through $\langle Q_6 \rangle$ are proportional to $\langle Q_8 \rangle$ and are usually taken into account with the introduction of the effective Wilson coefficient C_8^{eff} .

Within the SCET approach it is also possible to express f_T in terms of f_+ —schematically $f_T \sim (1 + \alpha_s) f_+ + \phi_B \star T \star \phi_P$. Because we have direct access to the lattice-QCD calculation of f_T , this step would only result in the unnecessary introduction of additional uncertainties.

4. Differential decay rates

The double differential $B \rightarrow K(\pi)\ell\ell$ rate can be written as

$$\frac{d^2\Gamma}{dq^2 d\cos\theta} = a + b \cos\theta + c \cos^2\theta, \quad (2.15)$$

where θ is the angle between the B meson and ℓ^- in the dilepton rest frame, and a, b, c are functions of q^2 that depend on the form factors and Wilson coefficients. The three main observables considered in the literature are the differential rate

$$\frac{d\Gamma}{dq^2} = 2 \left(a + \frac{c}{3} \right), \quad (2.16)$$

the forward-backward asymmetry, and the flat term [100]. There are two forms of the last two, either evaluated at a single value of q^2 [64]

$$A_{\text{FB}}(q^2) = \frac{b}{d\Gamma/dq^2}, \quad (2.17)$$

$$F_H(q^2) = \frac{2(a+c)}{d\Gamma/dq^2}, \quad (2.18)$$

which is useful for plotting, or a binned form [100]

$$A_{\text{FB}}(q_{\text{min}}^2, q_{\text{max}}^2) = \int_{q_{\text{min}}^2}^{q_{\text{max}}^2} b dq^2 \left[\int_{q_{\text{min}}^2}^{q_{\text{max}}^2} 2 \left(a + \frac{c}{3} \right) dq^2 \right]^{-1}, \quad (2.19)$$

$$F_H(q_{\text{min}}^2, q_{\text{max}}^2) = \int_{q_{\text{min}}^2}^{q_{\text{max}}^2} (a+c) dq^2 \left[\int_{q_{\text{min}}^2}^{q_{\text{max}}^2} \left(a + \frac{c}{3} \right) dq^2 \right]^{-1}, \quad (2.20)$$

which can be compared with experimental measurements. In the Standard Model $b = 0$, *i.e.*, the forward-backward asymmetry vanishes (neglecting tiny QED effects). Further, in the $m_\ell = 0$ limit (an excellent approximation for $\ell = e, \mu$), one finds $c = -a$, implying a very small flat term of order m_ℓ^2/M_B^2 . Thus both the forward-backward asymmetry and flat term are potentially sensitive to contributions beyond the Standard Model. In addition, it is possible to consider the isospin and CP asymmetries of the differential $d\Gamma/dq^2$ rate. Appendix B provides explicit expressions for a and c in the Standard Model.

C. Rare $b \rightarrow q \nu \bar{\nu}$ ($q = d, s$) decay processes

In the Standard Model, the effective Hamiltonian for the rare decay process $b \rightarrow q \nu \bar{\nu}$ ($q = d, s$) is given by

$$\mathcal{H}_{\text{eff}} = -\frac{4G_F}{\sqrt{2}} V_{tb} V_{tq}^* C_L Q_L, \quad (2.21)$$

where

$$Q_L = \frac{e^2}{16\pi^2} (\bar{q}_L \gamma_\mu b_L) \sum_\nu (\bar{\nu}_L \gamma^\mu \nu_L), \quad (2.22)$$

summing over $\nu = \nu_e, \nu_\mu, \nu_\tau$, and

$$C_L = -X_t / \sin^2 \theta_W. \quad (2.23)$$

The function X_t parametrizes top-quark-loop effects and includes next-to-leading-order QCD contributions [101–103] and two-loop electroweak corrections [104]. We take the numerical value $X_t = 1.469(17)$ from Ref. [104].

The neutrino-pair final state ensures that the complications discussed for $B \rightarrow K(\pi) \ell^+ \ell^-$ decays in Sec. II B do not arise in the calculation of the decay rate for this process. In particular, the decay rate receives no contributions from $u\bar{u}$ or $c\bar{c}$ resonances or nonfactorizable terms. Thus, the systematic uncertainties associated with power corrections, resonances, and duality violations are absent [18]. In summary, the short-distance flavor-changing-neutral-current-induced contribution to the Standard Model decay rate for $B \rightarrow P \nu \bar{\nu}$ ($P = K, \pi$), which proceeds via the flavor-changing-neutral-current interaction, depends only on the vector form factor $f_+(q^2)$ and can be calculated over the entire kinematic range with full control over the theoretical errors. The differential branching fraction takes the form [18, 105]

$$\frac{d\mathcal{B}(B \rightarrow P \nu \bar{\nu})_{\text{SD}}}{dq^2} = C_P \tau_B |V_{tb} V_{ts(d)}^*|^2 \frac{G_F^2 \alpha^2}{32\pi^5} \frac{X_t^2}{\sin^4 \theta_W} |\mathbf{p}_P|^3 f_+^2(q^2). \quad (2.24)$$

where $|\mathbf{p}_P|$ is the magnitude of the final-state meson three-momentum in the B -meson rest frame. The isospin factor $C_P = 1$ for decays to kaons and charged pions (K^\pm, K^0, π^\pm), while $C_P = \frac{1}{2}$ for decays to neutral pions (π^0).

For the neutral modes $B^0 \rightarrow K^0(\pi^0)\nu\bar{\nu}$, Eq. (2.24) provides a full Standard-Model description. For the charged modes $B^+ \rightarrow K^+(\pi^+)\nu\bar{\nu}$, however, a tree-level amplitude arises via an intermediate lepton between two charged interactions [106]. First the B^+ meson decays leptonically, *i.e.*, $B^+ \rightarrow \ell^+\nu$; subsequently, the charged lepton decays as $\ell^+ \rightarrow P^+\bar{\nu}$. For $\ell = \tau$, the intermediate lepton can be on shell, leading to a long-distance contribution. Interference between the long- and short-distance amplitudes is negligible [106], leaving the following long-distance contribution to the rate

$$\mathcal{B}(B^+ \rightarrow P^+\nu_\tau\bar{\nu}_\tau)_{\text{LD}} = \frac{\left|G_F^2 V_{ub} V_{us(d)}^* f_B f_P\right|^2}{256\pi^3 M_B^3} \frac{2\pi m_\tau (M_B^2 - m_\tau^2)^2 (M_P^2 - m_\tau^2)^2}{\Gamma_\tau \Gamma_B}. \quad (2.25)$$

Superficially, Eq. (2.25) is suppressed relative to the loop-induced rate in Eq. (2.24) by G_F^2 , but the τ width Γ_τ is of order G_F^2 , canceling this suppression. The long-distance contribution is also numerically significant because the τ mass is large. For $B^+ \rightarrow \pi^+\nu_\tau\bar{\nu}_\tau$, it is further enhanced relative to the short-distance contribution by the CKM factor $|V_{ud}/V_{td}|^2$.

Taking the CKM matrix element $|V_{ub}| = 3.72(16) \times 10^{-3}$ from Fermilab/MILC [48], the combinations $|V_{ud}|f_{\pi^-} = 127.13(2)(13)$ MeV and $|V_{us}|f_{K^+} = 35.09(4)(4)$ MeV from experiment [107], and all other inputs from Table XVII, we obtain for the ν_τ -pair final state:

$$\mathcal{B}(B^+ \rightarrow \pi^+\nu_\tau\bar{\nu}_\tau)_{\text{LD}} = 9.48(92) \times 10^{-6}, \quad (2.26)$$

$$\mathcal{B}(B^+ \rightarrow K^+\nu_\tau\bar{\nu}_\tau)_{\text{LD}} = 6.22(60) \times 10^{-7}, \quad (2.27)$$

where the errors stem from the uncertainties on f_B and $|V_{ub}|$, and other parametric errors are negligible. The long-distance contributions to the $B^+ \rightarrow K^+(\pi^+)\nu_\ell\bar{\nu}_\ell$ rate for $\ell = e, \mu$ are of order 10^{-17} – 10^{-18} [106]. Because lattice QCD provides reliable determinations of the hadronic inputs f_B [108–113] and $f_{\pi(K)}$ [114–121], the long-distance contributions to the $B^+ \rightarrow K^+(\pi^+)\nu\bar{\nu}$ decay rates are under good theoretical control.

D. Tree-level $b \rightarrow u\ell\nu$ decay processes

The tree-level semileptonic decay $B \rightarrow \pi\ell\nu_\ell$ ($\ell = e, \mu, \tau$) is mediated in the Standard Model by the charged current interaction, and the resulting Standard-Model differential decay rate is

$$\begin{aligned} \frac{d\Gamma(B \rightarrow \pi\ell\nu_\ell)}{dq^2} &= C_P \frac{G_F^2 |V_{ub}|^2}{24\pi^3} \frac{(q^2 - m_\ell^2)^2 |\mathbf{p}_P|}{q^4 M_B^2} \left[\left(1 + \frac{m_\ell^2}{2q^2}\right) M_B^2 |\mathbf{p}_P|^2 |f_+(q^2)|^2 \right. \\ &\quad \left. + \frac{3m_\ell^2}{8q^2} (M_B^2 - M_\pi^2)^2 |f_0(q^2)|^2 \right], \end{aligned} \quad (2.28)$$

where the isospin factor C_P is the same as in Eq. (2.24) above. The decay rate depends upon both the vector (f_+) and scalar (f_0) form factors. For decays to light charged leptons ($\ell = e, \mu$), the contribution from the scalar form factor is suppressed by m_ℓ^2 and hence negligibly small. In contrast, the scalar form-factor contribution to decays into τ leptons is numerically significant. While $B \rightarrow \pi\tau\nu_\tau$ decay is not a rare, loop-suppressed process in the Standard Model, the large τ -lepton mass makes it particularly sensitive to contributions mediated by charged Higgs bosons.

III. LATTICE-QCD FORM FACTORS AND SYMMETRY TESTS

The first *ab-initio* lattice-QCD results for the $B \rightarrow K$ form factors and for the $B \rightarrow \pi$ tensor form factor became available only recently [48, 62–64]. Consequently, previous theoretical calculations of $B \rightarrow K(\pi)\ell^+\ell^-$ observables have sometimes used expectations from heavy-quark and/or SU(3)-flavor symmetries to relate the unknown form factors to others that can be constrained from experiment or computed with QCD models (see, *e.g.*, Refs. [78, 122]).

In this section, we directly test these symmetry relations, at both high and low q^2 , using the complete set of Fermilab/MILC $B \rightarrow K$ and $B \rightarrow \pi$ form factors [48, 62, 63]. For the $B \rightarrow \pi$ case, we use the vector and scalar form factors f_+ and f_0 obtained from a combined fit of lattice-QCD data with experiment. This combination improves the precision on the form factors at low q^2 , but assumes that no significant new physics contributes to the tree-level $B \rightarrow \pi\ell\nu$ decays for $\ell = \mu, e$.

First, in Sec. III A, we briefly summarize the lattice form-factor calculations, highlighting the properties of the simulations and analysis that enable controlled systematic errors and high precision. Then, in Sec. III B, we present tests of heavy-quark symmetry relations for $B \rightarrow \pi$ and $B \rightarrow K$ form factors that were not already presented in Refs. [48] and [62]. Finally, we calculate the size of SU(3)-flavor-breaking effects between the $B \rightarrow K$ and $B \rightarrow \pi$ form factors and compare with power-counting expectations in Sec. III C.

A. Lattice-QCD form-factor calculations

The Fermilab Lattice and MILC Collaborations carried out the numerical lattice-QCD calculations in Refs. [48, 62, 63] in parallel. Here we summarize the features of the work that enabled both high precision and controlled uncertainties. Below we give the correlations between the $B \rightarrow \pi$ and $B \rightarrow K$ form factors, which have not appeared elsewhere. To put this new information in context, we summarize the similarities and slight differences between the $B \rightarrow \pi$ [48, 63] and $B \rightarrow K$ [62] Fermilab/MILC lattice-QCD calculations.

The calculations [48, 62, 63] employed the MILC asqtad ensembles [123–125] at four lattice spacings from approximately 0.12 fm down to 0.045 fm; physical volumes with linear size $L \gtrsim 3.8$ fm; and several choices for the masses of the sea-quarks, corresponding to pions with mass as low as 175 MeV. The strange sea-quark mass was chosen close to the physical strange-quark mass, but varied a bit with lattice spacing, allowing for adjustment of this mass *a posteriori*. The Fermilab method was used for the lattice b quark [126]. As in several other calculations, starting with Ref. [127], the matching of the currents from the lattice to the continuum was mostly nonperturbative, with a residual matching factor close to unity computed in one-loop perturbation theory, with matching scale $\mu = m_b$ for the tensor current. Because the one-loop calculation was separate from the Monte Carlo calculation of correlation functions, it was exploited to introduce a multiplicative “blinding” offset.

The matrix elements for the form factors were obtained from fits to two- and three-point correlation functions, including one excited B meson in the fit. After matching these lattice-QCD data to the continuum, as described above, two further analysis steps are crucial for the present paper. First, the form factors calculated in the kinematic region $q^2 \gtrsim 17 \text{ GeV}^2$ were extrapolated to zero lattice spacing and to the physical light-quark masses with a form of chiral perturbation theory (χ PT) for semileptonic decays [128] adapted to

staggered fermions [129]. Because the final-state pion and kaon energies can become large in the context of standard χ PT, the analyses found better fits with SU(2) hard-pion and hard-kaon χ PT [130]. This chiral-continuum extrapolation included terms for heavy-quark discretization effects, with a functional form taken from heavy-quark effective theory [131–133], as in Ref. [108].

Next, to extend the form-factor results to the whole kinematically allowed region, Refs. [48, 62, 63] used the model-independent z expansion based on the analytic structure of the form factors. In the present paper, we rely on the output of these fits, including correlations, so we repeat the most pertinent details. Following Refs. [134, 135], the complex q^2 plane is mapped to

$$z(q^2, t_0) = \frac{\sqrt{t_+ - q^2} - \sqrt{t_+ - t_0}}{\sqrt{t_+ - q^2} + \sqrt{t_+ - t_0}}, \quad (3.1)$$

which maps a cut at $q^2 > t_+ = (M_B + M_P)^2$ to the unit circle and maps the semileptonic region to an interval in z on the real axis. The extent of the interval can be minimized by choosing $t_0 = (M_B + M_P)(\sqrt{M_B} - \sqrt{M_P})^2$, where $M_P = M_\pi$ or M_K . Unitarity implies that a power series in z converges for $|z| < 1$. In Refs. [48, 62, 63], these series were used [135]:

$$f_+(q^2) = \frac{1}{P_+(q^2)} \sum_{n=0}^{K-1} b_n^+ \left[z^n - (-1)^{K-n} \frac{n}{K} z^K \right], \quad (3.2)$$

$$f_0(q^2) = \frac{1}{P_0(q^2)} \sum_{n=0}^{K-1} b_n^0 z^n, \quad (3.3)$$

and the same for f_T as for f_+ (with coefficients b_n^T). The pole factor $P_{+,0,T}(q^2) = 1 - q^2/M_{+,0,T}^2$, with $M_{+,0,T}$ chosen as follows: for $B \rightarrow \pi$, $M_+ = M_T = M_{B^*} = 5.3252$ GeV from experiment [136], $M_0 \rightarrow \infty$ (*i.e.*, no pole); for $B \rightarrow K$, $M_+ = M_T = M_{B_s^*} = 5.4154$ GeV from experiment [136], $M_0 = 5.711$ GeV from lattice QCD [137]. The output of the chiral-continuum extrapolation was propagated to Eqs. (3.2) and (3.3) using either synthetic data [62] or a functional fitting procedure [48, 63].

Reference [48] also presented determinations of the $B \rightarrow \pi$ form factors f_+ and f_0 from a combined z fit to the lattice-QCD form factors and experimental measurements of the $B \rightarrow \pi \ell \nu$ differential decay rate from the B factories [67–70]. This fit employed the same z expansions as above. The experimental data provides information on the shape of $f_+(q^2)$ at low q^2 beyond the direct reach of lattice-QCD simulations, thereby reducing the form-factor errors at low q^2 . In this paper, we use these more precise $B \rightarrow \pi$ vector and scalar form factors for all calculations of $B \rightarrow \pi$ observables, thereby improving the precision of the Standard-Model results at the expense of the assumption that new physics does not significantly alter the rate of this tree-level transition.

In Sec. III C, we present predictions for combinations of $B \rightarrow \pi$ and $B \rightarrow K$ observables, which require the correlations between the two channels, not provided before [48, 62, 63]. As co-authors of these papers, we have access to the relevant information. To enable others to study both modes together, we provide the correlation coefficients in Table I. With Eqs. (3.1)–(3.3) and the information contained in Table XIX of Ref. [48], Table XII of Ref. [62], and Table III of Ref. [63], the supplementary information provided in Table I enables the reader to reproduce the form factors and combinations of them.

The dominant correlations between the two sets of form factors are statistical, because both calculations used the same gauge-field ensembles. In practice, however, both the sta-

TABLE I. Correlations between the z -expansion coefficients of the $B \rightarrow \pi$ and $B \rightarrow K$ vector, scalar, and tensor form factors, where the $B \rightarrow \pi$ vector and scalar form factors include experimental shape information from $B \rightarrow \pi \ell \nu$ decay. These should be combined with Table XIX of Ref. [48], Table III of Ref. [63], and Table XII of Ref. [62], which give the central values of the coefficients as well as the remaining correlation information.

		$B \rightarrow K \ell \ell$								
		b_0^+	b_1^+	b_2^+	b_0^0	b_1^0	b_2^0	b_0^T	b_1^T	b_2^T
$B \rightarrow \pi \ell \ell$	b_0^+	0.273	-0.002	-0.029	0.227	0.063	0.034	0.333	-0.001	-0.005
	b_1^+	0.016	0.085	-0.006	-0.003	0.061	0.067	-0.011	0.075	0.017
	b_2^+	-0.133	-0.069	0.024	-0.094	-0.077	-0.064	-0.124	-0.053	0.006
	b_3^+	-0.077	-0.033	0.060	-0.030	-0.028	-0.023	-0.062	-0.021	0.031
	b_0^0	0.278	0.098	0.091	0.299	0.160	0.124	0.285	-0.005	-0.005
	b_1^0	-0.004	0.225	0.155	0.065	0.197	0.171	-0.079	0.153	0.092
	b_2^0	-0.120	-0.231	-0.163	-0.194	-0.232	-0.183	-0.020	-0.058	-0.006
	b_3^0	-0.085	-0.192	-0.155	-0.144	-0.195	-0.171	-0.041	-0.121	-0.079
	b_0^T	0.319	0.051	-0.005	0.279	0.115	0.088	0.392	0.037	0.008
	b_1^T	0.056	0.080	0.012	0.051	0.072	0.063	0.067	0.097	0.048
	b_2^T	0.014	0.022	0.029	0.030	0.026	0.019	0.018	0.014	0.025
	b_3^T	0.005	0.010	0.026	0.023	0.015	0.008	0.010	0.003	0.022

tistical and systematic correlations are diluted in the chiral-continuum extrapolations for $B \rightarrow \pi$ and $B \rightarrow K$, which were performed independently. The same holds for several important systematic uncertainties, namely from the chiral-continuum extrapolations, the uncertainty in the B^*-B - π coupling, and the heavy-quark discretization errors. The correlations became even smaller once the experimental $B \rightarrow \pi \ell \nu$ data were used to constrain the shape of the $B \rightarrow \pi$ vector and scalar form factors. In the end, the only significant correlations are among the leading coefficients b_0 , which correspond essentially to the normalization, and are therefore well determined by the data. Even these are typically only ~ 0.3 , with the largest being ~ 0.4 . Smaller correlations between the leading coefficients and the higher-order coefficients of ~ 0.1 – 0.2 arise from the kinematic constraint $f_+(0) = f_0(0)$ enforced in the z -expansion fits. The use of experimental $B \rightarrow \pi \ell \nu$ data to constrain the shape of the $B \rightarrow \pi$ vector and scalar form factors, when combined with the kinematic constraint, leads to the negative entries in the correlation matrix, which correspond to anticorrelations between b_i^+ and b_i^0 for $B \rightarrow \pi$ and the other coefficients.

B. Tests of heavy-quark symmetry

Several tests of heavy-quark-symmetry relations for $B \rightarrow \pi$ and $B \rightarrow K$ using the Fermilab/MILC form factors were already presented in Refs. [48, 62]. Figure 16 of Ref. [62] plots the $B \rightarrow K$ form-factor ratios f_0/f_+ and f_T/f_+ at high q^2 obtained from lattice QCD, and compares them with expectations from heavy-quark symmetry. Similarly, Fig. 25 of Ref. [48] compares the $B \rightarrow \pi$ form factor ratio f_0/f_+ with heavy-quark-symmetry expectations. Here we examine heavy-quark-symmetry tests of the $B \rightarrow \pi$ tensor form factor.

The simplest heavy-quark-symmetry relation between f_T and the other form factors

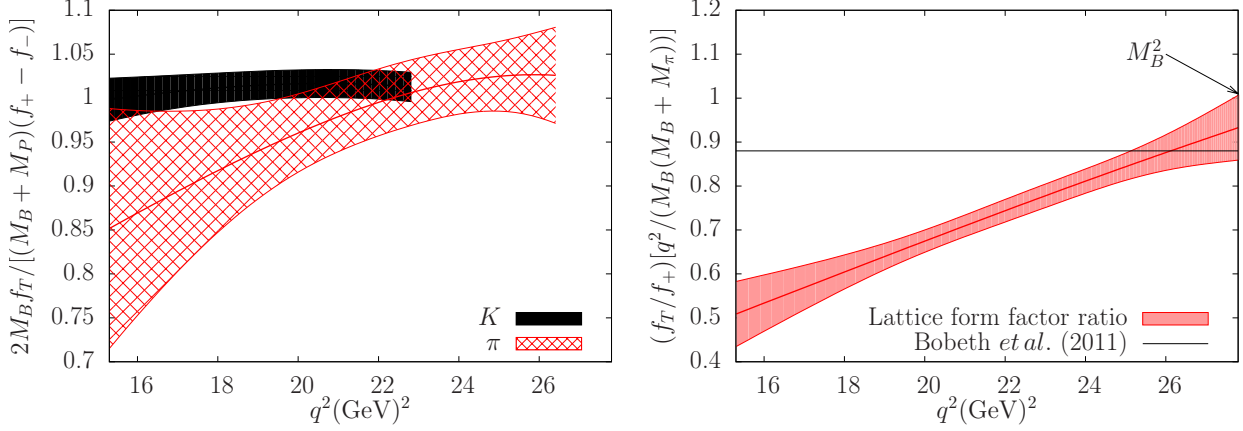


FIG. 1. Tests of the heavy-quark symmetry relations for the tensor form factor using the Fermilab/MILC form factors [48, 62, 63]. The left plot shows the ratio in Eq. (3.5) at low recoil for $B \rightarrow \pi$ (red hatched band) and $B \rightarrow K$ (black solid band), which would become unity as $m_b \rightarrow \infty$ [138, 139]. The right plot compares $(f_T/f_+) [q^2/(M_B(M_B + M_\pi))]$ at low recoil (red curve with error band), for $B \rightarrow \pi$ with the theoretical expectation for $\kappa(\mu)$ [78] (black horizontal line).

is [138, 139]

$$f_T(q^2) = \frac{M_B + M_P}{2M_B} [f_+(q^2) - f_-(q^2)] + \mathcal{O}(\alpha_s, \Lambda/m_b), \quad (3.4)$$

which follows because the right-hand side is proportional to the matrix element $\langle P | \bar{q} \gamma^i b | B \rangle$, while the left-hand side is proportional to $\langle P | \bar{q} \gamma^i \gamma^0 b | B \rangle$. In Fig. 1, left, we plot the ratio

$$\frac{2M_B}{M_B + M_P} \frac{f_T(q^2)}{f_+(q^2) - f_-(q^2)} \quad (3.5)$$

vs. q^2 , calculated directly from the Fermilab/MILC form factors [48, 62, 63]. We show the range $q^2 \gtrsim 15 \text{ GeV}^2$ where the error remains small enough to provide a meaningful test of the relation in Eq. (3.4). In this region, the approximation in Eq. (3.4) fares very well, especially for $B \rightarrow K$.

A refinement of this idea uses heavy-quark symmetry and m_b -scaling to eliminate f_- [73, 78, 93]:

$$\lim_{q^2 \rightarrow M_B^2} \frac{f_T(q^2, \mu)}{f_+(q^2)} = \kappa(\mu) \frac{M_B(M_B + M_\pi)}{q^2} + \mathcal{O}(\Lambda/m_b), \quad (3.6)$$

in which the scale-dependent coefficient $\kappa(\mu)$ incorporates radiative corrections and is given explicitly through order α_s^2 in Eq. (B49). Figure 1, right, compares the quantity $(f_T/f_+) [q^2/(M_B(M_B + M_\pi))]$ obtained from the Fermilab/MILC $B \rightarrow \pi$ form factors [48, 63] with the theoretical prediction from Eq. (3.6). For the theoretical estimate, we take $m_b = 4.18 \text{ GeV}$ and $\alpha_s^{(4)}(m_b) = 0.2268$, giving $\kappa(m_b) \approx 0.88$ [73, 78].

As observed in Ref. [62] for the $B \rightarrow K$ form factors, the ratio f_T/f_+ calculated directly from lattice QCD agrees well with the expectation from Eq. (3.6) for $q^2 \approx M_B^2$. Although we do not show any errors on the theoretical prediction, we can estimate the size of higher-order corrections in the heavy-quark expansion from power counting. Taking $\Lambda = 500 \text{ MeV}$ gives $\Lambda/m_b \sim 12\%$. Equation (3.6) also receives corrections from the pion recoil energy

of order E_π/m_b . This ratio grows rapidly from $E_\pi/m_b \sim 3\%$ at q_{\max}^2 to $E_\pi/m_b \sim 30\%$ at $q^2 \approx 14 \text{ GeV}^2$. The observed size of deviations from the leading heavy-quark-symmetry prediction are somewhat larger than the rough estimate based on power counting. Although form factors from *ab-initio* QCD are now available for $B \rightarrow \pi$ and $B \rightarrow K$, other analyses of semileptonic decay processes might still use heavy-quark-symmetry relations. Figure 1 provides quantitative, empirical guides for estimating the associated systematic uncertainty introduced by their use.

In the limit $q^2 \ll M_B^2$, a collinear spin symmetry emerges for the energetic daughter quark, and the vector, scalar, and tensor form factors are related to a universal M_B -independent form factor [98, 140]:

$$f_+(q^2) = \frac{M_B}{2E_P} f_0(q^2) = \frac{M_B}{M_B + M_P} f_T(q^2), \quad (q^2 \ll M_B^2). \quad (3.7)$$

The first relation merely recovers the kinematic constraint, $f_+(0) = f_0(0)$. Unfortunately, as q^2 decreases, so do the correlations between the lattice-QCD determinations of f_+ and f_T . The error on the ratio f_T/f_+ therefore increases, reaching 100% at $q^2 = 0$. Thus, we are unable to quantitatively test the predicted relationship between f_T and f_+ at large recoil.

C. Tests of SU(3)-flavor symmetry

The $B \rightarrow \pi$ and $B \rightarrow K$ form factors would be equal in the SU(3)-flavor limit $m_u = m_d = m_s$ and, thus, differ due to corrections that are suppressed by the factor $(m_s - m_{ud})/\Lambda$, where Λ is a typical QCD scale inside heavy-light mesons. Indeed, approximate SU(3) symmetry implies relations among all matrix elements of the form

$$\langle P_{q\bar{r}}(p_P) | \bar{q} \Gamma b | B_r(p_B) \rangle, \quad (3.8)$$

where r denotes the flavor of the spectator quark; Γ is γ^μ , 1, or $i\sigma^{\mu\nu}$; and the subscript on the final-state pseudoscalar denotes its flavor content.

A rule of thumb [141] for SU(3) breaking is that large effects can be traced to the pseudoscalar masses— $M_K^2 \gg M_\pi^2$ —while SU(3)-breaking effects in matrix elements per se are small. In considering the matrix elements in Eq. (3.8), the final-state four-momentum p_P cannot be the same for all $P_{q\bar{r}}$ mesons, because the mass shells differ. The masses affect the kinematic variables q^2 , E_P , and \mathbf{p}_P in different ways.

In Ref. [122] (see also Ref. [141]), SU(3)-breaking was considered as a function of q^2 , with the quantities $R_{+,0,T}(q^2)$ defined as

$$R_i(q^2) = \frac{f_i^{BK}(q^2)}{f_i^{B\pi}(q^2)} - 1, \quad (3.9)$$

where $i = +, 0, T$. In Ref. [122], the ratios $R_{+,0}(q^2)$ were calculated using lattice $B \rightarrow \pi$ and $B \rightarrow K$ form factors from Refs. [142] and [43, 143], respectively. Here we repeat the tests in Ref. [122] using the more precise Fermilab/MILC $B \rightarrow \pi$ vector and scalar form factors [48], and include an additional test using the Fermilab/MILC $B \rightarrow \pi$ tensor form factor [63], taking the $B \rightarrow K$ form factors from Fermilab/MILC [62] as well. Figure 2, left, plots the quantity $R_i(q^2)$, including correlations between the $B \rightarrow \pi$ and $B \rightarrow K$ form factors from statistics as well as the dominant systematic errors [48, 62, 63]. We find that the sizes

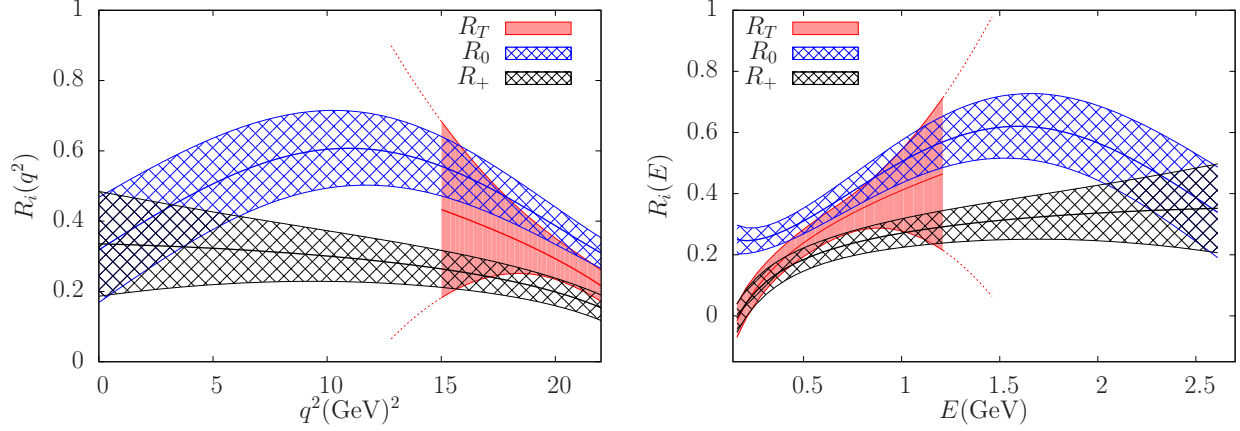


FIG. 2. SU(3)-flavor-breaking ratios using the Fermilab/MILC form factors [48, 62, 63] (solid and hatched curves with error bands). Left: ratios $R_{+,0,T}(q^2)$ [Eq. (3.9)]. Right: ratios $R_{+,0,T}(E)$ [Eq. (3.10)]. We do not show R_T when the error becomes too large to draw any useful inferences, although the trend of the error band is shown by the thin lines extending from the R_T error bands.

of $R_i(q^2)$ are between 20% and 60%, ranging from commensurate with $(m_s - m_{ud})/\Lambda$ (for $m_s \sim 100$ MeV, $\Lambda \sim 500$ MeV) to uncharacteristically large. In the region where the error on the tensor form factors remain manageable, we find that $R_T(q^2) \approx [R_+(q^2) + R_0(q^2)]/2$, as assumed in Ref. [122]. With the more precise Fermilab/MILC $B \rightarrow \pi$ form factors [48, 63], the resulting SU(3) breaking is larger than that deduced and employed in that work.

As an alternative to Eq. (3.9), we consider the analogous ratio with fixed final-state energy (in the B rest frame):

$$R_i(E) = \frac{f_i^{BK}(E)}{f_i^{B\pi}(E)} - 1. \quad (3.10)$$

As shown in Fig. 2, right, the SU(3) breaking in $R_i(E)$ is similar to that in $R_i(q^2)$.

A further alternative is to examine

$$\tilde{R}_i(|\mathbf{v}|) = \frac{f_i^{BK}(|\mathbf{v}|)P_i^{BK}}{f_i^{B\pi}(|\mathbf{v}|)P_i^{B\pi}} - 1, \quad (3.11)$$

where $\mathbf{v} = \mathbf{p}_P/M_P$ is the final-state three-velocity (in HQET conventions) in the B -meson rest frame. The factors $P_0^{B\pi} = P_0^{BK} = 1$, $P_{+,T}^{B\pi} = 1 - q^2/M_{B^*}^2$, and $P_{+,T}^{BK} = 1 - q^2/M_{B_s^*}^2$ are introduced to remove the kinematically important vector-meson pole from the vector and tensor form factors. As shown in Fig. 3, this measure of SU(3) breaking is under 20% for f_+ and f_T , and under 35% for f_0 (in the momentum range shown). The result for \tilde{R}_0 can be understood in the soft-pion (soft-kaon) limit, where $f_0 \propto f_B/f_P$, so

$$\tilde{R}_0(|\mathbf{v}| \rightarrow 0) = \frac{f_\pi}{f_K} - 1 \approx -0.16. \quad (3.12)$$

which agrees very well with our result in Fig. 3 (right). Similarly, for \tilde{R}_+

$$\tilde{R}_+(|\mathbf{v}| \rightarrow 0) = \frac{f_\pi g_{B_s^*BK}}{f_K g_{B^*B\pi}} - 1. \quad (3.13)$$

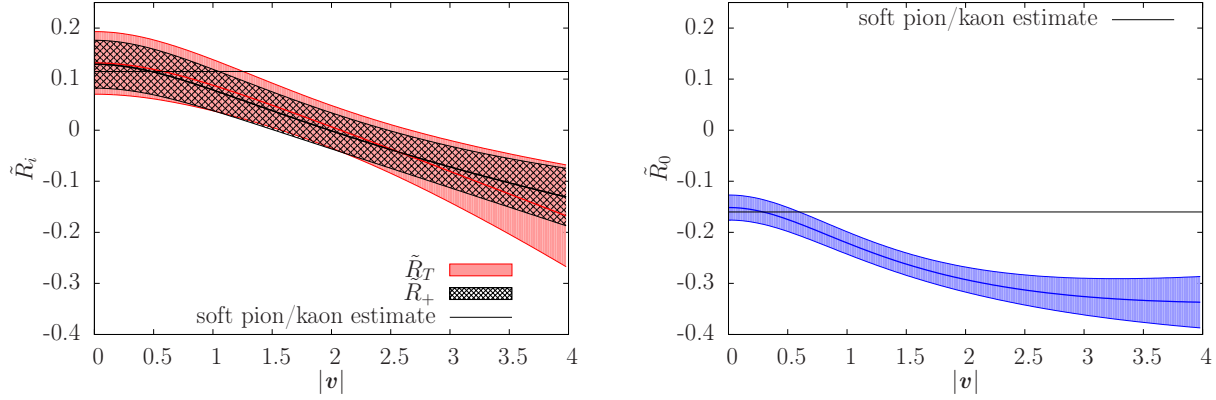


FIG. 3. Velocity-based SU(3)-flavor-breaking ratios $\tilde{R}_{+,T}(|v|)$ (left) and $\tilde{R}_0(|v|)$ (right) using the lattice-QCD form factors from Refs. [48, 62, 63].

The SU(3)-breaking effects in the couplings can be estimated from the chiral extrapolation of a recent calculation of $g_{B^*B\pi}$ [144]. The expression of the chiral extrapolation of $g_{B^*B\pi}$ was given in Eq. (28) of Ref. [144]. Replacing the pions in the loops with kaons, we estimate $g_{B_s^*BK}/g_{B^*B\pi} \approx 1.33$ and, consequently, $R_+ \approx 0.11$. Because of the heavy-quark relation between f_T and f_+ discussed above, \tilde{R}_T should be close to \tilde{R}_+ , and one can see in Fig. 3 (left) that this is indeed the case.

IV. STANDARD-MODEL RESULTS

We now use the Fermilab/MILC $B \rightarrow \pi$ and $B \rightarrow K$ form factors [48, 62, 63] to predict $B \rightarrow K(\pi)\ell^+\ell^-$, $B \rightarrow K(\pi)\nu\bar{\nu}$, and $B \rightarrow \pi\tau\nu$ observables (and their ratios) in the Standard Model. For predictions of $B \rightarrow \pi$ decay observables, as in the previous section, we use the more precise $B \rightarrow \pi$ vector and scalar form factors obtained using the measured $B \rightarrow \pi\ell\nu$ q^2 spectrum to constrain the shape. We present results for rare decays with a charged-lepton pair final state, $b \rightarrow q\ell\ell$ ($q = d, s$) in Sec. IV A, for rare decays with a neutrino pair final state $b \rightarrow q\nu\bar{\nu}$ ($q = d, s$) in Sec. IV B, and for tree-level $b \rightarrow u\tau\nu_\tau$ semileptonic decays in Sec. IV C. Where possible, we compare our results with experimental measurements.

We compile our numerical results for the partially integrated $B \rightarrow K(\pi)\ell^+\ell^-$ observables over different q^2 intervals in Tables II–XV of Appendix A. To enable comparison with the recent experimental measurements of $B \rightarrow K(\pi)\ell^+\ell^-$ from LHCb, we provide the matrix of correlations between our Standard-Model predictions for the binned branching fractions (and the ratio of $B \rightarrow \pi$ -to- $B \rightarrow K$ binned branching fractions) for the same wide q^2 bins below and above the charmonium resonances employed by LHCb [45, 55].

Appendix B provides the complete expressions for the Standard-Model $B \rightarrow K(\pi)\ell^+\ell^-$ ($\ell = e, \mu, \tau$) differential decay rates. The simpler expressions for the $B \rightarrow K(\pi)\nu\bar{\nu}$ and $B \rightarrow \pi\tau\nu$ decay rates are presented in the main text of Secs. II C and II D, respectively. The Wilson coefficients and other numerical inputs used for all of the phenomenological analyses in this work are given in Appendix C.

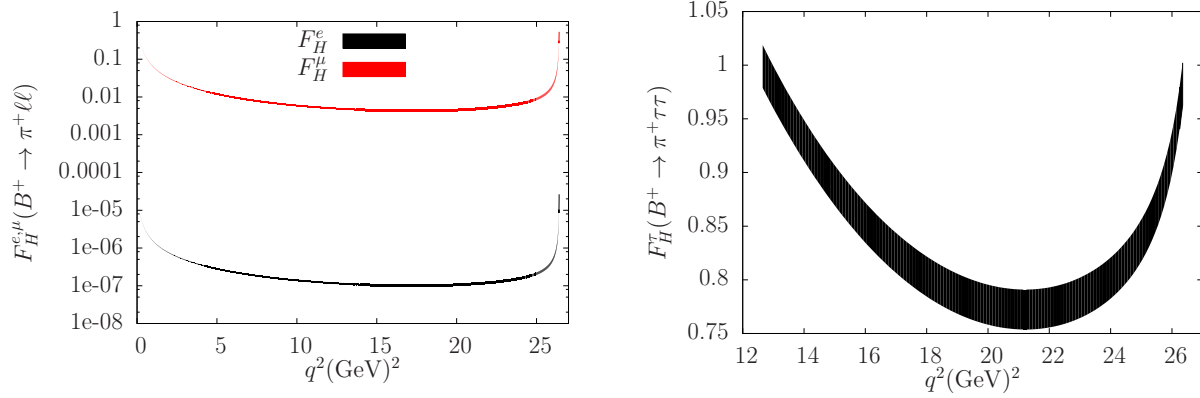


FIG. 4. Standard-Model predictions for the $B^+ \rightarrow \pi^+ \ell^+ \ell^-$ flat term $F_H^\ell(q^2)$ for $\ell = e, \mu$ (left) and $\ell = \tau$ (right) using the Fermilab/MILC form factors [48, 63].

A. Rare $b \rightarrow q \ell \ell$ ($q = d, s$) decay observables

1. $B \rightarrow \pi \ell^+ \ell^-$ observables

The Fermilab Lattice and MILC Collaborations already presented some Standard-Model predictions for $B \rightarrow \pi \ell^+ \ell^-$ [63]. Figure 4 of that work plots the differential branching fractions for $\ell = \mu, \tau$, while Table IV gives the partial branching fractions in selected intervals of q^2 below and above the charmonium resonances, and for the full kinematic range. To enable correlated analyses of the partially integrated branching fractions for $B \rightarrow \pi$ from Ref. [63] and those for $B \rightarrow K$ presented in Sec. IV A 2, we update the large-bin numerical results from Table IV of Ref. [63] in Table IV here by adding digits to the quoted uncertainties and combining the scale uncertainty (quoted separately in Ref. [63]) with the “other” error. In addition, we extend the phenomenological analysis of $B \rightarrow \pi \ell^+ \ell^-$ by providing predictions for the flat term of the angular distribution, cf. Eqs. (2.18) and (2.20).

Figure 4 plots our Standard-Model predictions for the $B^+ \rightarrow \pi^+ \ell^+ \ell^-$ flat term $F_H^\ell(q^2)$, $\ell = e, \mu, \tau$, while Tables II and III report numerical values for the binned version $F_H^\ell(q_{\min}^2, q_{\max}^2)$ for the charged and neutral decay modes, respectively. For the dimuon final state, we find $F_H^\mu(q^2) \sim 1\text{--}2\%$ for most of the kinematic range, which is large enough to be measured in future experiments. For the electron-positron final state, $F_H^e(q^2)$ is so small— 10^{-6} or smaller—that any foreseeable nonzero measurement would indicate the presence of new physics.

After the Fermilab Lattice and MILC Collaborations submitted Ref. [63] for publication, the LHCb experiment announced [145] a new measurement of the differential decay rate for $B \rightarrow \pi \mu^+ \mu^-$ decay, which is now finalized [55]. Here we repeat the main numerical results of Ref. [63] and compare them to the LHCb measurement. The Standard-Model predictions for the partially integrated branching ratio in the wide high- q^2 and low- q^2 bins are [63]

$$\Delta\mathcal{B}(B^+ \rightarrow \pi^+ \mu^+ \mu^-)^{\text{SM}} \times 10^9 = \begin{cases} 4.78(29)(54)(15)(6) & 1 \text{ GeV}^2 \leq q^2 \leq 6 \text{ GeV}^2, \\ 5.05(30)(34)(7)(15) & 15 \text{ GeV}^2 \leq q^2 \leq 22 \text{ GeV}^2, \end{cases} \quad (4.1)$$

where the errors are from the CKM matrix elements, form factors, the variation of the high and low matching scales, and the quadrature sum of all other contributions, respectively.

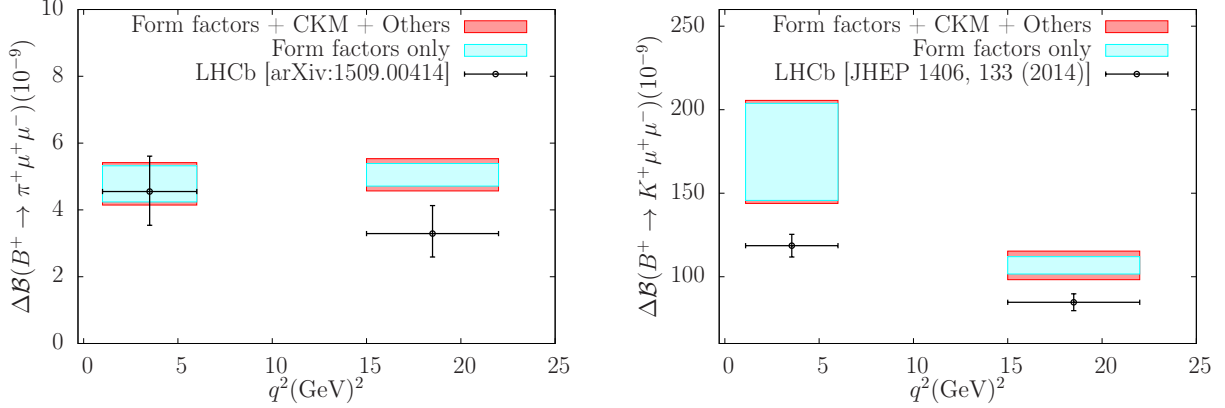


FIG. 5. Standard-Model partially integrated branching ratios for $B^+ \rightarrow \pi^+ \mu^+ \mu^-$ decay (left) and $B^+ \rightarrow K^+ \mu^+ \mu^-$ decay (right) using the Fermilab/MILC form factors [48, 62, 63] compared with experimental measurements from LHCb [45, 55] for the wide q^2 bins above and below the charmonium resonances.

LHCb quotes measured values for binned differential branching fractions [55], which we convert to partially integrated branching fractions for ease of comparison with Eq. (4.1):

$$\Delta\mathcal{B}(B^+ \rightarrow \pi^+ \mu^+ \mu^-)^{\text{exp}} \times 10^9 \text{ GeV}^2 = \begin{cases} 4.55 \left({}^{+1.05}_{-1.00} \right) (0.15) & 1 \text{ GeV}^2 \leq q^2 \leq 6 \text{ GeV}^2, \\ 3.29 \left({}^{+0.84}_{-0.70} \right) (0.07) & 15 \text{ GeV}^2 \leq q^2 \leq 22 \text{ GeV}^2, \end{cases} \quad (4.2)$$

where the two errors are statistical and systematic.

Figure 5 (left panel) compares the Standard-Model predictions from Ref. [63] and LHCb for the wide bins. The result for the low q^2 interval below the charm resonances agrees with the experimental measurement, but that for the high q^2 interval differs at the 1.9σ level. The combination of the two bins, including the theoretical correlations from Tables VII, and VIII and treating the experimental bins as uncorrelated, yields a $\chi^2/\text{dof} = 3.7/2$ ($p = 0.15$), and thus disfavors the Standard-Model hypothesis at 1.4σ confidence level.

Although LHCb's recent measurement of the $B \rightarrow \pi \ell^+ \ell^-$ differential decay rate [55] is compatible with the Standard-Model predictions, the uncertainties leave room for sizable new-physics contributions. In the high- q^2 interval, $15 \text{ GeV}^2 \leq q^2 \leq 22 \text{ GeV}^2$, the theoretical and experimental errors are commensurate. Future, more precise measurements after the LHCb upgrade will refine the comparison, thereby strengthening the test of the Standard Model.

2. $B \rightarrow K \ell^+ \ell^-$ observables

Here we present results for $B \rightarrow K \ell^+ \ell^-$ ($\ell = \mu, \tau$) observables in the Standard Model using the Fermilab/MILC $B \rightarrow K$ form factors [62]. Many previous phenomenological analyses of $B \rightarrow K \ell^+ \ell^-$ related the tensor form factor f_T to the vector form factor f_+ based on approximate symmetries [78, 100]. The HPQCD Collaboration has also presented results for $B \rightarrow K$ observables using their own lattice-QCD form-factor determinations [43]. We improve upon the Standard-Model predictions in that work and in Ref. [62] by incorporating hard-scattering contributions at low q^2 and by using Wilson coefficients that include

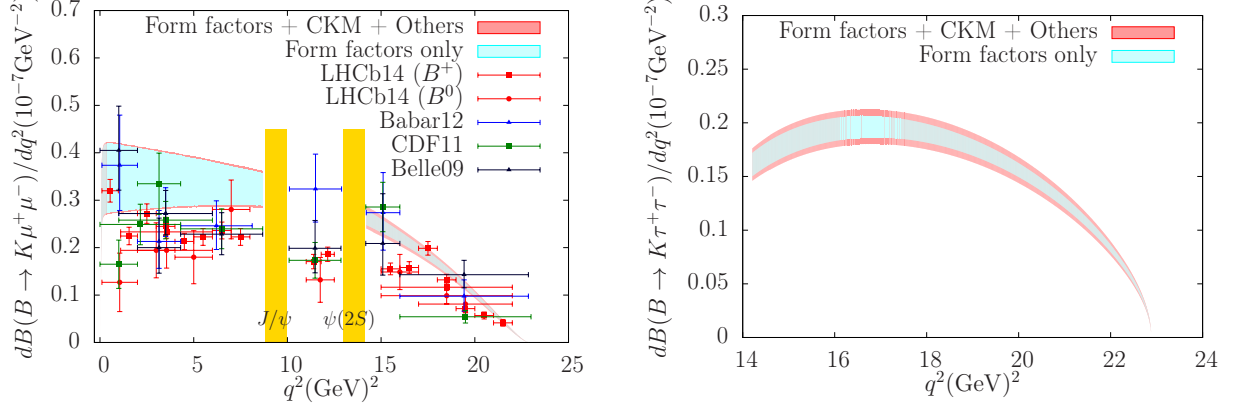


FIG. 6. Standard-Model differential branching fraction (gray band) for $B \rightarrow K\mu^+\mu^-$ decay (left) and $B \rightarrow K\tau^+\tau^-$ (right), where B denotes the isospin average, using the Fermilab/MILC form factors [62]. Experimental results for $B \rightarrow K\mu^+\mu^-$ are from Refs. [45, 146–148]. The BaBar, Belle, and CDF experiments report isospin-averaged measurements.

logarithmically enhanced QED corrections.

Figure 6 plots the isospin-averaged Standard-Model differential branching fractions for $B \rightarrow K\mu^+\mu^-$ and $B \rightarrow K\tau^+\tau^-$. For $B \rightarrow K\mu^+\mu^-$ decay, we compare our results with the latest measurements by BaBar [148], Belle [146], CDF [147], and LHCb [45]. Tables V and VI give the partially integrated branching fractions for the charged (B^+) and neutral (B^0) meson decays, respectively, for the same q^2 bins used by LHCb in Ref. [45]. In the regions $q^2 \lesssim 1 \text{ GeV}^2$ and $6 \text{ GeV}^2 \lesssim q^2 \lesssim 14 \text{ GeV}^2$, $u\bar{u}$ and $c\bar{c}$ resonances dominate the rate. To estimate the total branching ratio, we simply disregard them and interpolate linearly in q^2 between the QCD-factorization result at $q^2 \approx 8.5 \text{ GeV}^2$ and the OPE result at $q^2 \approx 13 \text{ GeV}^2$. Although this treatment does not yield the full branching ratio, it enables a comparison with the quoted experimental totals, which are obtained from a similar treatment of these regions. Away from the charmonium resonances, the Standard-Model calculation is under good theoretical control, and the partially integrated branching ratios in the wide high- q^2 and low- q^2 bins are our main results:

$$\Delta\mathcal{B}(B^+ \rightarrow K^+\mu^+\mu^-)^{\text{SM}} \times 10^9 = \begin{cases} 174.7(9.5)(29.1)(3.2)(2.2), & 1.1 \text{ GeV}^2 \leq q^2 \leq 6 \text{ GeV}^2, \\ 106.8(5.8)(5.2)(1.7)(3.1), & 15 \text{ GeV}^2 \leq q^2 \leq 22 \text{ GeV}^2, \end{cases} \quad (4.3)$$

$$\Delta\mathcal{B}(B^0 \rightarrow K^0\mu^+\mu^-)^{\text{SM}} \times 10^9 = \begin{cases} 160.8(8.8)(26.6)(3.0)(1.9), & 1.1 \text{ GeV}^2 \leq q^2 \leq 6 \text{ GeV}^2, \\ 98.5(5.4)(4.8)(1.6)(2.8), & 15 \text{ GeV}^2 \leq q^2 \leq 22 \text{ GeV}^2, \end{cases} \quad (4.4)$$

where the errors are from the CKM elements, form factors, variations of the high and low matching scales, and the quadrature sum of all other contributions, respectively. LHCb's measurements for the same wide bins are [45]

$$\Delta\mathcal{B}(B^+ \rightarrow K^+\mu^+\mu^-)^{\text{exp}} \times 10^9 \text{ GeV}^2 = \begin{cases} 118.6(3.4)(5.9) & 1.1 \text{ GeV}^2 \leq q^2 \leq 6 \text{ GeV}^2, \\ 84.7(2.8)(4.2) & 15 \text{ GeV}^2 \leq q^2 \leq 22 \text{ GeV}^2, \end{cases} \quad (4.5)$$

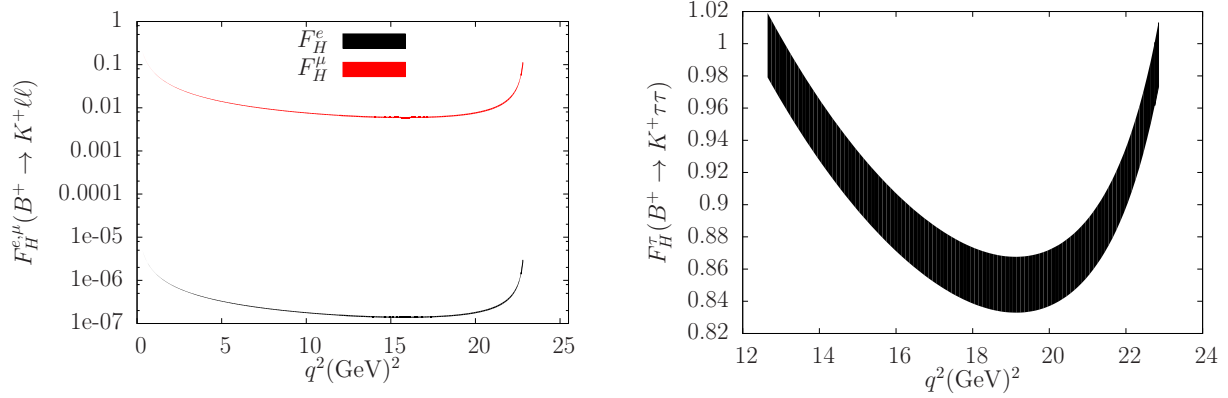


FIG. 7. Standard-Model predictions for the $B^+ \rightarrow K^+ \ell^+ \ell^-$ flat term $F_H^\ell(q^2)$ for $\ell = e, \mu$ (left) and $\ell = \tau$ (right) using the Fermilab/MILC form factors [62].

$$\Delta\mathcal{B}(B^0 \rightarrow K^0 \mu^+ \mu^-)^{\text{exp}} \times 10^9 \text{ GeV}^2 = \begin{cases} 91.6 \left({}^{+17.2}_{-15.7} \right) (4.4) & 1.1 \text{ GeV}^2 \leq q^2 \leq 6 \text{ GeV}^2, \\ 66.5 \left({}^{+11.2}_{-10.5} \right) (3.5) & 15 \text{ GeV}^2 \leq q^2 \leq 22 \text{ GeV}^2, \end{cases} \quad (4.6)$$

where the errors are statistical and systematic, respectively, and again we convert the quoted differential branching fractions to partially integrated branching fractions for direct comparison with Eqs. (4.3) and (4.4). Figure 5, right, shows the comparison between the Standard Model and the experimental measurements. The Standard-Model values are higher than the measurements by 1.8σ and 2.2σ for the low- and high- q^2 bins, respectively. The combination of the two bins, including the theoretical correlations from Tables VII and VIII of Appendix A and treating the experimental bins as uncorrelated, yields $\chi^2/\text{dof} = 5.7/2$, $p = 0.06$, thus disfavoring the Standard-Model hypothesis with 1.9σ significance. Note, however, that the structures observed in the LHCb data above the $\psi(2S)$ (red points with small errors bars in Fig. 6) warrant a great deal of caution in comparing theory and experiment for narrow bins [149].

We also calculate the Standard-Model flat term $F_H^\ell(q^2)$ with the Fermilab/MILC form factors [62] and plot it for $B^+ \rightarrow K^+ \ell^+ \ell^-$ ($\ell = e, \mu, \tau$) in Fig. 7. LHCb reported results for the binned flat term $F_H^\mu(q_{\min}^2, q_{\max}^2)$ [150] with uncertainties greater than 100% in every bin. The Standard-Model result for F_H^μ agrees with LHCb's measurement, but the comparison is limited by the large experimental errors, which will improve with new measurements after the LHCb upgrade. For future comparisons, Tables IX and X of Appendix A provide results for the binned $F_H^\ell(q_{\min}^2, q_{\max}^2)$ in both the charged and neutral decay modes, respectively.

3. Combinations of $B \rightarrow \pi$ and $B \rightarrow K$ observables

Figure 5 shows that the $B \rightarrow \pi \mu^+ \mu^-$ and $B \rightarrow K \mu^+ \mu^-$ Standard-Model partially integrated branching ratios are larger than the experimental results for all four wide q^2 bins. The four Standard-Model values are, however, highly correlated. Thus the combination of all four measurements disfavors the Standard-Model hypothesis at the 1.7σ level ($\chi^2/\text{dof} = 7.8/4$, $p = 0.10$). This significance lies in between the individual exclusions from the two $B \rightarrow \pi \mu^+ \mu^-$ bins and the two $B \rightarrow K \mu^+ \mu^-$ bins.

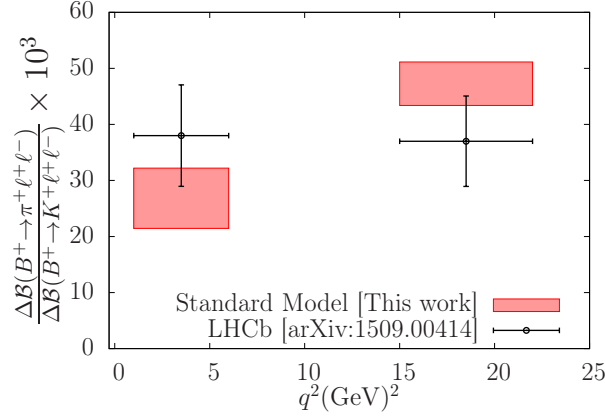


FIG. 8. Ratio of partially integrated branching ratios $\Delta\mathcal{B}(B^+ \rightarrow \pi^+ \mu^+ \mu^-)/\Delta\mathcal{B}(B^+ \rightarrow K^+ \mu^+ \mu^-)$ in the Standard Model using the Fermilab/MILC form factors [48, 62, 63], compared with experimental measurements from LHCb [55]. The errors in the Standard-Model results are dominated by the form-factor uncertainties; the others are too small to be shown separately.

The first observation of $B \rightarrow \pi \ell^+ \ell^-$ by LHCb implies that the ratio of branching fractions $\mathcal{B}(B^+ \rightarrow \pi^+ \mu^+ \mu^-)/\mathcal{B}(B^+ \rightarrow K^+ \mu^+ \mu^-) = 0.053(14)(1)$, where the errors are statistical and systematic, respectively [151]. More recently, LHCb reported first results for the partially integrated branching fractions for $B^+ \rightarrow \pi^+ \mu^+ \mu^-$ [55], and also provided the ratio of $\Delta\mathcal{B}(B^+ \rightarrow \pi^+ \mu^+ \mu^-)$ -to- $\Delta\mathcal{B}(B^+ \rightarrow K^+ \mu^+ \mu^-)$ for the same q^2 intervals above and below the charmonium resonances. This ratio probes new-physics scenarios that would affect the shape of the q^2 distribution differently for $B \rightarrow \pi \ell^+ \ell^-$ and $B \rightarrow K \ell^+ \ell^-$. On the other hand, it is not sensitive to new physics that would affect the overall $B \rightarrow \pi \ell^+ \ell^-$ and $B \rightarrow K \ell^+ \ell^-$ rates in the same way.

The ratios of partially integrated differential branching fractions in the wide high- q^2 and low- q^2 bins, using the Fermilab/MILC form factors [48, 62, 63], are our main results in this section:

$$\frac{\Delta\mathcal{B}(B^+ \rightarrow \pi^+ \mu^+ \mu^-)}{\Delta\mathcal{B}(B^+ \rightarrow K^+ \mu^+ \mu^-)}^{\text{SM}} \times 10^3 = \begin{cases} 26.8(0.8)(5.3)(0.4), & 1 \text{ GeV}^2 \leq q^2 \leq 6 \text{ GeV}^2, \\ 47.2(1.3)(3.4)(1.3), & 15 \text{ GeV}^2 \leq q^2 \leq 22 \text{ GeV}^2, \end{cases} \quad (4.7)$$

where the errors are from the CKM matrix elements, hadronic form factors, and all others added in quadrature, respectively. Binned Standard-Model values for additional q^2 intervals and for both the B^+ and B^0 decay modes are provided in Table XIII. Figure 8 compares the above Standard-Model values with recent measurements from LHCb for the same q^2 bins [55]:

$$\frac{\Delta\mathcal{B}(B^+ \rightarrow \pi^+ \mu^+ \mu^-)}{\Delta\mathcal{B}(B^+ \rightarrow K^+ \mu^+ \mu^-)}^{\text{exp}} \times 10^3 = \begin{cases} 38(9)(1), & 1 \text{ GeV}^2 \leq q^2 \leq 6 \text{ GeV}^2, \\ 37(8)(1), & 15 \text{ GeV}^2 \leq q^2 \leq 22 \text{ GeV}^2, \end{cases} \quad (4.8)$$

where the quoted errors are statistical and systematic, respectively. The Standard-Model result for each individual bin is consistent with its experimental measurement [55]—within 1.1σ —but the theory band lies below experiment for the $1 \text{ GeV}^2 \leq q^2 \leq 6 \text{ GeV}^2$ bin, while it lies above for the $15 \text{ GeV}^2 \leq q^2 \leq 22 \text{ GeV}^2$ bin. Combining the two bins, including the theoretical correlations from Tables XIV and XV, and treating the experimental bins as

uncorrelated, shows that the LHCb measurement is compatible with the Standard Model within 1.1σ ($\chi^2/\text{dof} = 2.7/2$ and $p = 0.26$). Given the present uncertainties, however, ample room remains for new-physics contributions that may be observable with improved measurements after the LHCb upgrade.

4. Lepton-universality-violating observables

Lepton-universality-violating effects may give rise to observable deviations in ratios of rare B decays to final states with different charged leptons [9, 13–18, 152–155], and would constitute a clear sign of physics beyond the Standard Model. A useful observable to look for such effects is the ratio of partially integrated decay rates to different charged-lepton final states with the same q^2 cuts [156]:

$$R_P^{\ell_1\ell_2}(q_{\min}^2, q_{\max}^2) = \frac{\int_{q_{\min}^2}^{q_{\max}^2} dq^2 d\mathcal{B}(B \rightarrow P\ell_1^+\ell_1^-)/dq^2}{\int_{q_{\min}^2}^{q_{\max}^2} dq^2 d\mathcal{B}(B \rightarrow P\ell_2^+\ell_2^-)/dq^2}, \quad (4.9)$$

where $P = \pi, K$ and $\ell_1, \ell_2 = e, \mu, \tau$. The quantities $R_{\pi}^{\mu e}$ and $R_K^{\mu e}$ are predicted to be unity in the Standard Model, up to corrections of order $(m_\ell^2/M_B^2, m_\ell^4/q^4)$ [100, 156], which are tiny for $\ell = e, \mu$. Thus any observed deviation of $R_{K(\pi)}^{\mu e}$ from unity would indicate the presence of physics beyond the Standard Model.

Measurements of R_K at e^+e^- colliders by BaBar [148] and Belle [146] are consistent with Standard-Model expectations within large experimental uncertainties of about 20–30%. The LHCb Collaboration, however, recently reported a measurement of the ratio $R_{K^+}^{\mu e}(1 \text{ GeV}^2, 6 \text{ GeV}^2) = 0.745 \left({}^{+97}_{-82} \right)$ [42] that is 2.6σ lower than Standard-Model expectations. Here we calculate lepton-universality-violating ratios in the Standard Model using the Fermilab/MILC $B \rightarrow K$ and $B \rightarrow \pi$ form factors [48, 62, 63]. Our predictions for $R_{\pi}^{\mu\ell}$ ($\ell = e, \tau$) are the first to use only *ab-initio* QCD information for the hadronic physics, while results for $R_K^{\ell_1\ell_2}$ ($\ell_1, \ell_2 = e, \mu, \tau$) were previously presented by the HPQCD Collaboration using their own lattice-QCD form-factor determinations [43].

Tables XI and XII show $R_{\pi}^{\mu\ell}$ and $R_K^{\mu\ell}$ for $\ell = e, \tau$, respectively, using the same q^2 bins employed by LHCb [55]. Figure 9 plots the difference from unity of $R_{K^+}^{\mu e}$ (left) and $R_{\pi^+}^{\mu e}$ (right) for the wide q^2 bins below and above the charmonium resonances. For the same q^2 cuts as LHCb’s measurement [42], we obtain

$$[R_{K^+}^{\mu e}(1 \text{ GeV}^2, 6 \text{ GeV}^2) - 1] \times 10^3 = 0.50(43), \quad (4.10)$$

where the error is predominantly from the form-factor uncertainties. This agrees with the earlier isospin-averaged Standard-Model value $(R_K^{\mu e} - 1) \times 10^3 = 0.74(35)$ from HPQCD for the same q^2 interval [43] with a similar error. Thus, explicit calculation with lattice QCD confirms the intuitively significant deviation between experiment and the Standard Model, observed by LHCb [42].

B. Rare $b \rightarrow q\nu\bar{\nu}$ ($q = d, s$) decay observables

Rare B decays into neutrino-pair final states have not yet been observed. The most recent bounds on $\mathcal{B}(B \rightarrow K\nu\bar{\nu})$ from Babar [157] and Belle [158] are, however, only about a factor

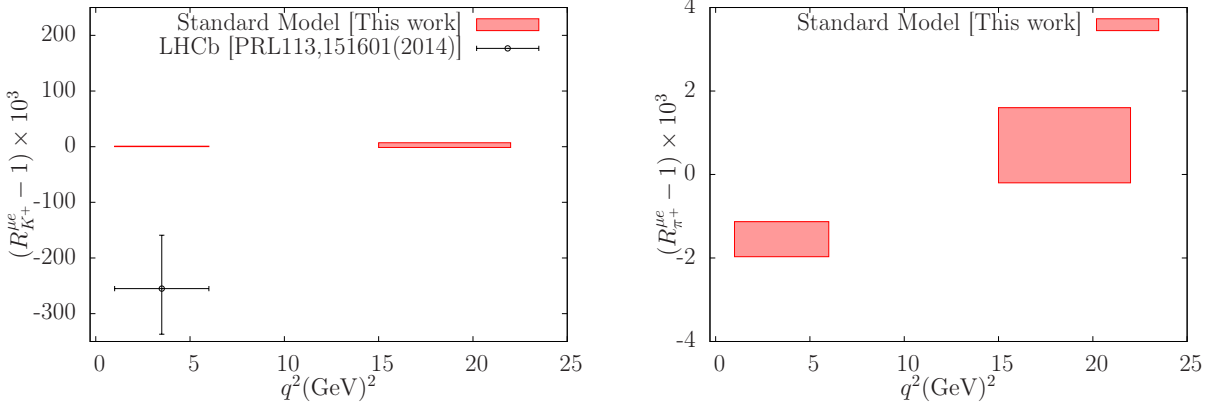


FIG. 9. Standard-Model lepton-universality-violating ratios $R_{K^+}^{\mu e} - 1$ (left) and $R_{\pi^+}^{\mu e} - 1$ (right) for $(q_{\min}^2, q_{\max}^2) = (1 \text{ GeV}^2, 6 \text{ GeV}^2)$ and $(15 \text{ GeV}^2, 22 \text{ GeV}^2)$ using the Fermilab/MILC form factors [48, 62, 63]. The errors in the Standard-Model results are dominated by the form-factor uncertainties; the remaining contributions are too small to be visible. The left plot also shows LHCb’s measurement for the low- q^2 bin [42].

of ten larger than Standard-Model expectations, so prospects are good for its observation by Belle II [57]. The Standard-Model decay rate for $B \rightarrow \pi \nu \bar{\nu}$ is further suppressed below $B \rightarrow K \nu \bar{\nu}$ by the relative CKM factor $|V_{td}/V_{ts}|^2 \approx 0.04$, except for $\mathcal{B}(B^+ \rightarrow \pi^+ \nu_\tau \bar{\nu}_\tau)$, which is enhanced by long-distance contributions. Indeed, $B^+ \rightarrow \pi^+ \nu_\tau \bar{\nu}_\tau$ events are included in measurements of the leptonic decay rate $\mathcal{B}(B^+ \rightarrow \tau^+ \nu_\tau)$, where the τ subsequently decays as $\tau \rightarrow \pi^+ \bar{\nu}_\tau$ [58–61].

In anticipation of such measurements, we provide Standard-Model predictions for $B \rightarrow K \nu \bar{\nu}$ and $B \rightarrow \pi \nu \bar{\nu}$ observables using the Fermilab/MILC form factors [48, 62]. Previous analyses of $B \rightarrow K(\pi) \nu \bar{\nu}$ used form factors from light-cone sum rules (LCSR) [83, 105] or perturbative QCD (pQCD) [159]. One recent study of $B \rightarrow K(\pi) \nu \bar{\nu}$ [18] combined lattice-QCD form factors at high q^2 [64] with LCSR form factors [160] at low q^2 in a simultaneous z -expansion fit. Our calculations of $B \rightarrow K(\pi) \nu \bar{\nu}$ observables are the first to use only *ab-initio* QCD information for the hadronic physics. Because experiments cannot identify the outgoing neutrino flavor, we present results for the sum of contributions from ν_e, ν_μ , and ν_τ .

For the neutral decay modes $B^0 \rightarrow K^0(\pi^0) \nu \bar{\nu}$, the dominant contributions to the Standard-Model decay rate are from FCNC transitions [see Eq. (2.24)]. Figure 10 shows our Standard-Model prediction for the differential branching fractions for $B^0 \rightarrow \pi^0 \nu \bar{\nu}$ and $B^0 \rightarrow K^0 \nu \bar{\nu}$. We obtain the total branching fractions

$$\mathcal{B}(B^0 \rightarrow \pi^0 \nu \bar{\nu}) \times 10^7 = 0.668(41)(49)(16), \quad (4.11)$$

$$\mathcal{B}(B^0 \rightarrow K^0 \nu \bar{\nu}) \times 10^7 = 40.1(2.2)(4.3)(0.9), \quad (4.12)$$

where the errors are from the CKM elements, form factors, and the quadrature sum of all other contributions, respectively. The “other” errors in Eqs. (4.11) and (4.12) are so much smaller than those from the CKM elements and form factors because $u\bar{u}$ and $c\bar{c}$ resonances do not contribute to the rate in Eq. (2.2), and because the perturbative contributions lumped into X_t are known to about a percent.

For the charged decay modes $B^+ \rightarrow K^+(\pi^+) \nu \bar{\nu}$, we obtain the following contributions to

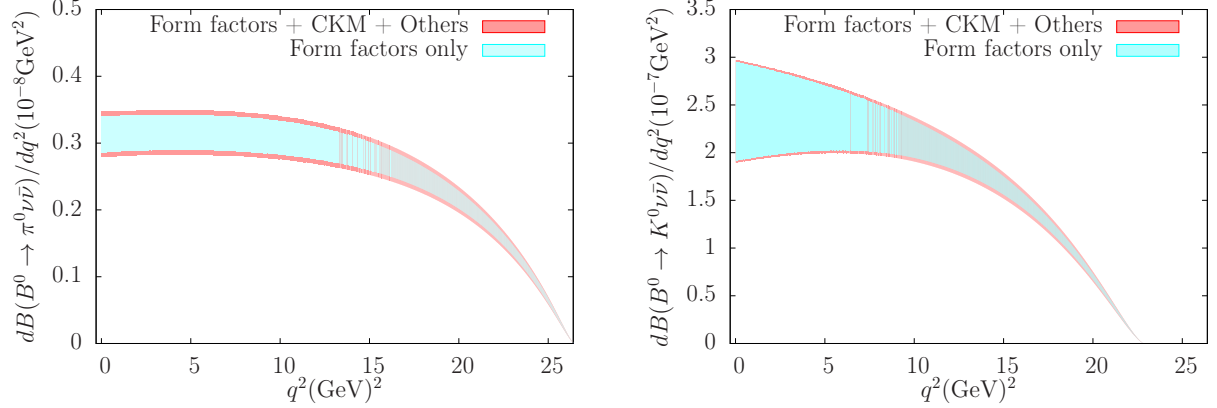


FIG. 10. Standard-Model differential branching fraction for $B^0 \rightarrow \pi^0 \nu \bar{\nu}$ decay (left) and $B^0 \rightarrow K^0 \nu \bar{\nu}$ (right) using the Fermilab/MILC form factors [48, 62].

the Standard-Model branching fractions from FCNC transitions:

$$\mathcal{B}(B^+ \rightarrow \pi^+ \nu \bar{\nu})_{\text{SD}} \times 10^7 = 1.456(89)(106)(34), \quad (4.13)$$

$$\mathcal{B}(B^+ \rightarrow K^+ \nu \bar{\nu})_{\text{SD}} \times 10^7 = 43.2(2.3)(4.6)(1.0), \quad (4.14)$$

where again the errors are from the CKM elements, form factors, and the quadrature sum of all other contributions. Our result for $\mathcal{B}(B^+ \rightarrow K^+ \nu \bar{\nu})_{\text{SD}}$ is consistent with that in Ref. [18], albeit with a slightly larger error. The smaller error in Ref. [18] stems from their use of an additional input at low- q^2 from LCSR [160]. The results quoted in Ref. [159] for the total $B \rightarrow K(\pi) \nu \bar{\nu}$ branching fractions for both the charged and neutral modes agree with ours, but they have significantly larger errors.

As discussed in Sec. II C, the decay rates for $B^+ \rightarrow K^+(\pi^+) \nu_\tau \bar{\nu}_\tau$ also receive substantial long-distance contributions from intermediate tree-level τ decays. The numerical values for the long-distance contributions are given in Eqs. (2.26) and (2.27). We add them to the short-distance contributions in Eqs. (4.13) and (4.14) to obtain the full branching ratios:

$$\mathcal{B}(B^+ \rightarrow \pi^+ \nu \bar{\nu}) \times 10^6 = 9.62(1)(92), \quad (4.15)$$

$$\mathcal{B}(B^+ \rightarrow K^+ \nu \bar{\nu}) \times 10^6 = 4.94(52)(6), \quad (4.16)$$

where here the errors are from the short-distance and long-distance contributions respectively. For $B^+ \rightarrow \pi^+ \nu \bar{\nu}$, the intermediate τ -decay channel increases the Standard-Model rate by an order of magnitude, whereas for $B^+ \rightarrow K^+ \nu \bar{\nu}$ it only generates about a 10% enhancement.

C. Tree-level $b \rightarrow u \ell \nu$ decay observables

The decay $B \rightarrow \pi \tau \nu$ has not yet been observed experimentally. Recently, however, the Belle Collaboration reported their first search for $B^0 \rightarrow \pi^- \tau^+ \nu_\tau$ decay [56], obtaining a result for the total branching fraction with a 2.4σ significance, corresponding to an upper limit not far from the Standard-Model prediction. The upcoming Belle II experiment is therefore well positioned to measure the branching fraction as well as the q^2 spectrum for this process.

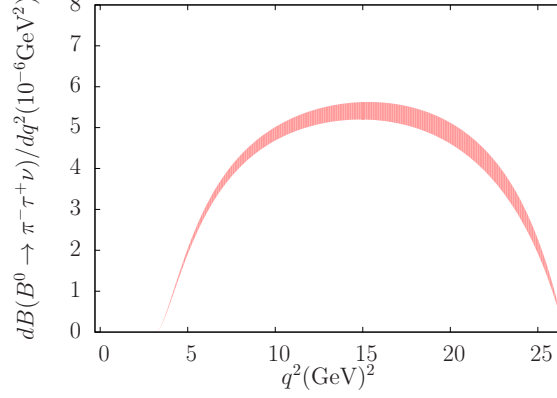


FIG. 11. Standard-Model differential branching fraction for $B^0 \rightarrow \pi^- \tau^+ \nu_\tau$ decay using the Fermilab/MILC form factors and determination of $|V_{ub}|$ from Ref. [48].

Most previous Standard-Model predictions for $B \rightarrow \pi \tau \nu$ have relied on estimates of the hadronic form factors from LCSR [161–163] or pQCD [159]. Reference [164] employs form factors from lattice QCD [65, 142]. The scalar form factor, however, was calculated only in Ref. [142], and disagrees with more recent continuum-limit results [48, 66]. Because the total uncertainty on $\mathcal{B}(B \rightarrow \pi \tau \nu)$ in Ref. [164] is dominated by the error on the scalar form factor, it is now possible to improve the Standard-Model estimate. Here we use the form factors and value of $|V_{ub}|$, $3.72(16) \times 10^{-3}$, from Fermilab/MILC [48], obtained from a simultaneous z -expansion fit of lattice-QCD results and the measured $B \rightarrow \pi \ell \nu$ partial branching fractions. These form factors and $|V_{ub}|$ carry significant correlations, which we incorporate below. We reiterate that with this choice of inputs we assume that there are no significant new-physics contributions to $B \rightarrow \pi \ell \nu$ decays with light charged leptons.

Figure 11 shows our Standard-Model prediction for the $B^0 \rightarrow \pi^- \tau^+ \nu_\tau$ differential branching fraction. For the total integrated branching fractions we find

$$\mathcal{B}(B^0 \rightarrow \pi^- \tau^+ \nu_\tau) = 9.35(38) \times 10^{-5}, \quad (4.17)$$

$$\mathcal{B}(B^+ \rightarrow \pi^0 \tau^+ \nu_\tau) = 4.99(20) \times 10^{-5}, \quad (4.18)$$

where the error includes the correlated uncertainties from the form factors and $|V_{ub}|$. Because of the correlations between the form factors and $|V_{ub}|$, it is not possible to quote their errors individually. The uncertainties stemming from the parametric inputs are negligible. Our results are consistent with those quoted in Refs. [159, 162] within their much larger uncertainties. Because the Standard-Model branching fraction for $B \rightarrow \pi \tau \nu$ is of the same order of magnitude as for $B \rightarrow \pi \mu \nu$, the Belle II experiment should be in a good position to test our prediction of its differential decay rate.

Deviations from Standard-Model expectations have been observed for semileptonic B -meson decays to $\tau \nu_\tau$ final states involving tree-level $b \rightarrow c$ charged-current interactions. Given the combined 3.9σ excess quoted by HFAG for their averages of $R(D)$ and $R(D^*)$ [41], it is interesting to consider the analogous ratio for $B \rightarrow \pi \ell \nu$ decay, which instead proceeds through a tree-level $b \rightarrow u$ transition. Assuming, again, that there are no new-physics contributions to decays to light charged leptons, $B \rightarrow \pi \ell \nu$ with $\ell = e, \mu$, the Fermilab/MILC

form factors [48] yield the Standard-Model prediction

$$R(\pi) \equiv \frac{\mathcal{B}(B \rightarrow \pi\tau\nu_\tau)}{\mathcal{B}(B \rightarrow \pi\ell\nu_\ell)} = 0.641(17), \quad (4.19)$$

for both the charged and neutral B -meson decay modes. Because $|V_{ub}|$ cancels in the ratio, $R(\pi)$ provides an especially clean probe of new physics, particularly charged Higgs bosons, independent of the currently observed tension between determinations of $|V_{ub}|$ from inclusive and exclusive semileptonic B -meson decays [41, 136, 165].

V. CKM MATRIX ELEMENTS AND WILSON COEFFICIENTS

We now illustrate the broader utility of the Fermilab/MILC form factors [48, 62, 63] for Standard-Model and beyond-the-Standard-Model phenomenology with two concrete examples. First, in Sec. V A, starting with the assumption that the Standard Model is a complete description of Nature, we combine our predicted branching fractions with the recent LHCb measurements to determine the CKM matrix elements $|V_{td}|$, $|V_{ts}|$, and their ratio. We then compare them with results from other processes. Second, in Sec. V B, we make no such assumption but take the CKM matrix elements from unitarity and combine our theoretical branching fractions with the experimental measurements to constrain the Wilson coefficients of the $b \rightarrow q\ell\ell$ ($q = d, s$) effective Hamiltonian. We then compare them with Standard-Model values.

These analyses are possible because, as stressed above, the $B \rightarrow \pi$ and $B \rightarrow K$ form factors are decoupled, via the effective Hamiltonian, from physics at energy scales above the electroweak scale.

A. Constraints on V_{ts} , V_{td} , and $|V_{td}/V_{ts}|$

In the Standard Model, the ratios of differential branching fractions

$$\frac{\Delta\mathcal{B}(B \rightarrow \pi\ell^+\ell^-)}{\Delta\mathcal{B}(B \rightarrow K\ell^+\ell^-)} \quad \text{and} \quad \frac{\Delta\mathcal{B}(B \rightarrow \pi\nu\bar{\nu})}{\Delta\mathcal{B}(B \rightarrow K\nu\bar{\nu})}$$

are both proportional to the ratio of CKM matrix elements $|V_{td}/V_{ts}|^2$. Thus, they enable determinations of $|V_{td}/V_{ts}|$, independent of that from the ratio of B_d -to- B_s -meson oscillation frequencies [136], which is currently the most precise.

The LHCb experiment's initial observation of $B \rightarrow \pi\mu^+\mu^-$ [151] enabled the first determination of this ratio of CKM matrix elements from rare semileptonic B decays. In that work, they obtained $|V_{td}/V_{ts}| = 0.266(35)$ using form factors from light-cone sum rules [166] and neglecting the theoretical uncertainty. More recently, LHCb measured the differential decay rate for $B \rightarrow \pi\mu^+\mu^-$ and the ratio $\Delta\mathcal{B}(B \rightarrow \pi\mu^+\mu^-)/\Delta\mathcal{B}(B \rightarrow K\mu^+\mu^-)$ in two bins of q^2 below and above the charmonium resonances [55]. Although the measurement errors decreased, the quoted error in $|V_{td}/V_{ts}| = 0.23(^{+5}_{-4})$ increased from including now the theory uncertainty. Here we obtain the first determination of $|V_{td}/V_{ts}|$ from rare $b \rightarrow d(s)\ell^+\ell^-$ decay processes using only *ab-initio* lattice-QCD information for the hadronic form factors.

Following Refs. [122, 151] we calculate

$$F^{\pi/K} \equiv \left| \frac{V_{ts}}{V_{td}} \right|^2 \frac{\Delta\mathcal{B}(B^+ \rightarrow \pi^+\mu^+\mu^-)}{\Delta\mathcal{B}(B^+ \rightarrow K^+\mu^+\mu^-)}, \quad (5.1)$$

which removes the CKM matrix elements. Taking Eq. (4.7) for the second factor in Eq. (5.1) and removing the CKM ratio used there (from Table XVII), we obtain

$$F^{\pi/K} = \begin{cases} 0.60(12), & 1 \text{ GeV}^2 \leq q^2 \leq 6 \text{ GeV}^2 \\ 1.055(81), & 15 \text{ GeV}^2 \leq q^2 \leq 22 \text{ GeV}^2 \end{cases}, \quad (5.2)$$

where the errors stem predominantly from the form-factor uncertainties. Combining this Standard-Model calculation of $F^{\pi/K}$ with LHCb's recent measurement [55], Eq. (4.8), yields

$$|V_{td}/V_{ts}| = \begin{cases} 0.252(25)(30), & 1 \text{ GeV}^2 \leq q^2 \leq 6 \text{ GeV}^2 \\ 0.187(7)(20), & 15 \text{ GeV}^2 \leq q^2 \leq 22 \text{ GeV}^2 \end{cases}, \quad (5.3)$$

where the errors are from theory and experiment, respectively. A joint fit over both bins including theoretical correlations (which in practice are negligible) yields our final result for the ratio of CKM matrix elements:

$$|V_{td}/V_{ts}| = 0.201(20), \quad (5.4)$$

where the error includes both experimental and theoretical uncertainties, and the combined $\chi^2/\text{dof} = 2.3/1$ ($p = 0.13$). Equation (5.4) agrees with the more precise determination from the oscillation frequencies of neutral $B_{d,s}$ mesons, $|V_{td}/V_{ts}| = 0.216(1)(11)$, as well as that from CKM unitarity, $|V_{td}/V_{ts}| = 0.2115(30)$ [167].

The error on $|V_{td}/V_{ts}|$ in Eq. (5.4) is more than two times smaller than that obtained by LHCb in Ref. [55] using the same experimental information. This improvement stems entirely from the more precise form factors. Because the error on $|V_{td}/V_{ts}|$ in Eq. (5.4) is dominated by the experimental uncertainty, especially for the high- q^2 bin, it will be reduced as measurements of $B \rightarrow K(\pi)\ell^+\ell^-$ decays improve. Better form-factor calculations will also aid the determination of $|V_{td}/V_{ts}|$ from the low- q^2 region. Future observations of $B \rightarrow K(\pi)\nu\bar{\nu}$ in combination with our Standard-Model predictions in Sec. II C will enable yet another way to determine $|V_{td}/V_{ts}|$.

We can also determine the products of CKM elements $|V_{tb}V_{td}^*|$ and $|V_{tb}V_{ts}^*|$ that appear in the individual decay rates for $B \rightarrow \pi\ell^+\ell^-$ and $B \rightarrow K\ell^+\ell^-$ decay, respectively. In analogy with the analysis above, we combine our calculations of the CKM-independent quantities $\Delta\mathcal{B}(B^+ \rightarrow \pi^+\mu^+\mu^-)/|V_{tb}V_{td}^*|^2$ and $\Delta\mathcal{B}(B^+ \rightarrow K^+\mu^+\mu^-)/|V_{tb}V_{ts}^*|^2$ with experimental measurements of the partial branching fractions for the same q^2 intervals. Using the $B \rightarrow \pi\mu^+\mu^-$ partial branching fractions measured by LHCb [55], and quoted in Eq. (4.2), we obtain

$$|V_{tb}V_{td}^*| \times 10^3 = \begin{cases} 8.34(49)(95), & 1 \text{ GeV}^2 \leq q^2 \leq 6 \text{ GeV}^2, \\ 6.90(26)(81), & 15 \text{ GeV}^2 \leq q^2 \leq 22 \text{ GeV}^2. \end{cases} \quad (5.5)$$

Similarly, using the $B \rightarrow K\mu^+\mu^-$ measurement from Ref. [45], quoted in Eq. (4.5), we obtain

$$|V_{tb}V_{ts}^*| \times 10^3 = \begin{cases} 33.3(2.8)(1.0), & 1.1 \text{ GeV}^2 \leq q^2 \leq 6 \text{ GeV}^2, \\ 36.0(1.1)(1.1), & 15 \text{ GeV}^2 \leq q^2 \leq 22 \text{ GeV}^2. \end{cases} \quad (5.6)$$

The errors given in Eqs. (5.5) and (5.6) are from theory and experiment, respectively. Combining the values from the individual q^2 bins above including correlations gives

$$|V_{tb}V_{td}^*| \times 10^3 = 7.45(69), \quad (5.7)$$

$$|V_{tb}V_{ts}^*| \times 10^3 = 35.7(15), \quad (5.8)$$

for our final results, where the errors include both the experimental and theoretical uncertainties.

Taking $|V_{tb}| = 0.9991$ from CKM unitarity [167], where the error is of order 10^{-5} and hence negligible, we can infer values for the magnitudes of the individual CKM elements $|V_{td}|$ and $|V_{ts}|$. We find

$$|V_{td}| = 7.45(69) \times 10^{-3}, \quad (5.9)$$

$$|V_{ts}| = 35.7(1.5) \times 10^{-3}, \quad (5.10)$$

where the errors include both the experimental and theoretical uncertainties. This determination of $|V_{td}|$ agrees with the Particle Data Group (PDG) value $|V_{td}| = 8.4(6) \times 10^{-3}$ [136] obtained from the oscillation frequency of neutral B_d mesons, with commensurate precision. Our $|V_{ts}|$ is 1.4σ lower than $|V_{ts}| = 40.0(2.7) \times 10^{-3}$ from B_s -meson oscillations with an error that is almost two times smaller. Compared with the determinations $|V_{td}| = 7.2^{(+9)}_{(-8)} \times 10^{-3}$ and $|V_{ts}| = 32(4) \times 10^{-3}$ by LHCb [55]—using the same experimental inputs but older form factors—the uncertainties in Eqs. (5.9) and (5.10) are 1.2 and 2.7 times smaller, respectively. Again, this illustrates the value added from using the more precise hadronic form factors. It is worth noting that the errors on the B -mixing results [136] are dominated by the uncertainties on the corresponding hadronic matrix elements [168, 169]. Therefore the errors on $|V_{td}|$ and $|V_{ts}|$ from both neutral B -meson oscillations and semileptonic B decays will decrease with anticipated lattice-QCD improvements (see Refs. [170, 171] and our discussion in Sec. VII).

Finally, assuming CKM unitarity, our result for $|V_{ts}|$ implies a value for $|V_{cb}|$ via $|V_{cb}| = |V_{ts}| = A\lambda^2 + O(\lambda^4)$, where the explicit expression for the correction can be found in Ref. [167]. Taking numerical values for $\{A, \lambda, \bar{\rho}, \bar{\eta}\}$ from Table XVII to estimate the correction term, we obtain $|V_{cb}| = 36.5(1.5) \times 10^{-3}$, where the error stems from the uncertainty in $|V_{ts}|$ in Eq. (5.9) and the parametric uncertainty due to higher-order corrections in λ is negligible. This alternate result for $|V_{cb}|$ is 1.6σ below the exclusive $|V_{cb}|$ determination from $B \rightarrow D^*\ell\nu$ [172], 2.6σ below that from $B \rightarrow D\ell\nu$ [53], and 3.5σ below the inclusive $|V_{cb}|$ determination [54]. This tension is simply another perspective on the differences we found between the experimental measurements for the $B \rightarrow K\mu^+\mu^-$ partially integrated branching fractions and our Standard-Model predictions, discussed in Sec. IV A 2.

B. Constraints on Wilson coefficients

In this section, we investigate the constraints on the Wilson coefficients of the effective Hamiltonian implied by present $B \rightarrow (K, \pi)\mu^+\mu^-$ measurements combined with the Fermilab/MILC form factors [48, 62, 63]. We focus on high-scale ($\mu_0 \simeq 120$ GeV) contributions to the Wilson coefficients C_9 and C_{10} :

$$C_9(\mu_0) = C_9^{\text{SM}}(\mu_0) + C_9^{\text{NP}}(\mu_0), \quad (5.11)$$

$$C_{10}(\mu_0) = C_{10}^{\text{SM}}(\mu_0) + C_{10}^{\text{NP}}(\mu_0), \quad (5.12)$$

where the Standard-Model matching conditions are given in Eqs. (25) and (26) of Ref. [82] and, for our choice of inputs, correspond to $C_9^{\text{SM}}(\mu_0) = 1.614$ and $C_{10}^{\text{SM}}(\mu_0) = -4.255$. The excellent agreement between the experimental and theoretical determinations of $B \rightarrow X_s\gamma$ (see, for instance, Ref. [173] and references therein) suggests that any new-physics contributions to C_7 and C_8 are small, so we do not consider them here. We also assume that

the Wilson coefficients for $b \rightarrow s\ell\ell$ and $b \rightarrow d\ell\ell$ transitions are identical, as they would be in minimal flavor violation, where new-physics contributions to the semileptonic operators for $b \rightarrow q\ell\ell$ are proportional to $V_{tb}V_{tq}^*$. We further assume that there are no new CP -violating phases and take $C_9^{\text{NP}}(\mu_0)$ and $C_{10}^{\text{NP}}(\mu_0)$ to be real.

To obtain the constraints shown here, we employ the measured $B^+ \rightarrow \pi^+\mu^+\mu^-$ and $B^+ \rightarrow K^+\mu^+\mu^-$ branching ratios in the wide q^2 intervals $[1(1.1), 6]$ GeV^2 and $[15, 22]$ GeV^2 from LHCb [45, 55], which are quoted in Eqs. (4.2) and (4.5). We adopt a frequentist approach, and construct a χ^2 statistic for these four measurements using a covariance matrix constructed from the correlation matrices given in Tables VII and VIII, and from the errors quoted in Table IV of Ref. [63] and in Table V. We obtain the experimental contribution to the covariance matrix by assuming that the four LHCb measurements in Eqs. (4.2) and (4.5) are uncorrelated, which should be a good approximation because the high- and low- q^2 bins are statistically independent, and the $B^+ \rightarrow \pi^+\mu^+\mu^-$ measurement is dominated by statistical errors, while that for $B^+ \rightarrow K^+\mu^+\mu^-$ is limited by systematics.

The resulting allowed regions in the $\text{Re}(C_9^{\text{NP}})$ - $\text{Re}(C_{10}^{\text{NP}})$ plane are shown in Fig. 12. In the top two panels we present the 1σ constraints from $B^+ \rightarrow K^+\mu^+\mu^-$ (left) and $B^+ \rightarrow \pi^+\mu^+\mu^-$ (right), where we show the allowed regions implied by each of the two bins separately (unfilled bands) as well as their combination (solid bands). The lower left panel shows the constraint from combining $B^+ \rightarrow K^+\mu^+\mu^-$ and $B^+ \rightarrow \pi^+\mu^+\mu^-$ branching ratios. Comparing the top and bottom left panels, we see that the combined $B \rightarrow (K, \pi)\mu^+\mu^-$ constraint is currently controlled by the high- q^2 $B^+ \rightarrow K^+\mu^+\mu^-$ $[15, 22]$ GeV^2 bin. In the lower right panel, the orange and yellow solid bands are the 1σ and 2σ regions allowed by $B \rightarrow (K, \pi)\mu^+\mu^-$ data. Allowing for new-physics contributions to C_9 and C_{10} yields a best fit with $\chi^2_{\text{min}}/\text{dof} = 1.8/2$, corresponding to $p = 0.41$. We find a 2.0σ tension between the Standard-Model values for $C_9^{\text{NP}} = C_{10}^{\text{NP}} = 0$ and those favored by the $B \rightarrow (K, \pi)\mu^+\mu^-$ branching ratios.

In the lower right panel of Fig. 12, we compare our allowed region in the $\text{Re}(C_9^{\text{NP}})$ - $\text{Re}(C_{10}^{\text{NP}})$ plane obtained from $B \rightarrow (K, \pi)\mu^+\mu^-$ branching fractions alone with the constraints from inclusive $B \rightarrow X_s\ell^+\ell^-$ and exclusive $B \rightarrow K^*\mu^+\mu^-$ measurements. The region favored by inclusive observables (black contours) is taken from Ref. [174], where the most recent experimental results from BaBar [175, 176] and Belle [177] were used. Similarly, the region favored by $B \rightarrow K^*\mu^+\mu^-$ angular observables (red contours) is taken from Ref. [36]. Global analyses of $b \rightarrow s$ data similar to that performed in Ref. [36] have also been presented in Refs. [9, 152, 178–186].

In Fig. 13 we add the constraint from the leptonic decay rate $\mathcal{B}(B_s \rightarrow \mu^+\mu^-)$, for which lattice QCD also gives a reliable input for the hadronic matrix element f_{B_s} [108–112, 187]. The expression for the Standard-Model rate is given in Eqs. (3) and (6) of Ref. [188], and is proportional to $f_{B_s}^2$ and to the CKM combination $|V_{tb}V_{ts}^*|^2$. For f_{B_s} we use the recent PDG value $f_{B_s} = 226.0(2.2)$ GeV [107], which was obtained by averaging the lattice QCD results of Refs. [108, 110, 112, 113, 187]. We take the remaining parametric inputs from Table XVII to obtain the Standard-Model total branching ratio

$$\mathcal{B}(B_s \rightarrow \mu^+\mu^-)^{\text{SM}} = 3.39(18)(7)(8) \times 10^{-9}, \quad (5.13)$$

where the errors are from the CKM elements, decay constant, and the quadrature sum of all other contributions, respectively. We take the nonparametric uncertainties to be 1.5% [188].

In the most general Standard-Model extension, new-physics contributions to $B_s \rightarrow \mu^+\mu^-$ decay can arise from six operators in the effective Hamiltonian: in addition to Q_{10} , there are operators with lepton currents $\bar{\ell}\ell$ and $\bar{\ell}\gamma_5\ell$, and three additional operators obtained

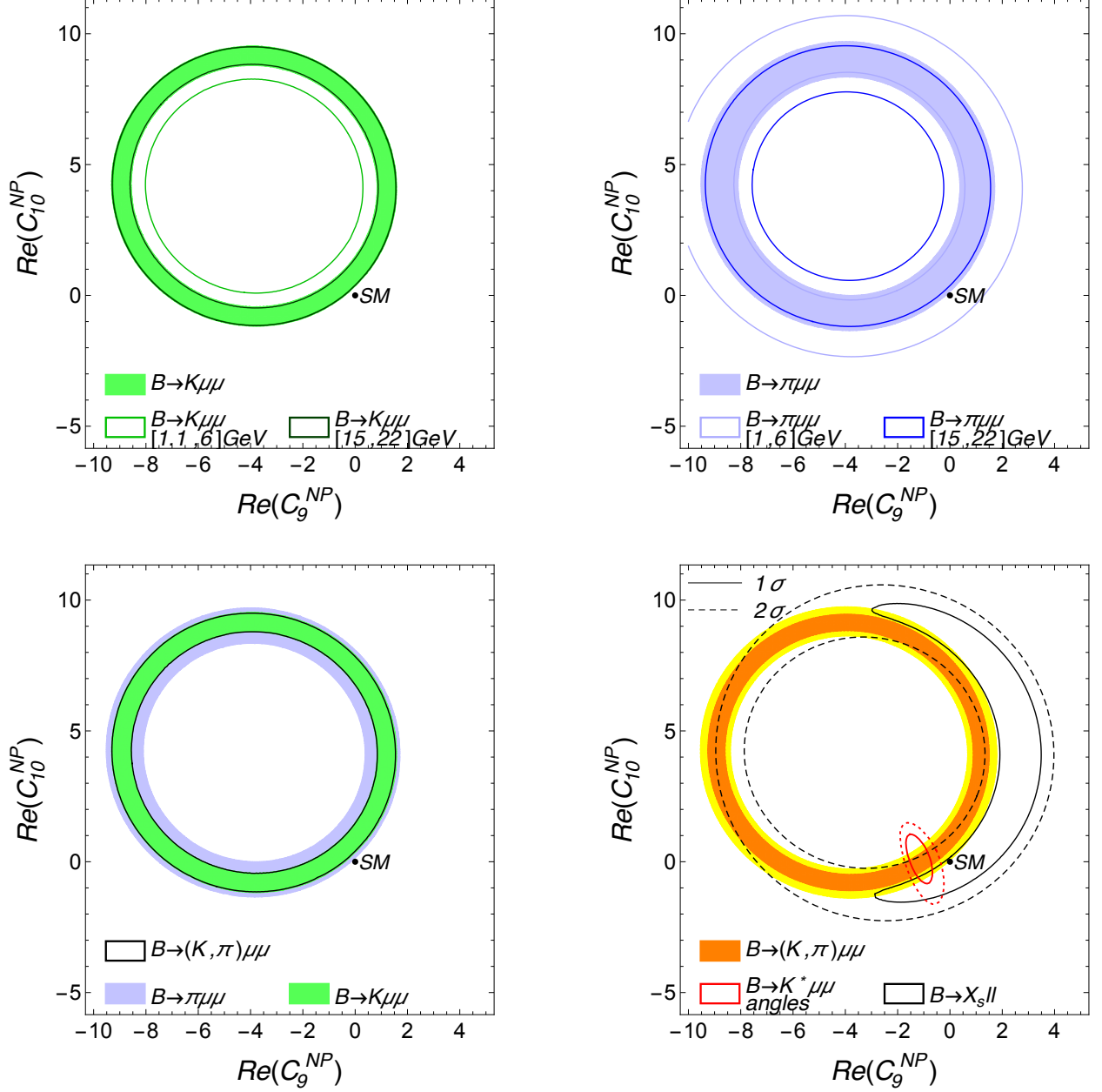


FIG. 12. Constraints on the $\text{Re}(C_9^{\text{NP}})$ - $\text{Re}(C_{10}^{\text{NP}})$ plane implied by $B \rightarrow (K, \pi) \mu^+ \mu^-$ data. In the top two panels, the light and dark unfilled bands show the 1σ constraints from the low- q^2 ($[1(1.1), 6] \text{ GeV}^2$) and high- q^2 ($[15, 22] \text{ GeV}^2$) bins, respectively, for $B^+ \rightarrow K^+ \mu^+ \mu^-$ (left) and $B^+ \rightarrow \pi^+ \mu^+ \mu^-$ (right). The filled bands show the 1σ allowed regions when the two bins are combined. Note that the outer low- and high- q^2 $B \rightarrow K$ contours almost completely overlap. The lower left panel shows these two 1σ regions with an unfilled band obtained from combining the two constraints (almost coincident with the filled $B \rightarrow K \ell^+ \ell^-$ band). The lower right panel compares the 1σ and 2σ bands [in orange (gray) and yellow (light gray), respectively] from the $B \rightarrow (K, \pi) \mu^+ \mu^-$ data with the constraints from $B \rightarrow K^* \ell \ell$ angular observables (red unfilled contours, dotted for 2σ) [36] and inclusive processes (black open contours, dashed for 2σ) [174].

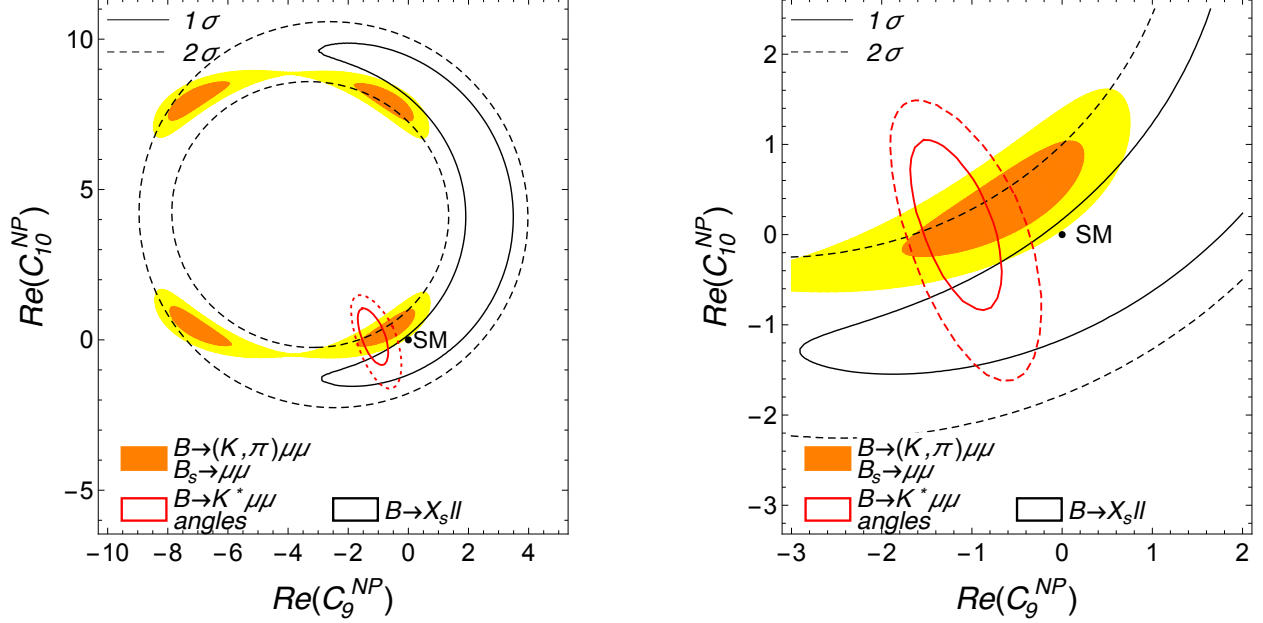


FIG. 13. Constraints on the $\text{Re}(C_9^{\text{NP}})$ - $\text{Re}(C_{10}^{\text{NP}})$ plane implied by $B \rightarrow (K, \pi)\mu^+\mu^-$ and $B_s \rightarrow \mu^+\mu^-$ data. The right panel shows the same contours as the left panel, but focuses on the region near the Standard-Model value. The color and styling is the same as in Fig. 12 (lower right).

by flipping the chirality of the quark current [189]. In order to combine information from $B_s \rightarrow \mu^+\mu^-$ with the constraints on the Wilson coefficients C_9 and C_{10} from $B \rightarrow K(\pi)\mu^+\mu^-$ branching ratios presented above, we assume that only C_{10} is affected by new physics. Under this assumption, the $B_s \rightarrow \mu^+\mu^-$ rate is proportional to $|C_{10}|^2$, so its inclusion reduces constraint from a ring to a smaller, roughly elliptical, region. Taking the measured branching ratio $\mathcal{B}(B_s \rightarrow \mu^+\mu^-)^{\text{exp}} = 2.8^{+0.7}_{-0.6} \times 10^{-9}$ from CMS and LHCb [190], we obtain the yellow and orange shaded bands in Fig. 13. As shown in the left panel, at the 1σ level there are four distinct allowed regions in the $\text{Re}(C_9^{\text{NP}})$ - $\text{Re}(C_{10}^{\text{NP}})$ plane, which merge into two larger nearly horizontal bands at 2σ . The lower-right orange contour is close to the Standard-Model value, and we zoom in on this region in Fig. 13, right. The region allowed by $B \rightarrow K(\pi)\mu^+\mu^-$ and $B_s \rightarrow \mu^+\mu^-$ branching ratios is compatible with the constraint from $B \rightarrow K^*\mu^+\mu^-$ angular observables, but is in slight tension with the constraint from inclusive $B \rightarrow X_s \ell^+\ell^-$ decays. Because the Standard-Model $B_s \rightarrow \mu^+\mu^-$ total branching ratio is compatible with experiment, including this information slightly decreases the tension between the Standard-Model prediction and experimental measurements of $B \rightarrow (K, \pi)\mu\mu$ branching ratios. The compatibility with the Standard-Model hypothesis increases from $p = 0.10$ to $p = 0.13$, and the significance of the tension decreases from 1.7σ to 1.5σ . Allowing for new physics in C_9 and C_{10} yields a best fit with $\chi^2_{\text{min}}/\text{dof} = 1.8/3$, corresponding to $p = 0.61$, and values of $\text{Re}(C_9^{\text{NP}})$ and $\text{Re}(C_{10}^{\text{NP}})$ that differ by 2.1σ from the Standard Model.

Because the constraints from $B \rightarrow \pi(K)\mu^+\mu^-$ branching ratios on the $\text{Re}(C_9^{\text{NP}})$ - $\text{Re}(C_{10}^{\text{NP}})$ plane are limited by the experimental uncertainties, the widths of the corresponding bands in Figs. 12 and 13 will be reduced with new measurements by LHCb from the recently started LHC run and by the upcoming Belle II experiment. Therefore, these decays will continue to squeeze the allowed region in the $\text{Re}(C_9^{\text{NP}})$ - $\text{Re}(C_{10}^{\text{NP}})$ plane.

VI. SUMMARY OF MAIN RESULTS

We now summarize our main results to help the reader digest the large quantity of information presented in the previous two sections. We present them in the same order in which they appeared above.

We begin with tests of heavy-quark and $SU(3)$ symmetries. By and large, the results given in Sec. III show marginal-to-excellent agreement with the symmetry limits, but the sizable q^2 dependence we observe is an obstacle to providing a simple rule of thumb.

Our findings for the Standard-Model observables for decays with a charged-lepton pair in the final state, $B \rightarrow K(\pi)\ell^+\ell^-$ with $\ell = e, \mu, \tau$ are more interesting. Here, the most reliable results are those for the wide q^2 regions above and below the charmonium resonances. For decays with a muon pair, we compare our results for the partially integrated branching fractions with the latest experimental measurements from the LHCb experiment [45, 55]. For the wide q^2 bins below and above the charmonium resonances, we find that the Standard-Model expectations for both $\Delta\mathcal{B}(B \rightarrow \pi\mu^+\mu^-)$ and $\Delta\mathcal{B}(B \rightarrow K\mu^+\mu^-)$ are in slight tension with the experimental measurements (see Fig. 5), with the Standard-Model values being 1–2 σ higher. The Standard-Model expectations for the ratio $\Delta\mathcal{B}(B \rightarrow \pi\mu^+\mu^-)/\Delta\mathcal{B}(B \rightarrow K\mu^+\mu^-)$ are compatible with experiment, however, within 1.1 σ (see Fig. 8). We also provide Standard-Model values for the flat terms and lepton-universality-violating ratios for all lepton final states $\ell = e, \mu, \tau$. We confirm the 2.6 σ discrepancy observed for $R_{K^+}^{\mu e}$ by LHCb [42]. Semileptonic B decays with τ pairs in the final state have yet to be observed, so our results for the associated observables are theoretical predictions that will be tested by experiment.

For decays with a neutrino pair in the final state, $B \rightarrow K(\pi)\nu\bar{\nu}$, we provide Standard-Model predictions for the total branching fractions. We do not present partially integrated branching fractions because there are not yet experimental measurements of these processes to guide our choice of q^2 intervals. Like $B \rightarrow K(\pi)\ell^+\ell^-$, these processes involve a $b \rightarrow d(s)$ FCNC transition, and thus probe some of the same underlying physics. The decay rates for $B \rightarrow K(\pi)\nu\bar{\nu}$, however, depend on only a single operator in the Standard-Model effective Hamiltonian. Hence, once measured, they will provide complementary information. Moreover, the $B \rightarrow K(\pi)\nu\bar{\nu}$ decay rates do not receive contributions from $u\bar{u}, c\bar{c}$ resonances or nonfactorizable terms, making the theoretical predictions particularly clean. Because the current bounds on $\mathcal{B}(B \rightarrow K\nu\bar{\nu})$ from Babar [157] and Belle [158] are only about a factor of ten larger than Standard-Model expectations, one may anticipate that this process will be observed by the forthcoming Belle II experiment [57]. Once experimental analyses of the $B \rightarrow K(\pi)\nu\bar{\nu}$ differential decay rates have settled on bin sizes, we can provide predictions for the partially integrated branching fractions matched to the q^2 bins employed.

We also predict the total branching ratio for the tree-level decay $B \rightarrow \pi\tau\nu$. Although this is not a FCNC process, the large τ -lepton mass makes this process sensitive to contributions from charged Higgs or other scalar bosons. The ratio of the decay rate for $B \rightarrow \pi\tau\nu$ over the decay rate for $B \rightarrow \pi\ell\nu$ ($\ell = e, \mu$) is of particular interest given the combined 3.9 σ deviation from the Standard Model for the analogous ratios for $B \rightarrow D\ell\nu$ and $B \rightarrow D^*\ell\nu$ semileptonic decays [41]. We obtain

$$R(\pi) \equiv \frac{\mathcal{B}(B \rightarrow \pi\tau\nu_\tau)}{\mathcal{B}(B \rightarrow \pi\ell\nu_\ell)} = 0.641(17), \quad (6.1)$$

where the error quoted includes statistical and systematic uncertainties. Because the CKM element $|V_{ub}|$ cancels in the ratio, $R(\pi)$ provides an especially clean test of the Standard

Model independent of the tension between inclusive and exclusive determinations [4, 41, 136, 165, 191]. The Belle experiment recently presented a preliminary 2.4σ measurement of the $B^0 \rightarrow \pi^- \tau^+ \nu_\tau$ total branching fraction, setting an upper limit only about five times greater than the Standard Model prediction, so Belle II may be able to measure not only the total branching fraction but also the q^2 spectrum for this process [57]. Again, we can provide partially integrated branching ratios corresponding to the bins used in future experimental analyses once they are needed.

The differential decay rates for $B \rightarrow \pi \ell^+ \ell^- (\nu \bar{\nu})$ and $B \rightarrow K \ell^+ \ell^- (\nu \bar{\nu})$ decay are proportional to the combinations of CKM elements $|V_{td} V_{tb}^*|$ and $|V_{ts} V_{tb}^*|$, respectively. Thus they enable determinations of $|V_{td}|$, $|V_{ts}|$, and their ratio that can be compared with the current most precise results obtained from the oscillation frequencies of neutral B_d and B_s mesons. Assuming the Standard Model, we combine the theoretical values for $\Delta\mathcal{B}(B \rightarrow \pi \ell^+ \ell^-)$, $\Delta\mathcal{B}(B \rightarrow K \ell^+ \ell^-)$, and their ratio with the recent experimental measurements from LHCb [45, 55] to obtain the CKM matrix elements

$$|V_{td}| = 7.45(69) \times 10^{-3}, \quad |V_{ts}| = 35.7(1.5) \times 10^{-3}, \quad \left| \frac{V_{td}}{V_{ts}} \right| = 0.201(20), \quad (6.2)$$

where we take $|V_{tb}|$ from CKM unitarity [167], and the errors include both experimental and theoretical uncertainties. These results are compatible with the PDG values from neutral B -meson oscillations [136], with a commensurate uncertainty for $|V_{td}|$, and an error on $|V_{ts}|$ that is almost two times smaller. Compared with the determinations $|V_{td}| = 7.2^{(+9)}_{(-8)} \times 10^{-3}$, $|V_{ts}| = 32(4) \times 10^{-3}$, and $|V_{td}/V_{ts}| = 0.24^{(+5)}_{(-4)}$ by LHCb [55] using the same experimental inputs but older form factors, the uncertainties above are 1.2, 2.7, and 2.3 times smaller, respectively. This illustrates the impact of using the precise hadronic form factors from *ab-initio* lattice QCD [48, 62, 63]. Further, our predictions for $\mathcal{B}(B \rightarrow \pi \nu \bar{\nu})$, $\mathcal{B}(B \rightarrow K \nu \bar{\nu})$, and their ratio will facilitate new, independent determinations of $|V_{td}|$, $|V_{ts}|$, and their ratio once these processes have been observed experimentally.

Finally, we also explore the constraints on possible new-physics contributions to the Wilson coefficients C_9 and C_{10} implied by the LHCb data for the partially integrated wide-bin $B \rightarrow K(\pi) \mu^+ \mu^-$ branching ratios when combined with the new lattice-QCD form factors. We find a 1.7σ tension between the Standard Model and the values for $\text{Re}(C_9)$ and $\text{Re}(C_{10})$ preferred by semileptonic B -meson decay data alone, as shown in Fig. 12. Including the constraint from $B_s \rightarrow \mu \mu$, for which reliable hadronic input from lattice QCD is also available, shrinks the allowed region and also slightly decreases the significance of the tension with the Standard Model. The region allowed by these theoretically clean decay modes is consistent with the constraints obtained from $B \rightarrow K^* \ell \ell$ observables, and the widths of the bands are comparable in size. The $B \rightarrow K^*$ constraints, however, make use of additional theoretical assumptions, which are not needed in lattice-QCD calculations of B -meson leptonic decays or semileptonic decays with a pseudoscalar meson in the final state. Hence, using the Fermilab/MILC form factors from *ab-initio* QCD [48, 62, 63], we obtain theoretically clean constraints on the Wilson coefficients with uncertainties similar to previous analyses.

VII. CONCLUSIONS AND OUTLOOK

Rare semileptonic B -meson decays provide a wealth of processes and observables with which to test the Standard Model and search for new physics. Exploiting this wealth, however, requires that both the experimental measurements and the corresponding theoretical

calculations are sufficiently precise and reliable. Recent progress in both areas has been significant, in particular, on the form factors that parametrize the momentum-dependent hadronic contributions to B -meson semileptonic decays with a pseudoscalar meson in the final state. In this paper, we explore the phenomenological implications of new calculations of the $B \rightarrow \pi$ [48, 63] and $B \rightarrow K$ [62] transition form factors by the Fermilab Lattice and MILC Collaborations. With the new *ab-initio* QCD information on the hadronic matrix elements, we are able to calculate the observables with fewer assumptions than previously possible. Indeed, the comparison of our Standard-Model results for the $B \rightarrow K(\pi)\mu^+\mu^-$ partial branching fractions with experimental measurements reveals that the theoretical uncertainties are now commensurate with the experimental errors, especially in the high- q^2 region. As a result, these decays are already providing theoretically clean and quantitatively meaningful tests of the Standard Model and constraints on new physics. Once the rare decays $B \rightarrow K(\pi)\nu\bar{\nu}$ and $B \rightarrow \pi\tau\nu$ are observed, our predictions for these processes will enable further Standard-Model tests, and, if deviations are seen, provide complementary information on the underlying new physics.

Our work reveals 1–2 σ deviations between the Standard Model and experiment for both $B \rightarrow \pi\mu^+\mu^-$ and $B \rightarrow K\mu^+\mu^-$ decays, where the theory values lie systematically above the measurements for all four wide q^2 bins outside the charmonium resonance region. Although the combined tension is less than 2 σ , at the current level of uncertainty, there is still ample room for new physics. Sharpening this and other tests and potentially revealing evidence for new physics will require improvements in both experiment and theory, both of which are expected. On the experimental side, measurements will continue to improve at the currently running LHCb experiment. Further, the soon-to-start Belle II experiment expects a great increase in luminosity compared to the previous Belle experiment. It may therefore observe heretofore unseen decays such as $B \rightarrow K(\pi)\nu\bar{\nu}$ and $B \rightarrow \pi\tau\nu$, for which the Standard-Model predictions are particularly clean. On the theoretical side, more precise $B \rightarrow K$ and $B \rightarrow \pi$ form factors from lattice QCD are anticipated. A dominant uncertainty in the form factors from Refs. [48, 62, 63] employed in this work, and for similar efforts using different light- and b -quark actions [66, 143, 192], is the combined statistical plus chiral-extrapolation error. Fortunately, three- and four-flavor lattice gauge-field ensembles with the average light-quark mass $(m_u + m_d)/2$ tuned to the physical value are becoming increasingly available [193–196], the use of which will essentially eliminate this source of error. Further, the form-factor uncertainties at $q^2 = 0$ are quite large due to the extrapolation from the range of simulated lattice momenta $q^2 \gtrsim 16 \text{ GeV}^2$ to the low- q^2 region using the model-independent z expansion. Reducing the form factor uncertainties at low- q^2 is necessary in order to make better use of experimental data at low- q^2 , and to sharpen comparisons of q^2 spectra between theory and experiment. Lattice-QCD ensembles with finer lattice spacings but similar spatial volumes will enable simulations with larger pion and kaon momenta, thereby shortening the extrapolation range and reducing the associated error. In particular, the form-factor calculations of Refs. [48, 62, 63] will be repeated by the Fermilab Lattice and MILC Collaborations on a new set of ensembles recently generated by the MILC Collaboration [196, 197] using the highly improved staggered quark action [198]. These four-flavor ensembles include dynamical up, down, strange, and charm quarks; physical-mass light quarks; and planned lattice spacings as small as approximately 0.03 fm.

We note that semileptonic B -meson decays with a vector meson in the final state, such as $B \rightarrow K^*\ell\ell$, provide an even richer set of observables with which to test the Standard Model, many of which are already measured experimentally. For example, for the analysis

of the Wilson coefficients, the constraint from $B \rightarrow K^* \mu^+ \mu^-$ angular observables in the $\text{Re}(C_9^{\text{NP}})$ - $\text{Re}(C_{10}^{\text{NP}})$ plane is approximately perpendicular to that from $B \rightarrow \pi(K) \mu^+ \mu^-$ branching ratios and provides complementary information. The presence of an unstable hadron in the final state, however, makes *ab initio* calculations of their form factors much more complicated. In fact, finite-volume methods for properly including the width of an unstable final state hadron in semileptonic B -meson decays are still being developed [72]. Once such methods are fully established, they will bring the hadronic uncertainties for $B \rightarrow K^* \mu^+ \mu^-$ observables under equally good theoretical control as for $B \rightarrow \pi(K) \mu^+ \mu^-$.

B -meson leptonic and semileptonic decays are already testing the Standard Model in the quark-flavor sector, in some cases yielding tantalizing discrepancies at the 2 - 3σ level. As discussed above, even more experimental and theoretical progress is anticipated. We are therefore optimistic that the rare semileptonic B -meson decays studied in this work— $B \rightarrow K(\pi) \mu^+ \mu^-$, $B \rightarrow K(\pi) \nu \bar{\nu}$, or $B \rightarrow \pi \tau \nu$ —may eventually reveal the presence of new flavor-changing interactions or sources of CP -violation in the quark sector.

ACKNOWLEDGMENTS

We thank our colleagues in the Fermilab Lattice and MILC Collaborations for an enjoyable collaboration that helped spur this work. We also thank Ulrik Egede and Tobias Tekampe for useful correspondence about LHCb’s recent $B \rightarrow K(\pi) \mu^+ \mu^-$ measurements, and Wolfgang Altmannshofer, Gudrun Hiller, Jernej Kamenik, Alexander Khodjamirian, David Straub, and Yuming Wang for valuable discussions about the theory. This work was supported in part by the U.S. Department of Energy under Grants No. DE-SC0010120 (S.G.) and No. DE-FG02-13ER42001 (A.X.K.); by the National Science Foundation under Grant No. PHY-1417805 (D.D., J.L.); and by the German Excellence Initiative, the European Union Seventh Framework Programme under grant agreement No. 291763, and the European Union’s Marie Curie COFUND program (A.S.K). Fermilab is operated by Fermi Research Alliance, LLC, under Contract No. DE-AC02-07CH11359 with the U.S. Department of Energy. S.G., A.S.K., E.L., and R.Z. thank the Kavli Institute for Theoretical Physics, which is supported by the National Science Foundation under Grant No. PHY11-25915, for its hospitality while this paper was being written. A.S.K., A.X.K., and D.D. thank the Mainz Institute for Theoretical Physics for its hospitality while part of this paper was written.

Appendix A: Numerical results for $B \rightarrow K(\pi) \ell^+ \ell^-$ observables

Here we tabulate the numerical values of $B \rightarrow K(\pi) \ell^+ \ell^-$ observables in the Standard Model integrated over different q^2 intervals. We select the same ranges of momentum transfer as the most recent experimental measurements from LHCb [45, 55].

TABLE II. Standard-Model binned flat term $F_H^\ell(q_{\min}^2, q_{\max}^2)$ for $B^+ \rightarrow \pi^+ \ell^+ \ell^-$ decay. Errors shown are from form factors and the quadrature sum of all other contributions, respectively.

$[q_{\min}^2, q_{\max}^2] \text{ (GeV}^2\text{)}$	$10^8 F_H^e$	$10^3 F_H^\mu$	$10^1 F_H^\tau$
[0.10, 2.00]	242.0(2.2,0.6)	96.1(0.8,0.2)	
[2.00, 4.00]	50.6(1.1,0.1)	21.5(0.5,0.1)	
[4.00, 6.00]	28.6(1.0,0.1)	12.2(0.4,0.0)	
[6.00, 8.00]	19.9(0.9,0.1)	8.5(0.4,0.0)	
[15.00, 17.00]	10.2(0.6,0.3)	4.3(0.3,0.1)	8.5(0.1,0.2)
[17.00, 19.00]	10.1(0.6,0.3)	4.3(0.3,0.1)	8.0(0.1,0.2)
[19.00, 22.00]	10.9(0.6,0.3)	4.7(0.3,0.1)	7.8(0.1,0.2)
[1.00, 6.00]	52.7(1.3,0.2)	22.3(0.5,0.1)	
[15.00, 22.00]	10.4(0.6,0.3)	4.4(0.3,0.1)	8.0(0.1,0.2)
$[4m_\ell^2, (M_{B^+} - M_{\pi^+})^2]$	55.6(3.6,1.8)	17.1(1.0,0.5)	8.2(0.1,0.2)

TABLE III. Standard-Model binned flat term $F_H^\ell(q_{\min}^2, q_{\max}^2)$ for $B^0 \rightarrow \pi^0 \ell^+ \ell^-$ decay. Errors shown are from form factors and the quadrature sum of all other contributions, respectively.

$[q_{\min}^2, q_{\max}^2] \text{ (GeV}^2\text{)}$	$10^8 F_H^e$	$10^3 F_H^\mu$	$10^1 F_H^\tau$
[0.10, 2.00]	249.6(1.8,0.8)	98.9(0.7,0.3)	
[2.00, 4.00]	51.0(1.0,0.1)	21.7(0.4,0.1)	
[4.00, 6.00]	28.7(0.9,0.1)	12.2(0.4,0.0)	
[6.00, 8.00]	19.9(0.8,0.1)	8.5(0.4,0.0)	
[15.00, 17.00]	10.1(0.6,0.3)	4.3(0.3,0.1)	8.5(0.1,0.2)
[17.00, 19.00]	10.0(0.6,0.3)	4.3(0.3,0.1)	8.0(0.1,0.2)
[19.00, 22.00]	10.8(0.6,0.3)	4.6(0.3,0.1)	7.7(0.1,0.2)
[1.00, 6.00]	53.1(1.2,0.2)	22.5(0.5,0.1)	
[15.00, 22.00]	10.3(0.6,0.3)	4.4(0.3,0.1)	8.0(0.1,0.2)
$[4m_\ell^2, (M_{B^0} - M_{\pi^0})^2]$	58.1(3.9,2.0)	17.4(1.0,0.6)	8.2(0.1,0.2)

TABLE IV. Standard-Model partially integrated branching fractions for $B^+ \rightarrow \pi^+ \mu^+ \mu^-$ decay. Results for $B^+ \rightarrow \pi^+ e^+ e^-$ are nearly identical. Errors shown are from the CKM elements, form factors, and the quadrature sum of all other contributions, respectively. Results are from Ref. [63], but additional digits are presented and the scale error has been included in the “other” error quoted here, to facilitate use with the correlation matrices in Tables VII and VIII.

$[q_{\min}^2, q_{\max}^2] \text{ (GeV}^2\text{)}$	$10^9 \Delta\mathcal{B}(B^+ \rightarrow \pi^+ \mu^+ \mu^-)$
[1.00, 6.00]	4.781(0.286,0.541,0.165)
[15.00, 22.00]	5.046(0.303,0.338,0.162)

TABLE V. Standard-Model partially integrated branching fractions for $B^+ \rightarrow K^+ \ell^+ \ell^-$ decay. Results for $B^+ \rightarrow K^+ e^+ e^-$ are nearly the same as for $B^+ \rightarrow K^+ \mu^+ \mu^-$. Errors shown are from the CKM elements, form factors, and the quadrature sum of all other contributions, respectively. Results for the electron and muon final states are indistinguishable at the current level of precision. At low q^2 , we present two wide bins $[1 \text{ GeV}^2, 6 \text{ GeV}^2]$ and $[1.1 \text{ GeV}^2, 6 \text{ GeV}^2]$ to enable comparison with the LHCb measurements in Refs. [55] and [45], respectively.

$[q_{\min}^2, q_{\max}^2] \text{ (GeV}^2\text{)}$	$10^9 \Delta\mathcal{B}(B^+ \rightarrow K^+ \mu^+ \mu^-)$	$10^9 \Delta\mathcal{B}(B^+ \rightarrow K^+ \tau^+ \tau^-)$
[0.10, 2.00]	68.03(3.70,13.72,1.55)	
[2.00, 4.00]	71.72(3.91,12.44,1.63)	
[4.00, 6.00]	70.59(3.84,10.36,1.54)	
[6.00, 8.00]	68.94(3.75,8.47,1.46)	
[15.00, 17.00]	46.15(2.51,2.48,1.62)	39.92(2.17,2.22,1.40)
[17.00, 19.00]	34.91(1.90,1.68,1.13)	39.31(2.14,1.81,1.33)
[19.00, 22.00]	25.73(1.40,1.17,0.86)	43.23(2.35,1.80,1.57)
[1.00, 6.00]	178.35(9.71,29.80,4.00)	
[1.10, 6.00]	174.75(9.52,29.07,3.92)	
[15.00, 22.00]	106.79(5.82,5.21,3.49)	122.46(6.67,5.63,4.17)
$[4m_\ell^2, (M_{B^+} - M_{K^+})^2]$	605.33(32.96,65.14,17.03)	160.36(8.73,7.87,5.46)

TABLE VI. Standard-Model partially integrated branching fractions for $B^0 \rightarrow K^0 \ell^+ \ell^-$ decay. Results for $B^0 \rightarrow K^0 e^+ e^-$ are nearly the same as for $B^0 \rightarrow K^0 \mu^+ \mu^-$. Errors shown are from the CKM elements, form factors, and the quadrature sum of all other contributions, respectively. Results for the electron and muon final states are indistinguishable at the current level of precision. At low q^2 , we present two wide bins $[1 \text{ GeV}^2, 6 \text{ GeV}^2]$ and $[1.1 \text{ GeV}^2, 6 \text{ GeV}^2]$ to enable comparison with the LHCb measurements in Refs. [55] and [45], respectively.

$[q_{\min}^2, q_{\max}^2] \text{ (GeV}^2\text{)}$	$10^9 \Delta\mathcal{B}(B^0 \rightarrow K^0 \mu^+ \mu^-)$	$10^9 \Delta\mathcal{B}(B^0 \rightarrow K^0 \tau^+ \tau^-)$
[0.10, 2.00]	63.38(3.45,12.70,1.51)	
[2.00, 4.00]	65.88(3.59,11.35,1.46)	
[4.00, 6.00]	64.94(3.54,9.47,1.37)	
[6.00, 8.00]	63.60(3.46,7.76,1.32)	
[15.00, 17.00]	42.76(2.33,2.30,1.51)	36.96(2.01,2.04,1.30)
[17.00, 19.00]	32.25(1.76,1.55,1.04)	36.34(1.98,1.67,1.23)
[19.00, 22.00]	23.53(1.28,1.07,0.79)	39.74(2.16,1.65,1.44)
[1.00, 6.00]	164.09(8.94,27.23,3.59)	
[1.10, 6.00]	160.75(8.75,26.56,3.51)	
[15.00, 22.00]	98.54(5.37,4.80,3.22)	113.05(6.16,5.19,3.85)
$[4m_\ell^2, (M_{B^0} - M_{K^0})^2]$	558.80(30.43,59.72,15.73)	147.45(8.03,7.22,5.02)

TABLE VII. Correlations between the form-factor contributions to the errors in the Standard-Model partially integrated branching fractions for $B^+ \rightarrow \pi^+ \ell^+ \ell^-$ decay and $B^+ \rightarrow K^+ \ell^+ \ell^-$ decay. These should be combined with the central values and form-factor errors in the bottom panels of Table IV from Ref. [63] and Table V above. The results for the neutral decay modes $B^0 \rightarrow \pi^0(K^0) \ell^+ \ell^-$ should be taken as 100% correlated with those for the charged decays.

$[q_{\min}^2, q_{\max}^2] \text{ (GeV}^2\text{)}$	$[1, 6]_{\pi^+}$	$[15, 22]_{\pi^+}$	$[1, 6]_{K^+}$	$[1.1, 6]_{K^+}$	$[15, 22]_{K^+}$
$[1, 6]_{\pi^+}$	1.0000	0.6071	0.0426	0.0428	0.1190
$[15, 22]_{\pi^+}$	0.6071	1.0000	0.1020	0.1023	0.2631
$[1, 6]_{K^+}$	0.0426	0.1020	1.0000	1.0000	0.5099
$[1.1, 6]_{K^+}$	0.0428	0.1023	1.0000	1.0000	0.5112
$[15, 22]_{K^+}$	0.1190	0.2631	0.5099	0.5112	1.0000

TABLE VIII. Correlations between the “other” contributions to the errors in the Standard-Model partially integrated branching fractions for $B^+ \rightarrow \pi^+ \ell^+ \ell^-$ decay and $B^+ \rightarrow K^+ \ell^+ \ell^-$ decay. These should be combined with the central values and “other” errors in the bottom panels of Table IV from Ref. [63] and Table V above. The correlation between the combinations of CKM elements that enter the $B^+ \rightarrow \pi^+ \ell^+ \ell^-$ and $B^+ \rightarrow K^+ \ell^+ \ell^-$ decay rates ($|V_{td}V_{tb}^*|$ and $|V_{ts}V_{tb}^*|$) is 0.878. The results for the neutral decay modes $B^0 \rightarrow \pi^0(K^0) \ell^+ \ell^-$ should be taken as 100% correlated with those for the charged decays.

$[q_{\min}^2, q_{\max}^2] \text{ (GeV}^2\text{)}$	$[1, 6]_{\pi^+}$	$[15, 22]_{\pi^+}$	$[1, 6]_{K^+}$	$[1.1, 6]_{K^+}$	$[15, 22]_{K^+}$
$[1, 6]_{\pi^+}$	1.0000	0.4504	0.9730	0.9728	0.4860
$[15, 22]_{\pi^+}$	0.4504	1.0000	0.4212	0.4207	0.6098
$[1, 6]_{K^+}$	0.9730	0.4212	1.0000	1.0000	0.4510
$[1.1, 6]_{K^+}$	0.9728	0.4207	1.0000	1.0000	0.4504
$[15, 22]_{K^+}$	0.4860	0.6098	0.4510	0.4504	1.0000

TABLE IX. Standard-Model binned flat term $F_H^\ell(q_{\min}^2, q_{\max}^2)$ for $B^+ \rightarrow K^+ \ell^+ \ell^-$ decay. Errors shown are from form factors and the quadrature sum of all other contributions, respectively.

$[q_{\min}^2, q_{\max}^2] \text{ (GeV}^2\text{)}$	$10^8 F_H^e$	$10^3 F_H^\mu$	$10^1 F_H^\tau$
$[0.10, 2.00]$	248.0(2.2,0.5)	98.3(0.8,0.2)	
$[2.00, 4.00]$	55.7(0.7,0.0)	23.6(0.3,0.0)	
$[4.00, 6.00]$	33.3(0.6,0.0)	14.2(0.2,0.0)	
$[6.00, 8.00]$	24.3(0.5,0.0)	10.3(0.2,0.0)	
$[15.00, 17.00]$	14.0(0.3,0.4)	6.0(0.1,0.2)	8.9(0.0,0.3)
$[17.00, 19.00]$	14.7(0.3,0.5)	6.3(0.1,0.2)	8.6(0.0,0.2)
$[19.00, 22.00]$	19.7(0.4,0.7)	8.4(0.2,0.3)	8.7(0.0,0.2)
$[1.00, 6.00]$	57.8(1.1,0.1)	24.5(0.5,0.0)	
$[15.00, 22.00]$	15.6(0.3,0.5)	6.6(0.1,0.2)	8.7(0.0,0.2)
$[4m_\ell^2, (M_{B^+} - M_{K^+})^2]$	71.5(6.1,2.1)	22.2(1.7,0.7)	8.9(0.0,0.3)

TABLE X. Standard-Model binned flat term $F_H^\ell(q_{\min}^2, q_{\max}^2)$ for $B^0 \rightarrow K^0 \ell^+ \ell^-$ decay. Errors shown are from the form factors and the quadrature sum of all other contributions, respectively.

$[q_{\min}^2, q_{\max}^2]$ (GeV ²)	$10^8 F_H^e$	$10^3 F_H^\mu$	$10^1 F_H^\tau$
[0.10, 2.00]	258.6(2.4,0.4)	101.8(0.9,0.2)	
[2.00, 4.00]	55.8(0.7,0.0)	23.6(0.3,0.0)	
[4.00, 6.00]	33.3(0.6,0.0)	14.2(0.2,0.0)	
[6.00, 8.00]	24.3(0.5,0.0)	10.3(0.2,0.0)	
[15.00, 17.00]	14.0(0.3,0.4)	6.0(0.1,0.2)	8.9(0.0,0.3)
[17.00, 19.00]	14.7(0.3,0.5)	6.3(0.1,0.2)	8.6(0.0,0.2)
[19.00, 22.00]	19.8(0.4,0.7)	8.4(0.2,0.3)	8.7(0.0,0.2)
[1.00, 6.00]	58.0(1.1,0.1)	24.5(0.5,0.0)	
[15.00, 22.00]	15.6(0.3,0.5)	6.7(0.1,0.2)	8.7(0.0,0.2)
$[4m_\ell^2, (M_{B^0} - M_{K^0})^2]$	73.5(6.4,2.2)	22.4(1.7,0.7)	8.9(0.0,0.3)

TABLE XI. Standard-Model lepton-universality-violating ratios for $B \rightarrow \pi \ell^+ \ell^-$ decay. Results are shown for both the charged (R_{π^+} , left) and neutral (R_{π^0} , right) modes. Errors shown are from the form factors and the quadrature sum of all other contributions, respectively.

$[q_{\min}^2, q_{\max}^2]$ (GeV ²)	$10^3 (R_{\pi^+}^{\mu e} - 1)$	$R_{\pi^+}^{\mu\tau}$	$10^3 (R_{\pi^0}^{\mu e} - 1)$	$R_{\pi^0}^{\mu\tau}$
[0.10, 2.00]	-5.81(0.62 0.07)		-4.70(0.50 0.02)	
[2.00, 4.00]	-1.66(0.46 0.06)		-1.49(0.41 0.05)	
[4.00, 6.00]	-1.38(0.42 0.05)		-1.33(0.40 0.04)	
[6.00, 8.00]	-1.14(0.39 0.04)		-1.13(0.39 0.04)	
[15.00, 17.00]	0.14(0.64 0.01)	0.52(0.08 0.00)	0.11(0.63 0.00)	0.54(0.08 0.00)
[17.00, 19.00]	0.58(0.82 0.02)	0.21(0.06 0.00)	0.54(0.82 0.02)	0.22(0.06 0.00)
[19.00, 22.00]	1.38(1.21 0.05)	-0.05(0.04 0.01)	1.33(1.21 0.05)	-0.04(0.04 0.01)
[1.00, 6.00]	-1.64(0.45 0.06)		-1.45(0.40 0.05)	
[15.00, 22.00]	0.72(0.90 0.02)	0.18(0.06 0.01)	0.68(0.90 0.02)	0.19(0.06 0.01)

TABLE XII. Standard-Model lepton-universality-violating ratios for $B \rightarrow K \ell^+ \ell^-$ decay. Results are shown for both the charged (R_{K^+} , left) and neutral (R_{K^0} , right) modes. Errors shown are from the form factors and the quadrature sum of all other contributions, respectively.

$[q_{\min}^2, q_{\max}^2]$ (GeV ²)	$10^3 (R_{K^+}^{\mu e} - 1)$	$R_{K^+}^{\mu\tau}$	$10^3 (R_{K^0}^{\mu e} - 1)$	$R_{K^0}^{\mu\tau}$
[0.10, 2.00]	-3.30(0.20 0.02)		-4.27(0.22 0.03)	
[2.00, 4.00]	0.50(0.38 0.02)		0.44(0.39 0.02)	
[4.00, 6.00]	0.62(0.59 0.02)		0.59(0.59 0.02)	
[6.00, 8.00]	0.72(0.86 0.02)		0.70(0.85 0.02)	
[15.00, 17.00]	1.79(3.20 0.06)	0.16(0.02 0.01)	1.78(3.20 0.06)	0.16(0.02 0.01)
[17.00, 19.00]	2.55(4.23 0.09)	-0.11(0.02 0.01)	2.56(4.23 0.09)	-0.11(0.02 0.01)
[19.00, 22.00]	5.08(5.95 0.19)	-0.40(0.01 0.01)	5.13(5.94 0.19)	-0.41(0.01 0.01)
[1.00, 6.00]	0.50(0.43 0.02)		0.43(0.44 0.02)	
[15.00, 22.00]	2.83(4.20 0.10)	-0.13(0.02 0.01)	2.84(4.19 0.10)	-0.13(0.02 0.01)

TABLE XIII. Standard-Model ratio of partially integrated branching ratios $\Delta\mathcal{B}(B \rightarrow \pi\ell^+\ell^-)/\Delta\mathcal{B}(B \rightarrow K\ell^+\ell^-)$. Errors shown are from the CKM elements, form factors, and the quadrature sum of all other contributions, respectively.

$[q_{\min}^2, q_{\max}^2] \text{ (GeV}^2\text{)}$	$10^3 \frac{\Delta\mathcal{B}(B^+ \rightarrow \pi^+ \mu^+ \mu^-)}{\Delta\mathcal{B}(B^+ \rightarrow K^+ \mu^+ \mu^-)}$	$10^3 \frac{\Delta\mathcal{B}(B^0 \rightarrow \pi^0 \mu^+ \mu^-)}{\Delta\mathcal{B}(B^0 \rightarrow K^0 \mu^+ \mu^-)}$
[0.10, 2.00]	26.63(0.76, 6.31, 0.42)	13.07(0.37, 3.12, 0.20)
[2.0, 4.0]	26.73(0.76, 5.48, 0.37)	13.04(0.37, 2.68, 0.17)
[4.0, 6.0]	27.01(0.77, 4.74, 0.35)	13.20(0.37, 2.32, 0.16)
[6.0, 8.0]	27.47(0.78, 4.11, 0.34)	13.46(0.38, 2.02, 0.16)
[15.0, 17.0]	36.64(1.04, 2.95, 1.05)	18.18(0.52, 1.47, 0.52)
[17.0, 19.0]	43.37(1.23, 3.15, 1.24)	21.63(0.61, 1.58, 0.62)
[19.0, 22.0]	71.37(2.02, 4.69, 2.03)	36.11(1.02, 2.38, 1.03)
[1.0, 6.0]	26.82(0.76, 5.30, 0.37)	13.09(0.37, 2.60, 0.17)
[15.0, 22.0]	47.21(1.34, 3.38, 1.34)	23.59(0.67, 1.70, 0.67)

TABLE XIV. Correlations between the form-factor contributions to the errors in the Standard-Model ratio of partially integrated branching ratios $\Delta\mathcal{B}(B \rightarrow \pi\ell^+\ell^-)/\Delta\mathcal{B}(B \rightarrow K\ell^+\ell^-)$. These should be combined with the central values and form-factor errors in the bottom panel of Table XIII above. The results for the ratio of neutral decay modes should be taken as 100% correlated with those for the charged decays.

$[q_{\min}^2, q_{\max}^2] \text{ (GeV}^2\text{)}$	[1, 6]	[15, 22]
[1, 6]	1.0000	0.4905
[15, 22]	0.4905	1.0000

TABLE XV. Correlations between the “other” contributions to the errors in the Standard-Model ratio of partially integrated branching ratios $\Delta\mathcal{B}(B \rightarrow \pi\ell^+\ell^-)/\Delta\mathcal{B}(B \rightarrow K\ell^+\ell^-)$. These should be combined with the central values and “other” errors in the bottom panel of Table XIII above. The CKM errors are 100% correlated between the two bins. The results for the ratio of neutral decay modes should be taken as 100% correlated with those for the charged decays.

$[q_{\min}^2, q_{\max}^2] \text{ (GeV}^2\text{)}$	[1, 6]	[15, 22]
[1, 6]	1.0000	0.0917
[15, 22]	0.0917	1.0000

Appendix B: $B \rightarrow K(\pi)\ell^+\ell^-$ differential decay rates

Here we summarize the theoretical expressions for the $B \rightarrow K(\pi)\ell^+\ell^-$ differential decay rates in the Standard Model, including the complete dependence on the charged-lepton mass m_ℓ . We encourage the users of these formulae to cite explicitly the original papers [73, 76–78, 90, 91, 98, 99, 199–204], in which the results collected below were first derived. In Appendix B 1 we present a complete set of expressions needed to describe the high- q^2 region. The discussion of the running of the tensor form factor f_T surrounding Eq. (B9) has not been discussed in reference to exclusive $b \rightarrow s\ell\ell$ decays elsewhere in the literature. The additional nonfactorizable terms of the type $\phi_B \star T \star \Phi_P$ required at low- q^2 are collected in Appendix B 2. For the $\ell = \tau$ case, the lower boundary of kinematic range, $q_{\min}^2 = 4m_\tau^2$, is larger than the ψ' mass implying that the high- q^2 OPE is sufficient to completely describe this mode. Relations between the form factors f_T and f_+ valid at low and high- q^2 are presented in Appendix B 3. A discussion of scale and power-correction uncertainties is given in Appendix B 4.

1. Main formulas

The double differential $B \rightarrow P\ell\ell$ ($P = K, \pi$; $\ell = e, \mu, \tau$) decay rate is given by (see, for instance, Ref. [78])

$$\frac{d^2\Gamma}{dq^2 d\cos\theta} = a + b\cos\theta + c\cos^2\theta, \quad (\text{B1})$$

$$a = \Gamma_0\lambda_0^{1/2}\beta_\ell \left[\frac{\lambda_0}{4}|G|^2 + |C_{10}|^2 \left(\frac{\lambda_0}{4}\beta_\ell^2|f_+|^2 + \frac{m_\ell^2}{q^2}(M_B^2 - M_P^2)^2|f_0|^2 \right) \right] \quad (\text{B2})$$

$$b = 0, \quad (\text{B3})$$

$$c = -\frac{1}{4}\Gamma_0\lambda_0^{3/2}\beta_\ell^3 (|G|^2 + |C_{10}f_+|^2), \quad (\text{B4})$$

$$G = C_9^{\text{eff}}f_+ + \frac{2m_b^{\overline{\text{MS}}}(\mu)}{M_B + M_P}C_7^{\text{eff}}f_T, \quad (\text{B5})$$

$$\Gamma_0 = C_P \frac{G_F^2\alpha_e^2|V_{tb}V_{tq}^*|^2}{512\pi^5 M_B^3}, \quad (\text{B6})$$

$$\lambda_0 = 4M_B^2|\mathbf{p}_P|^2 = M_B^4 + M_P^4 + q^4 - 2(M_B^2M_P^2 + M_B^2q^2 + M_P^2q^2), \quad (\text{B7})$$

$$\beta_\ell = \sqrt{1 - \frac{4m_\ell^2}{q^2}}, \quad (\text{B8})$$

where θ is the angle between the negative lepton direction and the B incoming direction in the dilepton center of mass frame, and $|\mathbf{p}_P| = \sqrt{E_P^2 - M_P^2}$ is the three-momentum of the final-state meson in the B -meson rest frame. The isospin factor in Eq. (B6) $C_P = 1$ for decays to kaons and charged pions (π^\pm), while $C_P = 1/2$ for decays to neutral pions (π^0). When $m_\ell = 0$, $c = -a$.

The form factor f_+ is scale independent while the scale dependence of f_T is simply

controlled by the anomalous dimension of the tensor current:

$$f_T(\mu_2) = f_T(\mu_1) \left(\frac{\alpha_s(\mu_2)}{\alpha_s(\mu_1)} \right)^{-\gamma_T^{(0)}/2\beta_0}, \quad (\text{B9})$$

where $\beta_0 = (11N_c - 2N_f)/3 = 23/3$ (with $N_f = 5$ active flavors) is the leading order QCD beta function, and the leading order anomalous dimension of the tensor current is given by the anomalous dimension of the operator Q_7 minus the contribution of the explicit bottom mass that appears in Q_7 , $\gamma_T^{(0)} = \gamma_7^{(0)} - \gamma_m^{(0)} = 8C_F - 6C_F = 2C_F = 8/3$ (see, for instance, Ref. [205]).

We obtain the expressions for the effective Wilson coefficients C_7^{eff} and C_9^{eff} starting from Eq. (47) of Ref. [201] where the notation $\tilde{C}_{7,9}^{\text{eff}}$ is used; we also use results from Refs. [90, 99, 204]. We have made a number of changes in notation, however, and also removed some terms, as described below. Reference [201] uses the notation $\xi_i = V_{ib}V_{id}^*$ with $i = u, c, t$, which can be generalized to replace d by q so that the final state quark can be either d or s . In either case, third-column and q^{th} -column unitarity implies $\xi_u + \xi_c + \xi_t = 0$, or equivalently, $\xi_c/\xi_t = -1 - \xi_u/\xi_t = -1 - \lambda_u^{(q)}$, defining $\lambda_u^{(q)} = V_{uq}^*V_{ub}/(V_{tq}^*V_{tb})$. Also, the extra factor $\alpha_s/(4\pi)$ in the definition of the operators $Q_{7,9}$ has to be taken into account by replacing $4\pi/\alpha_s C_{7,9} \rightarrow C_{7,9}$ in Eq. (48) of Ref. [201]. Our notation simplifies that of Ref. [201] by not being explicit about the μ dependence of the C_i . We set $\omega_{7,9} \rightarrow 0$ to remove bremsstrahlung contributions. We absorb the terms proportional to $\ln(m_b/\mu)$ in Eq. (48) of Ref. [201] into the definitions of the functions $h(m, q^2)$ that we adopt here in Eqs. (B12)-(B14), so that they are scale dependent. We use the exact relation $F_{2,c}^{(7)} = -6F_{1,c}^{(7)}$ to simplify Eq. (B10). Finally, we keep only the first term for A_8 in Eq. (48) of Ref [201] since the other terms are higher order, and take $A_8 = C_8$ because of different operator normalization.

With the above choices, our expressions for C_7^{eff} and C_9^{eff} become

$$C_7^{\text{eff}} = C_7 - \frac{1}{3} \left[C_3 + \frac{4}{3} C_4 + 20 C_5 + \frac{80}{3} C_6 \right] - \frac{\alpha_s}{4\pi} \left[(C_1 - 6 C_2) F_{1,c}^{(7)} + C_8 F_8^{(7)} \right] \\ - \frac{\alpha_s}{4\pi} \lambda_u^{(q)} (C_1 - 6 C_2) \left(F_{1,c}^{(7)} - F_{1,u}^{(7)} \right), \quad (\text{B10})$$

$$C_9^{\text{eff}} = C_9 + \frac{4}{3} C_3 + \frac{64}{9} C_5 + \frac{64}{27} C_6 + h(0, q^2) \left(-\frac{1}{2} C_3 - \frac{2}{3} C_4 - 8 C_5 - \frac{32}{3} C_6 \right) \\ + h(m_b, q^2) \left(-\frac{7}{2} C_3 - \frac{2}{3} C_4 - 38 C_5 - \frac{32}{3} C_6 \right) \\ + h(m_c, q^2) \left(\frac{4}{3} C_1 + C_2 + 6 C_3 + 60 C_5 \right) + \lambda_u^{(q)} \left[h(m_c, q^2) - h(0, q^2) \right] \left(\frac{4}{3} C_1 + C_2 \right) \\ - \frac{\alpha_s}{4\pi} \left[C_1 F_{1,c}^{(9)} + C_2 F_{2,c}^{(9)} + C_8 F_8^{(9)} \right] \\ - \frac{\alpha_s}{4\pi} \lambda_u^{(q)} \left[C_1 \left(F_{1,c}^{(9)} - F_{1,u}^{(9)} \right) + C_2 \left(F_{2,c}^{(9)} - F_{2,u}^{(9)} \right) \right]. \quad (\text{B11})$$

Numerically, the CKM factor $|\lambda_u^{(s)}| \simeq 0.02 \ll |\lambda_u^{(d)}| \simeq 0.4$; thus terms proportional to $\lambda_u^{(q)}$ are significant only for the $B \rightarrow \pi$ mode. Reference [204] provides a *Mathematica* notebook for the functions $F_{1,2}^{(7,9)}$ in the charm-pole-mass scheme. Our expressions for C_7^{eff} and C_9^{eff} are similar to Eqs. (2.6) and (2.7) in Ref. [90]; however, we have included terms proportional to

$\lambda_u^{(q)}$ for C_7^{eff} , and for C_9^{eff} we have not expanded $h(m_c, q^2)$ and $F_{i,c}^{(7,9)}$ in powers of m_c^2/q^2 as in Eq. (2.7) of Ref. [90].

The function $h(m_q, q^2)$ is given in Eq. (11) of Ref. [99]. The function $h(m_q, q^2)$ for $m_q = 0, m_b$ is also given explicitly in Eqs. (3.11) and (3.12) of Ref. [76]. The functions $F_8^{(7,9)}$, B_0 , and C_0 are given in Eqs. (B.1)–(B.3), and (29) of Ref. [99]. The functions $F_{1,u}^{(7,9)}$, $F_{2,u}^{(7,9)}$ are given in Eqs. (22)–(31) of Ref. [202] but with an extra minus sign compared with the convention adopted here and in Refs. [200, 201, 204]). For the convenience of the reader, we present the explicit expressions for all required functions here:

$$h(m_c, q^2) = \frac{4}{9} \left(\ln \frac{\mu^2}{m_c^2} + \frac{2}{3} + z \right) - \frac{4}{9} (2+z) \sqrt{|z-1|} \begin{cases} \arctan \frac{1}{\sqrt{z-1}} & z = \frac{4m_c^2}{q^2} > 1 \\ \ln \frac{1+\sqrt{1-z}}{\sqrt{z}} - \frac{i\pi}{2} & z = \frac{4m_c^2}{q^2} \leq 1 \end{cases}, \quad (\text{B12})$$

$$h(0, q^2) = \frac{8}{27} + \frac{4}{9} \left(\ln \frac{\mu^2}{q^2} + i\pi \right), \quad (\text{B13})$$

$$h(m_b, q^2) = \frac{4}{9} \left(\ln \frac{\mu^2}{m_b^2} + \frac{2}{3} + z \right) - \frac{4}{9} (2+z) \sqrt{z-1} \arctan \frac{1}{\sqrt{z-1}}, \quad z = \frac{4m_b^2}{q^2}, \quad (\text{B14})$$

$$F_8^{(7)} = -\frac{32}{9} \ln \frac{\mu}{m_b} - \frac{8}{9} \frac{\hat{s}}{1-\hat{s}} \ln \hat{s} - \frac{8}{9} i\pi - \frac{4}{9} \frac{11-16\hat{s}+8\hat{s}^2}{(1-\hat{s})^2} + \frac{4}{9} \frac{1}{(1-\hat{s})^3} [(9\hat{s}-5\hat{s}^2+2\hat{s}^3) B_0(\hat{s}) - (4+2\hat{s}) C_0(\hat{s})], \quad (\text{B15})$$

$$F_8^{(9)} = \frac{16}{9} \frac{1}{1-\hat{s}} \ln \hat{s} + \frac{8}{9} \frac{5-2\hat{s}}{(1-\hat{s})^2} - \frac{8}{9} \frac{4-\hat{s}}{(1-\hat{s})^3} [(1+\hat{s}) B_0(\hat{s}) - 2 C_0(\hat{s})], \quad (\text{B16})$$

$$B_0(\hat{s}) = -2 \sqrt{4/\hat{s}-1} \arctan \frac{1}{\sqrt{4/\hat{s}-1}}, \quad (\text{B17})$$

$$C_0(\hat{s}) = \int_0^1 dx \frac{1}{x(1-\hat{s})+1} \ln \frac{x^2}{1-x(1-x)\hat{s}}, \quad (\text{B18})$$

$$F_{1,u}^{(7)} = F_{1,c}^{(7)}|_{m_c \rightarrow 0} = -A(\hat{s}), \quad (\text{B19})$$

$$F_{2,u}^{(7)} = F_{2,c}^{(7)}|_{m_c \rightarrow 0} = -6F_{1,c}^{(7)}|_{m_c \rightarrow 0} = 6A(\hat{s}), \quad (\text{B20})$$

$$F_{1,u}^{(9)} = F_{1,c}^{(9)}|_{m_c \rightarrow 0} = -B(\hat{s}) - 4C(\hat{s}), \quad (\text{B21})$$

$$F_{2,u}^{(9)} = F_{2,c}^{(9)}|_{m_c \rightarrow 0} = -3C(\hat{s}) + 6B(\hat{s}), \quad (\text{B22})$$

$$A(\hat{s}) = -\frac{104}{243} \ln \left(\frac{m_b^2}{\mu^2} \right) + \frac{4\hat{s}}{27(1-\hat{s})} \left[\text{Li}_2(\hat{s}) + \ln(\hat{s}) \ln(1-\hat{s}) \right] + \frac{1}{729(1-\hat{s})^2} \left[6\hat{s}(29-47\hat{s}) \ln(\hat{s}) + 785 - 1600\hat{s} + 833\hat{s}^2 + 6\pi i(20-49\hat{s}+47\hat{s}^2) \right] - \frac{2}{243(1-\hat{s})^3} \left[2\sqrt{z-1}(-4+9\hat{s}-15\hat{s}^2+4\hat{s}^3) \text{arccot}(\sqrt{z-1}) + 9\hat{s}^3 \ln^2(\hat{s}) + 18\pi i\hat{s}(1-2\hat{s}) \ln(\hat{s}) \right] + \frac{2\hat{s}}{243(1-\hat{s})^4} \left[36 \text{arccot}^2(\sqrt{z-1}) + \pi^2(-4+9\hat{s}-9\hat{s}^2+3\hat{s}^3) \right], \quad (\text{B23})$$

$$\begin{aligned}
B(\hat{s}) = & \frac{8}{243\hat{s}} \left[(4 - 34\hat{s} - 17\pi i\hat{s}) \ln\left(\frac{m_b^2}{\mu^2}\right) + 8\hat{s} \ln^2\left(\frac{m_b^2}{\mu^2}\right) + 17\hat{s} \ln(\hat{s}) \ln\left(\frac{m_b^2}{\mu^2}\right) \right] \\
& + \frac{(2 + \hat{s})\sqrt{z-1}}{729\hat{s}} \left[-48 \ln\left(\frac{m_b^2}{\mu^2}\right) \operatorname{arccot}(\sqrt{z-1}) - 18\pi \ln(z-1) + 3i \ln^2(z-1) \right. \\
& - 24i \operatorname{Li}_2(-x_2/x_1) - 5\pi^2 i + 6i \left(-9 \ln^2(x_1) + \ln^2(x_2) - 2 \ln^2(x_4) \right. \\
& \quad \left. \left. + 6 \ln(x_1) \ln(x_2) - 4 \ln(x_1) \ln(x_3) + 8 \ln(x_1) \ln(x_4) \right) \right. \\
& \left. - 12\pi \left(2 \ln(x_1) + \ln(x_3) + \ln(x_4) \right) \right] \\
& - \frac{2}{243\hat{s}(1-\hat{s})} \left[4\hat{s} \left(-8 + 17\hat{s} \right) \left(\operatorname{Li}_2(\hat{s}) + \ln(\hat{s}) \ln(1-\hat{s}) \right) \right. \\
& \quad \left. + 3 \left(2 + \hat{s} \right) \left(3 - \hat{s} \right) \ln^2(x_2/x_1) + 12\pi \left(-6 - \hat{s} + \hat{s}^2 \right) \operatorname{arccot}(\sqrt{z-1}) \right] \\
& + \frac{2}{2187\hat{s}(1-\hat{s})^2} \left[-18\hat{s} \left(120 - 211\hat{s} + 73\hat{s}^2 \right) \ln(\hat{s}) \right. \\
& \quad \left. - 288 - 8\hat{s} + 934\hat{s}^2 - 692\hat{s}^3 + 18\pi i\hat{s} \left(82 - 173\hat{s} + 73\hat{s}^2 \right) \right] \\
& - \frac{4}{243\hat{s}(1-\hat{s})^3} \left[-2\sqrt{z-1} \left(4 - 3\hat{s} - 18\hat{s}^2 + 16\hat{s}^3 - 5\hat{s}^4 \right) \operatorname{arccot}(\sqrt{z-1}) \right. \\
& \quad \left. - 9\hat{s}^3 \ln^2(\hat{s}) + 2\pi i\hat{s} \left(8 - 33\hat{s} + 51\hat{s}^2 - 17\hat{s}^3 \right) \ln(\hat{s}) \right] \\
& + \frac{2}{729\hat{s}(1-\hat{s})^4} \left[72 \left(3 - 8\hat{s} + 2\hat{s}^2 \right) \operatorname{arccot}^2(\sqrt{z-1}) \right. \\
& \quad \left. - \pi^2 \left(54 - 53\hat{s} - 286\hat{s}^2 + 612\hat{s}^3 - 446\hat{s}^4 + 113\hat{s}^5 \right) \right], \tag{B24}
\end{aligned}$$

$$C(\hat{s}) = -\frac{16}{81} \ln\left(\hat{s} \frac{m_b^2}{\mu^2}\right) + \frac{428}{243} - \frac{64}{27} \zeta(3) + \frac{16}{81} \pi i, \tag{B25}$$

where $\hat{s} = q^2/m_b^2$, $x_1 = (1 + i\sqrt{z-1})/2$, $x_2 = (1 - i\sqrt{z-1})/2$, $x_3 = (1 + i/\sqrt{z-1})/2$, $x_4 = (1 - i/\sqrt{z-1})/2$ and $z = 4/\hat{s}$. Note that our functions $F_i^{(9)}$ follow the conventions used in Ref. [204]. All charm- and bottom-quark masses that appear in these formulae are in the pole scheme, with the exception of the explicit instance of the bottom $\overline{\text{MS}}$ mass in Eq. (B5).

2. Additional nonfactorizable contributions required at low q^2

The additional contributions of the form $\phi_B \star T \star \phi_P$ that arise in the SCET expansion at low q^2 have been calculated in the $m_\ell = 0$ limit in Ref. [99]. Some of these terms are truly nonfactorizable effects while others appear when f_T is expressed in terms of f_+ [see Eq. (B48) below]; the latter have to be removed because, in this work, we use the tensor form factor f_T computed directly from lattice QCD.

Following the notation of Ref. [100], all of these terms are included in the quantity τ_P defined in Eq. (B.1) of that work. Compared to that work,² we set the terms $C_P^{(0,\text{f,nf})}$ and

² Note that in Eq. (B.2) of Ref. [100] there is a typo in the definition of $C_P^{(\text{f})}$ and its overall sign has to be reversed.

$T_{P,\pm}^{(f)}$ to zero in our formulae (where the superscripts “f” and “nf” denote factorizable and nonfactorizable, respectively). Some of these terms correspond to contributions that we have already included in $C_{7,9}^{\text{eff}}$. Others appear in the SCET expansion of f_T , which we do not use here because we have the tensor form factor from lattice QCD, or in the perturbative expansion of the $\overline{\text{MS}}$ b -quark mass in terms of the potential subtracted one, which is not relevant because we adopt the $\overline{\text{MS}}$ scheme.

The remaining contributions $T_{P,\pm}^{(0,\text{nf})}$ are genuine nonfactorizable corrections. From the expression for $F_V = G/f_+$ given in Eq. (3.2) of Ref. [100], we see that these terms all can be included in a shift in the effective coefficient C_9^{eff} :

$$\Delta C_9^{\text{eff}} = \frac{2m_b}{M_B} \frac{\Delta\tau_P}{f_+}, \quad (\text{B26})$$

$$\Delta\tau_P = \frac{\pi^2}{N_c} \frac{f_B f_P}{M_B} \sum_{\pm} \int \frac{d\omega}{\omega} \Phi_{B,\pm}(\omega) \int_0^1 du \Phi_P(u) \left[T_{P,\pm}^{(0)} + \tilde{\alpha}_s C_F T_{P,\pm}^{(\text{nf})} \right]. \quad (\text{B27})$$

The functions $T_{P,\pm}^{(0,\text{nf})} = -T_{\parallel,\pm}^{(0,\text{nf})}$ are given in Eqs. (17) and (18), (25) and (26), and (28)–(32) of Ref. [99] and read

$$T_{P,+}^{(0)} = 0, \quad (\text{B28})$$

$$T_{P,-}^{(0)} = e_q \frac{M_B \omega}{M_B \omega - q^2 - i\epsilon} \frac{4M_B}{m_b} \left(C_3 + \frac{4}{3} C_4 + 16C_5 + \frac{64}{3} C_6 \right), \quad (\text{B29})$$

$$\begin{aligned} T_{P,+}^{(\text{nf})} = & -\frac{M_B}{m_b} \left[e_u t_{\parallel}(u, m_c) (-C_1/6 + C_2 + 6C_6) \right. \\ & + e_d t_{\parallel}(u, m_b) (C_3 - C_4/6 + 16C_5 + 10C_6/3), \\ & \left. + e_d t_{\parallel}(u, 0) (C_3 - C_4/6 + 16C_5 - 8C_6/3) \right] \end{aligned} \quad (\text{B30})$$

$$t_{\parallel}(u, m_q) = \frac{2M_B}{\bar{u}E} I_1(m_q) + \frac{\bar{u}M_B^2 + uq^2}{\bar{u}^2 E^2} (B_0(\bar{u}M_B^2 + uq^2, m_q) - B_0(q^2, m_q)), \quad (\text{B31})$$

$$E = \frac{M_B^2 + M_P^2 - q^2}{2M_B}, \quad (\text{B32})$$

$$I_1(m_q) = 1 + \frac{2m_q^2}{\bar{u}(M_B^2 - q^2)} \left[L_1(x_+) + L_1(x_-) - L_1(y_+) - L_1(y_-) \right], \quad (\text{B33})$$

$$L_1(x) = \ln \frac{x-1}{x} \ln(1-x) - \frac{\pi^2}{6} + \text{Li}_2 \left(\frac{x}{x-1} \right), \quad (\text{B34})$$

$$x_{\pm} = \frac{1}{2} \pm \left(\frac{1}{4} - \frac{m_q^2}{\bar{u}M_B^2 + uq^2} \right)^{1/2}, \quad (\text{B35})$$

$$y_{\pm} = \frac{1}{2} \pm \left(\frac{1}{4} - \frac{m_q^2}{q^2} \right)^{1/2}, \quad (\text{B36})$$

$$B_0(q^2, m_q) = -2 \sqrt{4m_q^2/q^2 - 1} \arctan \frac{1}{\sqrt{4m_q^2/q^2 - 1}}, \quad (\text{B37})$$

$$T_{P,-}^{(\text{nf})} = -e_q \frac{M_B \omega}{M_B \omega - q^2 - i\epsilon} \left[\frac{8 C_8^{\text{eff}}}{\bar{u} + uq^2/M_B^2} \right]$$

$$\begin{aligned}
& + \frac{6M_B}{m_b} \left(h(m_c, \bar{u}M_B^2 + uq^2) (-C_1/6 + C_2 + C_4 + 10C_6) \right. \\
& + h(m_b, \bar{u}M_B^2 + uq^2) (C_3 + 5C_4/6 + 16C_5 + 22C_6/3) \\
& + h(0, \bar{u}M_B^2 + uq^2) (C_3 + 17C_4/6 + 16C_5 + 82C_6/3) \\
& \left. - \frac{8}{27} (-15C_4/2 + 12C_5 - 32C_6) \right), \tag{B38}
\end{aligned}$$

$$C_8^{\text{eff}} = C_8 + C_3 - \frac{1}{6}C_4 + 20C_5 - \frac{10}{3}C_6, \tag{B39}$$

where $\tilde{\alpha}_s = \alpha_s/(4\pi)$, $\bar{u} = 1 - u$, $h(m_q, q^2)$ is defined in Eq. (B12), and e_q , which appears in Eq. (B29), is the charge of the spectator quark (*i.e.*, $e_q = -1/3$ for neutral B and $e_q = 2/3$ for B^\pm). The correct imaginary parts are obtained by replacing $m_q^2 \rightarrow m_q^2 - i\epsilon$. Note that in Ref. [99] the functions repeated above are given in terms of barred coefficients \bar{C}_i that are simple linear combinations of the coefficients C_i (explicit expressions that relate the two sets of coefficients are given in Appendix A of Ref. [99]). The nonfactorizable contribution $\Delta\tau_P$ in Eq. (B27) depends upon the light-cone distribution amplitudes (LCDA) of the kaon, $\Phi_K(u)$, of the pion, $\Phi_\pi(u)$, and of the B meson, $\Phi_{B,\pm}(\omega)$. It is customary to expand the kaon and pion LCDAs in terms of Gegenbauer polynomials and keep only the first few terms [206] (see Eqs. (48)–(54) in Ref. [99]):

$$\Phi_K(u) = 6u(1-u) \left[1 + a_1^K C_1^{(3/2)}(2u-1) + a_2^K C_2^{(3/2)}(2u-1) + \dots \right], \tag{B40}$$

$$\Phi_\pi(u) = 6u(1-u) \left[1 + a_2^\pi C_2^{(3/2)}(2u-1) + a_4^\pi C_4^{(3/2)}(2u-1) + \dots \right]. \tag{B41}$$

Note that a_1^π vanishes due to G -parity. The u dependence of $\Phi_P(u)$ is needed because the convolutions involve nontrivial functions of u . The first few coefficients $a_i^{\pi,K}$ have been computed in lattice QCD [206–209]. The B -meson LCDAs are known less precisely, but enter only through the first inverse moments:

$$\lambda_{B,+}^{-1} = \int_0^\infty d\omega \frac{\Phi_{B,+}(\omega)}{\omega}, \tag{B42}$$

$$\lambda_{B,-}^{-1}(q^2) = \int_0^\infty d\omega \frac{\Phi_{B,-}(\omega)}{\omega - q^2/M_B - i\epsilon}. \tag{B43}$$

Following Ref. [99], we model $\Phi_{B,+}$ and $\Phi_{B,-}$ as

$$\Phi_{B,+}(\omega) = \frac{\omega}{\omega_0^2} e^{-\omega/\omega_0}, \tag{B44}$$

$$\Phi_{B,-}(\omega) = \frac{1}{\omega_0} e^{-\omega/\omega_0}. \tag{B45}$$

The value of ω_0 can be fixed using $\lambda_{B,+}$, giving

$$\omega_0 = \lambda_{B,+}, \tag{B46}$$

$$\lambda_{B,-}^{-1}(q^2) = \frac{e^{-q^2/(M_B\lambda_{B,+})}}{\lambda_{B,+}} \left[-\text{Ei} \left(\frac{q^2}{M_B} \lambda_{B,+} \right) + i\pi \right]. \tag{B47}$$

3. Form-factor relations

We now present details on the relations between the form factors f_T and f_+ , tested in Sec. III B. At low- q^2 SCET gives [98]

$$\begin{aligned} \frac{M_B}{M_B + M_P} f_T = f_+ & \left[1 + \frac{\alpha_s}{4\pi} C_F \left(\ln \frac{m_b^2}{\mu^2} + 2L \right) \right] \\ & - \frac{\pi}{N_c} \frac{f_B f_P}{E} \alpha_s C_F \int \frac{d\omega}{\omega} \Phi_{B,+}(\omega) \int_0^1 \frac{du}{\bar{u}} \Phi_P(u), \end{aligned} \quad (\text{B48})$$

where $L = -[2E/(M_B - 2E)] \ln(2E/M_B)$. The extension of this relation to order α_s^2 is also available [210].

At high- q^2 the corresponding relation obtained from the high- q^2 OPE reads [73, 78]

$$\frac{M_B}{M_B + M_P} f_T = \frac{M_B^2}{q^2} f_+ \kappa(\mu) = \frac{M_B^2}{q^2} f_+ \left(1 + 2 \frac{D_0^{(v)}}{C_0^{(v)}} \right) \frac{m_b}{M_B}, \quad (\text{B49})$$

$$D_0^{(v)} = \frac{\alpha_s}{4\pi} C_F \left(2 \ln \frac{\mu}{m_b} + 2 \right), \quad (\text{B50})$$

$$C_0^{(v)} = 1 - \frac{\alpha_s}{4\pi} C_F \left(3 \ln \frac{\mu}{m_b} + 4 \right). \quad (\text{B51})$$

Note that we do not use these expressions, except to test them, because we take the form factors directly from lattice QCD.

4. Scale and power-correction uncertainties

Scale uncertainties are intended to account for errors introduced by truncating a perturbative expansion, and should reflect the size of omitted higher-order perturbative corrections. The standard approach for estimating such missing terms is to vary the unphysical scales: in our case we vary the two scales $\mu_b \sim m_b$ and $\mu_0 \sim m_W, m_t$. Higher-order corrections will cancel exactly the explicit dependence in the expressions for the branching ratios that we use, while the residual scale dependence will be suppressed by one more power of the strong coupling α_s . In this work we adopt the standard choices $\mu_b = 5$ GeV and $\mu_0 = \sqrt{m_W m_t} = 120$ GeV. The scale uncertainty is then obtained by varying *simultaneously* these scales by a factor of two and taking half the difference between the maximum and minimum observed values.

Uncertainties associated with power corrections are more difficult to estimate because higher-order terms in the OPE are dynamically suppressed; *i.e.*, the suppression is expected to appear in the nonperturbative calculation of the matrix elements of higher-dimensional operators. We estimate this uncertainty by varying by 10% all terms in the amplitude that are not directly proportional to $C_{9,10} f_+$ or $C_7 f_T$.

Appendix C: Numerical inputs

Here we tabulate the numerical inputs used for the Standard-Model predictions in Secs. IV and V. Table XVI provides the Wilson coefficients, while Table XVII provides the other inputs.

TABLE XVI. Numerical values of the Standard-Model Wilson coefficients used for the calculations in this work, taken from Ref. [82]. The dominant source of error in the coefficients is from the variation of the scale $\mu_{\text{low}} \in [2.5, 10]$ GeV. The scale dependencies of the coefficients in some cases are somewhat large, but are meant to cancel against the corresponding scale dependence of the matrix elements.

$C_i(\mu_b)$	value
C_1	-0.29(16)
C_2	1.009(10)
C_3	-0.0047(42)
C_4	-0.081(39)
C_5	0.00036(31)
C_6	0.00082(97)
C_7	-0.297(26)
C_8	-0.152(15)
C_9	4.04(33)
C_{10}	-4.292(73)

TABLE XVII. Numerical inputs used in the phenomenological analysis of this paper. The CKM combinations are obtained using the determinations of the Wolfenstein parameters $\{A, \lambda, \bar{\rho}, \bar{\eta}\} = \{0.810(^{+18}_{-24}), 0.22548(^{+68}_{-34}), 0.1453(^{+133}_{-73}), 0.343(^{+11}_{-12})\}$ from the CKMfitter group's global analysis including results through CKM 2014 [167]. The hadronic parameters (decay constants and light-cone distribution amplitudes) are taken from unquenched lattice-QCD calculations except for $\lambda_{B,+}$, for which lattice results are unavailable. Coupling constants, masses, and lifetimes are taken from the PDG [136] unless otherwise specified.

$\alpha_s(m_Z) = 0.1185(6)$	$\alpha_e(m_Z) = 1/127.940(18)$
$s_W^2 \equiv \sin^2 \theta_W = 0.23126(5)$	$G_F = 1.1663787(6) \times 10^{-5} \text{ GeV}^{-2}$
$m_W = 80.385(15) \text{ GeV}$	$m_Z = 91.1876(21) \text{ GeV}$
$m_e = 510.998928(11) \text{ keV}$	$m_\mu = 105.6583715(35) \text{ MeV}$
$m_\tau = 1.77682(16) \text{ GeV}$	$m_{t,\text{pole}} = 173.21(87) \text{ GeV}$
$M_{B^\pm} = 5.27926(17) \text{ GeV}$	$M_{B^0} = 5.27958(17) \text{ GeV}$
$\tau_{B^\pm} = 1.638(4) \text{ ps}$	$\tau_{B^0} = 1.519(5) \text{ ps}$
$M_{\pi^\pm} = 139.57018(35) \text{ MeV}$	$M_{\pi^0} = 134.9766(6) \text{ MeV}$
$M_{K^\pm} = 493.677(16) \text{ MeV}$	$M_{K^0} = 497.614(24) \text{ MeV}$
$m_b^{\text{pole}} = 4.91(12) \text{ GeV}$ [122]	$m_c^{\text{pole}} = 1.77(14) \text{ GeV}$ [122]
$m_b^{\overline{\text{MS}}}(m_b) = 4.18(3) \text{ GeV}$	$m_c^{\overline{\text{MS}}}(m_c) = 1.275(25) \text{ GeV}$
$ V_{ts}^* V_{tb} = 4.04(11) \times 10^{-2}$	$ V_{td}^* V_{tb} = 8.55(26) \times 10^{-3}$
$ \lambda_u^{(s)} = 0.01980(62)$	$\arg(\lambda_u^{(s)}) = 114.0(1.9)^\circ$
$ \lambda_u^{(d)} = 0.404(14)$	$\arg(\lambda_u^{(d)}) = -88.9(2.0)^\circ$
$ V_{td}/V_{ts} = 0.2115(30)$	
$f_B = 190.5(4.2) \text{ MeV}$ [211]	$f_K = 156.3(9) \text{ MeV}$ [211]
$a_1^K = 0.061(4)$ [209]	$a_2^K = 0.18(7)$ [209]
$a_2^\pi = 0.23(7)$ [209]	$\lambda_{B,+}(1.5 \text{ GeV}) = 0.51(12) \text{ GeV}$ [212–214]
$\mu_b = 5 \left(^{+5}_{-2.5}\right) \text{ GeV}$	$\mu_0 = 120 \left(^{+120}_{-60}\right) \text{ GeV}$
$\mu_f = 2 \text{ GeV}$	

-
- [1] J. L. Hewett, H. Weerts, *et al.*, *Fundamental Physics at the Intensity Frontier* (U.S. Department of Energy, 2012) [arXiv:1205.2671 \[hep-ex\]](#).
 - [2] J. Albrecht *et al.* (Charged Leptons Working Group), (2013), [arXiv:1311.5278 \[hep-ex\]](#).
 - [3] S. Dawson *et al.* (Higgs Boson Working Group), (2013), [arXiv:1310.8361 \[hep-ex\]](#).
 - [4] J. N. Butler *et al.* (Quark Flavor Physics Working Group), (2013), [arXiv:1311.1076 \[hep-ex\]](#).
 - [5] C. Bobeth, T. Ewerth, F. Krüger, and J. Urban, *Phys. Rev.* **D64**, 074014 (2001), [arXiv:hep-ph/0104284](#).
 - [6] D. A. Demir, K. A. Olive, and M. B. Voloshin, *Phys. Rev.* **D66**, 034015 (2002), [arXiv:hep-ph/0204119](#).
 - [7] S. R. Choudhury and N. Gaur, *Phys. Rev.* **D66**, 094015 (2002), [arXiv:hep-ph/0206128](#).
 - [8] J.-J. Wang, R.-M. Wang, Y.-G. Xu, and Y.-D. Yang, *Phys. Rev.* **D77**, 014017 (2008), [arXiv:0711.0321 \[hep-ph\]](#).
 - [9] G. Hiller and M. Schmaltz, *Phys. Rev.* **D90**, 054014 (2014), [arXiv:1408.1627 \[hep-ph\]](#).
 - [10] B. Gripaios, M. Nardecchia, and S. A. Renner, *JHEP* **05**, 006 (2015), [arXiv:1412.1791 \[hep-ph\]](#).
 - [11] S. Sahoo and R. Mohanta, *Phys. Rev.* **D91**, 094019 (2015), [arXiv:1501.05193 \[hep-ph\]](#).
 - [12] W.-S. Hou, M. Kohda, and F. Xu, *Phys. Rev.* **D87**, 094005 (2013), [arXiv:1302.1471 \[hep-ph\]](#).
 - [13] R. Gauld, F. Goertz, and U. Haisch, *Phys. Rev.* **D89**, 015005 (2014), [arXiv:1308.1959 \[hep-ph\]](#).
 - [14] A. J. Buras and J. Girrbach, *JHEP* **1312**, 009 (2013), [arXiv:1309.2466 \[hep-ph\]](#).
 - [15] R. Gauld, F. Goertz, and U. Haisch, *JHEP* **1401**, 069 (2014), [arXiv:1310.1082 \[hep-ph\]](#).
 - [16] A. J. Buras, F. De Fazio, and J. Girrbach, *JHEP* **1402**, 112 (2014), [arXiv:1311.6729 \[hep-ph\]](#).
 - [17] W. Altmannshofer, S. Gori, M. Pospelov, and I. Yavin, *Phys. Rev.* **D89**, 095033 (2014), [arXiv:1403.1269 \[hep-ph\]](#).
 - [18] A. J. Buras, J. Girrbach-Noe, C. Niehoff, and D. M. Straub, *JHEP* **1502**, 184 (2015), [arXiv:1409.4557 \[hep-ph\]](#).
 - [19] A. Crivellin, G. D'Ambrosio, and J. Heeck, *Phys. Rev. Lett.* **114**, 151801 (2015), [arXiv:1501.00993 \[hep-ph\]](#).
 - [20] A. Crivellin, G. D'Ambrosio, and J. Heeck, *Phys. Rev.* **D91**, 075006 (2015), [arXiv:1503.03477 \[hep-ph\]](#).
 - [21] T. M. Aliev and M. Savci, *Phys. Rev.* **D60**, 014005 (1999), [arXiv:hep-ph/9812272](#).
 - [22] E. O. Iltan, *Int. J. Mod. Phys.* **A14**, 4365 (1999), [arXiv:hep-ph/9807256](#).
 - [23] G. Erkol and G. Turan, *JHEP* **0202**, 015 (2002), [arXiv:hep-ph/0201055](#).
 - [24] G. Erkol, J. W. Wagenaar, and G. Turan, *Eur. Phys. J.* **C41**, 189 (2005), [arXiv:hep-ph/0408186](#).
 - [25] H.-Z. Song, L.-X. Lü, and G.-R. Lu, *Commun. Theor. Phys.* **50**, 696 (2008).
 - [26] C.-H. Chen and C.-Q. Geng, *JHEP* **0610**, 053 (2006), [arXiv:hep-ph/0608166](#).
 - [27] U. Nierste, S. Trine, and S. Westhoff, *Phys. Rev.* **D78**, 015006 (2008), [arXiv:0801.4938 \[hep-ph\]](#).
 - [28] M. Tanaka and R. Watanabe, *Phys. Rev.* **D82**, 034027 (2010), [arXiv:1005.4306 \[hep-ph\]](#).
 - [29] A. Crivellin, C. Greub, and A. Kokulu, *Phys. Rev.* **D86**, 054014 (2012), [arXiv:1206.2634 \[hep-ph\]](#).
 - [30] Y. Sakaki and H. Tanaka, *Phys. Rev.* **D87**, 054002 (2013), [arXiv:1205.4908 \[hep-ph\]](#).

- [31] A. Celis, M. Jung, X.-Q. Li, and A. Pich, *JHEP* **1301**, 054 (2013), [arXiv:1210.8443 \[hep-ph\]](#).
- [32] A. Crivellin, *Phys. Rev.* **D81**, 031301 (2010), [arXiv:0907.2461 \[hep-ph\]](#).
- [33] R. Feger, T. Mannel, V. Klose, H. Lacker, and T. Lück, *Phys. Rev.* **D82**, 073002 (2010), [arXiv:1003.4022 \[hep-ph\]](#).
- [34] F. U. Bernlochner, Z. Ligeti, and S. Turczyk, *Phys. Rev.* **D90**, 094003 (2014), [arXiv:1408.2516 \[hep-ph\]](#).
- [35] A. J. Buras and J. Girrbach, *Rept. Prog. Phys.* **77**, 086201 (2014), [arXiv:1306.3775 \[hep-ph\]](#).
- [36] W. Altmannshofer and D. M. Straub, in *50th Rencontres de Moriond on Electroweak Interactions and Unified Theories* (2015) [arXiv:1503.06199 \[hep-ph\]](#).
- [37] J. P. Lees *et al.* (BaBar Collaboration), *Phys. Rev. Lett.* **109**, 101802 (2012), [arXiv:1205.5442 \[hep-ex\]](#).
- [38] J. A. Bailey *et al.* (Fermilab Lattice and MILC Collaborations), *Phys. Rev. Lett.* **109**, 071802 (2012), [arXiv:1206.4992 \[hep-ph\]](#).
- [39] M. Huschle *et al.* (Belle Collaboration), *Phys. Rev.* **D92**, 072014 (2015), [arXiv:1507.03233 \[hep-ex\]](#).
- [40] R. Aaij *et al.* (LHCb Collaboration), *Phys. Rev. Lett.* **115**, 111803 (2015), [arXiv:1506.08614 \[hep-ex\]](#).
- [41] Y. Amhis *et al.* (Heavy Flavor Averaging Group), (2014), [arXiv:1412.7515 \[hep-ex\]](#).
- [42] R. Aaij *et al.* (LHCb Collaboration), *Phys. Rev. Lett.* **113**, 151601 (2014), [arXiv:1406.6482 \[hep-ex\]](#).
- [43] C. Bouchard, G. P. Lepage, C. Monahan, H. Na, and J. Shigemitsu (HPQCD Collaboration), *Phys. Rev. Lett.* **111**, 162002 (2013), (E) *Phys. Rev. Lett.* **112**, 149902 (2013), [arXiv:1306.0434 \[hep-ph\]](#).
- [44] R. R. Horgan, Z. Liu, S. Meinel, and M. Wingate, *Phys. Rev. Lett.* **112**, 212003 (2014), [arXiv:1310.3887 \[hep-ph\]](#).
- [45] R. Aaij *et al.* (LHCb Collaboration), *JHEP* **1406**, 133 (2014), [arXiv:1403.8044 \[hep-ex\]](#).
- [46] R. Aaij *et al.* (LHCb Collaboration), *Phys. Rev. Lett.* **111**, 191801 (2013), [arXiv:1308.1707 \[hep-ex\]](#).
- [47] C. Langenbruch (LHCb Collaboration), in *50th Rencontres de Moriond on Electroweak Interactions and Unified Theories* (2015) [arXiv:1505.04160 \[hep-ex\]](#).
- [48] J. A. Bailey *et al.* (Fermilab Lattice and MILC Collaborations), *Phys. Rev.* **D92**, 014024 (2015), [arXiv:1503.07839 \[hep-lat\]](#).
- [49] J. A. Bailey *et al.* (Fermilab Lattice and MILC Collaborations), *Phys. Rev.* **D92**, 034506 (2015), [arXiv:1503.07237 \[hep-lat\]](#).
- [50] H. Na, C. M. Bouchard, G. P. Lepage, C. Monahan, and J. Shigemitsu (HPQCD Collaboration), *Phys. Rev.* **D92**, 054510 (2015), [arXiv:1505.03925 \[hep-lat\]](#).
- [51] W. Detmold, C. Lehner, and S. Meinel, *Phys. Rev.* **D92**, 034503 (2015), [arXiv:1503.01421 \[hep-lat\]](#).
- [52] R. Glattauer (Belle Collaboration), “Semileptonic B and B_s decays at Belle,” talk presented at [EPS-HEP 2015](#) (2015).
- [53] P. Gambino, “ V_{cb} and V_{ub} : Where do we stand?” talk presented at [EPS-HEP 2015](#) (2015).
- [54] A. Alberti, P. Gambino, K. J. Healey, and S. Nandi, *Phys. Rev. Lett.* **114**, 061802 (2015), [arXiv:1411.6560 \[hep-ph\]](#).
- [55] R. Aaij *et al.* (LHCb Collaboration), *JHEP* **10**, 034 (2015), [arXiv:1509.00414 \[hep-ex\]](#).
- [56] P. Hamer *et al.* (Belle Collaboration), (2015), [arXiv:1509.06521 \[hep-ex\]](#).

- [57] T. Aushev *et al.*, “Physics at Super B Factory,” KEK report (2010), [arXiv:1002.5012 \[hep-ex\]](#).
- [58] B. Aubert *et al.* (BaBar), [Phys. Rev. **D81**, 051101 \(2010\)](#), [arXiv:0912.2453 \[hep-ex\]](#).
- [59] J. P. Lees *et al.* (BaBar), [Phys. Rev. **D88**, 031102 \(2013\)](#), [arXiv:1207.0698 \[hep-ex\]](#).
- [60] I. Adachi *et al.* (Belle), [Phys. Rev. Lett. **110**, 131801 \(2013\)](#), [arXiv:1208.4678 \[hep-ex\]](#).
- [61] B. Kronenbitter *et al.* (Belle), [Phys. Rev. **D92**, 051102 \(2015\)](#), [arXiv:1503.05613 \[hep-ex\]](#).
- [62] J. A. Bailey *et al.* (Fermilab Lattice and MILC Collaborations), (2015), [arXiv:1509.06235 \[hep-lat\]](#).
- [63] J. A. Bailey *et al.* (Fermilab Lattice and MILC Collaborations), [Phys. Rev. Lett. **115**, 152002 \(2015\)](#), [arXiv:1507.01618 \[hep-ph\]](#).
- [64] C. Bouchard, G. P. Lepage, C. Monahan, H. Na, and J. Shigemitsu (HPQCD Collaboration), [Phys. Rev. **D88**, 054509 \(2013\)](#), [arXiv:1306.2384 \[hep-lat\]](#).
- [65] J. A. Bailey *et al.* (Fermilab Lattice and MILC Collaborations), [Phys. Rev. **D79**, 054507 \(2009\)](#), [arXiv:0811.3640 \[hep-lat\]](#).
- [66] J. M. Flynn *et al.* (RBC and UKQCD Collaborations), [Phys. Rev. **D91**, 074510 \(2015\)](#), [arXiv:1501.05373 \[hep-lat\]](#).
- [67] P. del Amo Sanchez *et al.* (BaBar Collaboration), [Phys. Rev. **D83**, 032007 \(2011\)](#), [arXiv:1005.3288 \[hep-ex\]](#).
- [68] H. Ha *et al.* (Belle Collaboration), [Phys. Rev. **D83**, 071101 \(2011\)](#), [arXiv:1012.0090 \[hep-ex\]](#).
- [69] J. P. Lees *et al.* (BaBar Collaboration), [Phys. Rev. **D86**, 092004 \(2012\)](#), [arXiv:1208.1253 \[hep-ex\]](#).
- [70] A. Sibidanov *et al.* (Belle Collaboration), [Phys. Rev. **D88**, 032005 \(2013\)](#), [arXiv:1306.2781 \[hep-ex\]](#).
- [71] R. R. Horgan, Z. Liu, S. Meinel, and M. Wingate, [Phys. Rev. **D89**, 094501 \(2014\)](#), [arXiv:1310.3722 \[hep-lat\]](#).
- [72] R. A. Briceño, M. T. Hansen, and A. Walker-Loud, [Phys. Rev. **D91**, 034501 \(2015\)](#), [arXiv:1406.5965 \[hep-lat\]](#).
- [73] B. Grinstein and D. Pirjol, [Phys. Rev. **D70**, 114005 \(2004\)](#), [arXiv:hep-ph/0404250](#).
- [74] T. Becher, R. J. Hill, and M. Neubert, [Phys. Rev. **D72**, 094017 \(2005\)](#), [arXiv:hep-ph/0503263](#).
- [75] A. Ali, B. D. Pecjak, and C. Greub, [Eur. Phys. J. **C55**, 577 \(2008\)](#), [arXiv:0709.4422 \[hep-ph\]](#).
- [76] C. Bobeth, G. Hiller, and D. van Dyk, [JHEP **1007**, 098 \(2010\)](#), [arXiv:1006.5013 \[hep-ph\]](#).
- [77] M. Beylich, G. Buchalla, and T. Feldmann, [Eur. Phys. J. **C71**, 1635 \(2011\)](#), [arXiv:1101.5118 \[hep-ph\]](#).
- [78] C. Bobeth, G. Hiller, D. van Dyk, and C. Wacker, [JHEP **1201**, 107 \(2012\)](#), [arXiv:1111.2558 \[hep-ph\]](#).
- [79] W.-S. Hou, M. Kohda, and F. Xu, [Phys. Rev. **D90**, 013002 \(2014\)](#), [arXiv:1403.7410 \[hep-ph\]](#).
- [80] B. Grinstein, M. J. Savage, and M. B. Wise, [Nucl. Phys. **B319**, 271 \(1989\)](#).
- [81] A. J. Buras, M. Misiak, M. Münz, and S. Pokorski, [Nucl. Phys. **B424**, 374 \(1994\)](#), [arXiv:hep-ph/9311345](#).
- [82] T. Huber, E. Lunghi, M. Misiak, and D. Wyler, [Nucl. Phys. **B740**, 105 \(2006\)](#), [arXiv:hep-ph/0512066](#).
- [83] W. Altmannshofer, P. Ball, A. Bharucha, A. J. Buras, D. M. Straub, and M. Wick, [JHEP **0901**, 019 \(2009\)](#), [arXiv:0811.1214 \[hep-ph\]](#).
- [84] M. Misiak, [Nucl. Phys. **B393**, 23 \(1993\)](#).
- [85] A. J. Buras and M. Münz, [Phys. Rev. **D52**, 186 \(1995\)](#), [arXiv:hep-ph/9501281](#).

- [86] R. Aaij *et al.* (LHCb), *Phys. Rev. Lett.* **111**, 112003 (2013), [arXiv:1307.7595 \[hep-ex\]](#).
- [87] A. Khodjamirian, T. Mannel, and Y. M. Wang, *JHEP* **02**, 010 (2013), [arXiv:1211.0234 \[hep-ph\]](#).
- [88] C. Hambrock, A. Khodjamirian, and A. Rusov, *Phys. Rev.* **D92**, 074020 (2015), [arXiv:1506.07760 \[hep-ph\]](#).
- [89] A. Khodjamirian, T. Mannel, A. A. Pivovarov, and Y.-M. Wang, *JHEP* **1009**, 089 (2010), [arXiv:1006.4945 \[hep-ph\]](#).
- [90] C. Bobeth, G. Hiller, and D. van Dyk, *JHEP* **1107**, 067 (2011), [arXiv:1105.0376 \[hep-ph\]](#).
- [91] C. Bobeth, G. Hiller, and D. van Dyk, *Phys. Rev.* **D87**, 034016 (2013), [arXiv:1212.2321 \[hep-ph\]](#).
- [92] B. Grinstein and D. Pirjol, *Phys. Lett.* **B533**, 8 (2002), [arXiv:hep-ph/0201298](#).
- [93] J. L. Hewett *et al.*, eds., *The Discovery potential of a Super B Factory* (SLAC, Menlo Park, 2004) [arXiv:hep-ph/0503261](#).
- [94] M. Beneke, G. Buchalla, M. Neubert, and C. T. Sachrajda, *Phys. Rev. Lett.* **83**, 1914 (1999), [arXiv:hep-ph/9905312](#).
- [95] M. Beneke, G. Buchalla, M. Neubert, and C. T. Sachrajda, *Nucl. Phys.* **B591**, 313 (2000), [arXiv:hep-ph/0006124](#).
- [96] C. W. Bauer, S. Fleming, D. Pirjol, and I. W. Stewart, *Phys. Rev.* **D63**, 114020 (2001), [arXiv:hep-ph/0011336](#).
- [97] C. W. Bauer, D. Pirjol, and I. W. Stewart, *Phys. Rev.* **D65**, 054022 (2002), [arXiv:hep-ph/0109045](#).
- [98] M. Beneke and T. Feldmann, *Nucl. Phys.* **B592**, 3 (2001), [arXiv:hep-ph/0008255](#).
- [99] M. Beneke, T. Feldmann, and D. Seidel, *Nucl. Phys.* **B612**, 25 (2001), [arXiv:hep-ph/0106067](#).
- [100] C. Bobeth, G. Hiller, and G. Piranishvili, *JHEP* **0712**, 040 (2007), [arXiv:0709.4174 \[hep-ph\]](#).
- [101] G. Buchalla and A. J. Buras, *Nucl. Phys.* **B400**, 225 (1993).
- [102] M. Misiak and J. Urban, *Phys. Lett.* **B451**, 161 (1999), [arXiv:hep-ph/9901278](#).
- [103] G. Buchalla and A. J. Buras, *Nucl. Phys.* **B548**, 309 (1999), [arXiv:hep-ph/9901288](#).
- [104] J. Brod, M. Gorbahn, and E. Stamou, *Phys. Rev.* **D83**, 034030 (2011), [arXiv:1009.0947 \[hep-ph\]](#).
- [105] W. Altmannshofer, A. J. Buras, D. M. Straub, and M. Wick, *JHEP* **0904**, 022 (2009), [arXiv:0902.0160 \[hep-ph\]](#).
- [106] J. F. Kamenik and C. Smith, *Phys. Lett.* **B680**, 471 (2009), [arXiv:0908.1174 \[hep-ph\]](#).
- [107] J. L. Rosner, S. Stone, and R. S. Van de Water, (2015), [arXiv:1509.02220 \[hep-ph\]](#).
- [108] A. Bazavov *et al.* (Fermilab Lattice and MILC Collaborations), *Phys. Rev.* **D85**, 114506 (2012), [arXiv:1112.3051 \[hep-lat\]](#).
- [109] H. Na, C. J. Monahan, C. T. H. Davies, R. Horgan, G. P. Lepage, and J. Shigemitsu (HPQCD Collaboration), *Phys. Rev.* **D86**, 034506 (2012), [arXiv:1202.4914 \[hep-lat\]](#).
- [110] R. J. Dowdall, C. T. H. Davies, R. R. Horgan, C. J. Monahan, and J. Shigemitsu (HPQCD Collaboration), *Phys. Rev. Lett.* **110**, 222003 (2013), [arXiv:1302.2644 \[hep-lat\]](#).
- [111] N. Carrasco *et al.* (ETM Collaboration), PoS **LATTICE2013**, 313 (2014), [arXiv:1311.2837 \[hep-lat\]](#).
- [112] N. H. Christ, J. M. Flynn, T. Izubuchi, T. Kawanai, C. Lehner, A. Soni, R. S. Van de Water, and O. Witzel (RBC and UKQCD Collaborations), *Phys. Rev.* **D91**, 054502 (2015), [arXiv:1404.4670 \[hep-lat\]](#).

- [113] Y. Aoki, T. Ishikawa, T. Izubuchi, C. Lehner, and A. Soni, *Phys. Rev.* **D91**, 114505 (2015), [arXiv:1406.6192 \[hep-lat\]](#).
- [114] E. Follana, C. T. H. Davies, G. P. Lepage, and J. Shigemitsu (HPQCD, UKQCD), *Phys. Rev. Lett.* **100**, 062002 (2008), [arXiv:0706.1726 \[hep-lat\]](#).
- [115] S. Dürr, Z. Fodor, C. Hoelbling, S. D. Katz, S. Krieg, T. Kurth, L. Lellouch, T. Lippert, A. Ramos, and K. K. Szabo (Budapest-Marseille-Wuppertal Collaboration), *Phys. Rev.* **D81**, 054507 (2010), [arXiv:1001.4692 \[hep-lat\]](#).
- [116] A. Bazavov *et al.* (MILC), *Proceedings, 28th International Symposium on Lattice field theory (Lattice 2010)*, PoS **LATTICE2010**, 074 (2010), [arXiv:1012.0868 \[hep-lat\]](#).
- [117] J. Laiho and R. S. Van de Water, *Proceedings, 29th International Symposium on Lattice field theory (Lattice 2011)*, PoS **LATTICE2011**, 293 (2011), [arXiv:1112.4861 \[hep-lat\]](#).
- [118] R. Arthur *et al.* (RBC/UKQCD), *Phys. Rev.* **D87**, 094514 (2013), [arXiv:1208.4412 \[hep-lat\]](#).
- [119] R. Dowdall, C. Davies, G. Lepage, and C. McNeile (HPQCD), *Phys. Rev.* **D88**, 074504 (2013), [arXiv:1303.1670 \[hep-lat\]](#).
- [120] A. Bazavov *et al.* (Fermilab Lattice and MILC), *Phys. Rev.* **D90**, 074509 (2014), [arXiv:1407.3772 \[hep-lat\]](#).
- [121] N. Carrasco *et al.* (ETM), *Phys. Rev.* **D91**, 054507 (2015), [arXiv:1411.7908 \[hep-lat\]](#).
- [122] A. Ali, A. Y. Parkhomenko, and A. V. Rusov, *Phys. Rev.* **D89**, 094021 (2014), [arXiv:1312.2523 \[hep-ph\]](#).
- [123] C. W. Bernard *et al.*, *Phys. Rev.* **D64**, 054506 (2001), [arXiv:hep-lat/0104002](#).
- [124] C. Aubin *et al.*, *Phys. Rev.* **D70**, 094505 (2004), [arXiv:hep-lat/0402030 \[hep-lat\]](#).
- [125] A. Bazavov *et al.*, *Rev. Mod. Phys.* **82**, 1349 (2010), [arXiv:0903.3598 \[hep-lat\]](#).
- [126] A. X. El-Khadra, A. S. Kronfeld, and P. B. Mackenzie, *Phys. Rev.* **D55**, 3933 (1997), [arXiv:hep-lat/9604004](#).
- [127] A. X. El-Khadra, A. S. Kronfeld, P. B. Mackenzie, S. M. Ryan, and J. N. Simone, *Phys. Rev.* **D64**, 014502 (2001), [arXiv:hep-ph/0101023](#).
- [128] D. Bećirević, S. Prelovšek, and J. Zupan, *Phys. Rev.* **D67**, 054010 (2003), [arXiv:hep-lat/0210048](#).
- [129] C. Aubin and C. Bernard, *Phys. Rev.* **D76**, 014002 (2007), [arXiv:0704.0795 \[hep-lat\]](#).
- [130] J. Bijnens and I. Jemos, *Nucl. Phys.* **B840**, 54 (2010), [arXiv:1006.1197 \[hep-ph\]](#).
- [131] A. S. Kronfeld, *Phys. Rev.* **D62**, 014505 (2000), [arXiv:hep-lat/0002008](#).
- [132] J. Harada, S. Hashimoto, K.-I. Ishikawa, A. S. Kronfeld, T. Onogi, and N. Yamada, *Phys. Rev.* **D65**, 094513 (2002), [arXiv:hep-lat/0112044](#).
- [133] M. B. Oktay and A. S. Kronfeld, *Phys. Rev.* **D78**, 014504 (2008), [arXiv:0803.0523 \[hep-lat\]](#).
- [134] C. G. Boyd, B. Grinstein, and R. F. Lebed, *Phys. Rev. Lett.* **74**, 4603 (1995), [arXiv:hep-ph/9412324](#).
- [135] C. Bourrely, I. Caprini, and L. Lellouch, *Phys. Rev.* **D79**, 013008 (2009), [arXiv:0807.2722 \[hep-ph\]](#).
- [136] K. A. Olive *et al.* (Particle Data Group), *Chin. Phys.* **C38**, 090001 (2014).
- [137] C. B. Lang, D. Mohler, S. Prelovšek, and R. M. Woloshyn, *Phys. Lett.* **B750**, 17 (2015), [arXiv:1501.01646 \[hep-lat\]](#).
- [138] N. Isgur and M. B. Wise, *Phys. Rev.* **D42**, 2388 (1990).
- [139] G. Burdman and J. F. Donoghue, *Phys. Lett.* **B270**, 55 (1991).
- [140] J. Charles, A. Le Yaouanc, L. Oliver, O. Pene, and J. C. Raynal, *Phys. Rev.* **D60**, 014001 (1999), [arXiv:hep-ph/9812358](#).
- [141] B. Bajc, S. Fajfer, and R. J. Oakes, (1996), [arXiv:hep-ph/9612276](#).

- [142] E. Gulez, A. Gray, M. Wingate, C. T. H. Davies, G. P. Lepage, and J. Shigemitsu (HPQCD Collaboration), *Phys. Rev.* **D73**, 074502 (2006), (E) *Phys. Rev.* **D75**, 119906 (2007), [arXiv:hep-lat/0601021](#).
- [143] C. Bouchard, G. P. Lepage, C. Monahan, H. Na, and J. Shigemitsu (HPQCD Collaboration), *Phys. Rev.* **D88**, 054509 (2013), (E) *Phys. Rev.* **D88**, 079901 (2013), [arXiv:1306.2384 \[hep-lat\]](#).
- [144] J. M. Flynn, P. Fritzsche, T. Kawanai, C. Lehner, B. Samways, C. T. Sachrajda, R. S. Van de Water, and O. Witzel (RBC and UKQCD Collaborations), (2015), [arXiv:1506.06413 \[hep-lat\]](#).
- [145] T. Tekampe (LHCb Collaboration), “First measurement of the differential branching fraction and CP asymmetry of the $B^+ \rightarrow \pi^+ \mu^+ \mu^-$ decay,” [talk presented at DPF 2015](#) (2015).
- [146] J.-T. Wei *et al.* (Belle Collaboration), *Phys. Rev. Lett.* **103**, 171801 (2009), [arXiv:0904.0770 \[hep-ex\]](#).
- [147] T. Aaltonen *et al.* (CDF Collaboration), *Phys. Rev. Lett.* **107**, 201802 (2011), [arXiv:1107.3753 \[hep-ex\]](#).
- [148] J. P. Lees *et al.* (BaBar Collaboration), *Phys. Rev.* **D86**, 032012 (2012), [arXiv:1204.3933 \[hep-ex\]](#).
- [149] J. Lyon and R. Zwicky, (2014), [arXiv:1406.0566 \[hep-ph\]](#).
- [150] R. Aaij *et al.* (LHCb Collaboration), *JHEP* **1302**, 105 (2013), [arXiv:1209.4284 \[hep-ex\]](#).
- [151] R. Aaij *et al.* (LHCb Collaboration), *JHEP* **1212**, 125 (2012), [arXiv:1210.2645 \[hep-ex\]](#).
- [152] W. Altmannshofer and D. M. Straub, *Eur. Phys. J.* **C73**, 2646 (2013), [arXiv:1308.1501 \[hep-ph\]](#).
- [153] A. Datta, M. Duraisamy, and D. Ghosh, *Phys. Rev.* **D89**, 071501 (2014), [arXiv:1310.1937 \[hep-ph\]](#).
- [154] S. Biswas, D. Chowdhury, S. Han, and S. J. Lee, *JHEP* **02**, 142 (2015), [arXiv:1409.0882 \[hep-ph\]](#).
- [155] S. L. Glashow, D. Guadagnoli, and K. Lane, *Phys. Rev. Lett.* **114**, 091801 (2015), [arXiv:1411.0565 \[hep-ph\]](#).
- [156] G. Hiller and F. Krüger, *Phys. Rev.* **D69**, 074020 (2004), [arXiv:hep-ph/0310219](#).
- [157] J. P. Lees *et al.* (BaBar Collaboration), *Phys. Rev.* **D87**, 112005 (2013), [arXiv:1303.7465 \[hep-ex\]](#).
- [158] O. Lutz *et al.* (Belle Collaboration), *Phys. Rev.* **D87**, 111103 (2013), [arXiv:1303.3719 \[hep-ex\]](#).
- [159] W.-F. Wang and Z.-J. Xiao, *Phys. Rev.* **D86**, 114025 (2012), [arXiv:1207.0265 \[hep-ph\]](#).
- [160] A. Bharucha, D. M. Straub, and R. Zwicky, (2015), [arXiv:1503.05534 \[hep-ph\]](#).
- [161] A. Khodjamirian, T. Mannel, N. Offen, and Y. M. Wang, *Phys. Rev.* **D83**, 094031 (2011), [arXiv:1103.2655 \[hep-ph\]](#).
- [162] R. Dutta, A. Bhol, and A. K. Giri, *Phys. Rev.* **D88**, 114023 (2013), [arXiv:1307.6653 \[hep-ph\]](#).
- [163] Y.-M. Wang and Y.-L. Shen, *Nucl. Phys.* **B898**, 563 (2015), [arXiv:1506.00667 \[hep-ph\]](#).
- [164] S. Fajfer, J. F. Kamenik, I. Nisandzic, and J. Zupan, *Phys. Rev. Lett.* **109**, 161801 (2012), [arXiv:1206.1872 \[hep-ph\]](#).
- [165] A. J. Bevan *et al.* (Belle and BaBar Collaborations), *Eur. Phys. J.* **C74**, 3026 (2014), [arXiv:1406.6311 \[hep-ex\]](#).
- [166] P. Ball and R. Zwicky, *Phys. Rev.* **D71**, 014015 (2005), [arXiv:hep-ph/0406232](#).
- [167] J. Charles *et al.* (CKMfitter Group), *Eur. Phys. J.* **C41**, 1 (2005), [arXiv:hep-ph/0406184](#).

- [168] E. Gámiz, C. T. H. Davies, G. P. Lepage, J. Shigemitsu, and M. Wingate (HPQCD Collaboration), *Phys. Rev.* **D80**, 014503 (2009), [arXiv:0902.1815 \[hep-lat\]](#).
- [169] A. Bazavov *et al.* (Fermilab Lattice and MILC Collaborations), *Phys. Rev.* **D86**, 034503 (2012), [arXiv:1205.7013 \[hep-lat\]](#).
- [170] R. J. Dowdall, C. T. H. Davies, R. R. Horgan, G. P. Lepage, C. J. Monahan, and J. Shigemitsu (HPQCD Collaboration), *PoS LATTICE2014*, 373 (2014), [arXiv:1411.6989 \[hep-lat\]](#).
- [171] C. M. Bouchard, E. Freeland, C. W. Bernard, C. C. Chang, A. X. El-Khadra, M. E. Gmiz, A. S. Kronfeld, J. Laiho, and R. S. Van de Water (Fermilab Lattice and MILC Collaborations), *PoS LATTICE2014*, 378 (2014), [arXiv:1412.5097 \[hep-lat\]](#).
- [172] J. A. Bailey *et al.* (Fermilab Lattice and MILC Collaborations), *Phys. Rev.* **D89**, 114504 (2014), [arXiv:1403.0635 \[hep-lat\]](#).
- [173] M. Misiak *et al.*, *Phys. Rev. Lett.* **114**, 221801 (2015), [arXiv:1503.01789 \[hep-ph\]](#).
- [174] T. Huber, T. Hurth, and E. Lunghi, *JHEP* **06**, 176 (2015), [arXiv:1503.04849 \[hep-ph\]](#).
- [175] J. P. Lees *et al.* (BaBar Collaboration), *Phys. Rev. Lett.* **112**, 211802 (2014), [arXiv:1312.5364 \[hep-ex\]](#).
- [176] B. Aubert *et al.* (BaBar Collaboration), *Phys. Rev. Lett.* **93**, 081802 (2004), [arXiv:hep-ex/0404006 \[hep-ex\]](#).
- [177] M. Iwasaki *et al.* (Belle Collaboration), *Phys. Rev.* **D72**, 092005 (2005), [arXiv:hep-ex/0503044 \[hep-ex\]](#).
- [178] S. Descotes-Genon, J. Matias, and J. Virto, *Phys. Rev.* **D88**, 074002 (2013), [arXiv:1307.5683 \[hep-ph\]](#).
- [179] F. Beaujean, C. Bobeth, and D. van Dyk, *Eur. Phys. J.* **C74**, 2897 (2014), (E) *Eur. Phys. J.* **C74**, 3179 (2014), [arXiv:1310.2478 \[hep-ph\]](#).
- [180] S. Descotes-Genon, J. Matias, and J. Virto, *PoS EPS-HEP2013*, 361 (2013), [arXiv:1311.3876 \[hep-ph\]](#).
- [181] T. Hurth and F. Mahmoudi, *JHEP* **04**, 097 (2014), [arXiv:1312.5267 \[hep-ph\]](#).
- [182] S. Descotes-Genon, L. Hofer, J. Matias, and J. Virto, *JHEP* **12**, 125 (2014), [arXiv:1407.8526 \[hep-ph\]](#).
- [183] T. Hurth, F. Mahmoudi, and S. Neshatpour, *JHEP* **12**, 053 (2014), [arXiv:1410.4545 \[hep-ph\]](#).
- [184] S. Descotes-Genon, L. Hofer, J. Matias, and J. Virto, (2014), [arXiv:1411.0922 \[hep-ph\]](#).
- [185] G. Hiller and M. Schmaltz, *JHEP* **02**, 055 (2015), [arXiv:1411.4773 \[hep-ph\]](#).
- [186] S. Descotes-Genon, L. Hofer, J. Matias, and J. Virto, *J. Phys. Conf. Ser.* **631**, 012027 (2015), [arXiv:1503.03328 \[hep-ph\]](#).
- [187] C. McNeile, C. T. H. Davies, E. Follana, K. Hornbostel, and G. P. Lepage (HPQCD Collaboration), *Phys. Rev.* **D85**, 031503 (2012), [arXiv:1110.4510 \[hep-lat\]](#).
- [188] C. Bobeth, M. Gorbahn, T. Hermann, M. Misiak, E. Stamou, and M. Steinhauser, *Phys. Rev. Lett.* **112**, 101801 (2014), [arXiv:1311.0903 \[hep-ph\]](#).
- [189] R. Fleischer, *Int. J. Mod. Phys.* **A29**, 1444004 (2014), [arXiv:1407.0916 \[hep-ph\]](#).
- [190] V. Khachatryan *et al.* (LHCb and CMS Collaborations), *Nature* **522**, 68 (2015), [arXiv:1411.4413 \[hep-ex\]](#).
- [191] M. Antonelli *et al.*, *Phys. Rept.* **494**, 197 (2010), [arXiv:0907.5386 \[hep-ph\]](#).
- [192] C. M. Bouchard, G. P. Lepage, C. J. Monahan, H. Na, and J. Shigemitsu (HPQCD Collaboration), *PoS LATTICE2013*, 387 (2014), [arXiv:1310.3207 \[hep-lat\]](#).
- [193] S. Dürr, Z. Fodor, C. Hoelbling, S. D. Katz, S. Krieg, T. Kurth, L. Lellouch, T. Lippert, K. K. Szabo, and G. Vulvert (Budapest-Marseille-Wuppertal Collaboration), *JHEP* **08**, 148

- (2011), [arXiv:1011.2711 \[hep-lat\]](#).
- [194] M. Bruno *et al.*, **JHEP** **02**, 043 (2015), [arXiv:1411.3982 \[hep-lat\]](#).
 - [195] T. Blum *et al.* (RBC and UKQCD Collaborations), (2014), [arXiv:1411.7017 \[hep-lat\]](#).
 - [196] A. Bazavov *et al.* (MILC Collaboration), (2015), [arXiv:1503.02769 \[hep-lat\]](#).
 - [197] A. Bazavov *et al.* (MILC Collaboration), **Phys. Rev.** **D82**, 074501 (2010), [arXiv:1004.0342 \[hep-lat\]](#).
 - [198] E. Follana, Q. Mason, C. Davies, K. Hornbostel, G. P. Lepage, J. Shigemitsu, H. Trottier, and K. Wong (HPQCD Collaboration), **Phys. Rev.** **D75**, 054502 (2007), [arXiv:hep-lat/0610092 \[hep-lat\]](#).
 - [199] H. H. Asatryan, H. M. Asatrian, C. Greub, and M. Walker, **Phys. Lett.** **B507**, 162 (2001), [arXiv:hep-ph/0103087](#).
 - [200] H. H. Asatryan, H. M. Asatrian, C. Greub, and M. Walker, **Phys. Rev.** **D65**, 074004 (2002), [arXiv:hep-ph/0109140](#).
 - [201] H. M. Asatrian, K. Bieri, C. Greub, and M. Walker, **Phys. Rev.** **D69**, 074007 (2004), [arXiv:hep-ph/0312063](#).
 - [202] D. Seidel, **Phys. Rev.** **D70**, 094038 (2004), [arXiv:hep-ph/0403185](#).
 - [203] M. Beneke, T. Feldmann, and D. Seidel, **Eur. Phys. J.** **C41**, 173 (2005), [arXiv:hep-ph/0412400](#).
 - [204] C. Greub, V. Pilipp, and C. Schupbach, **JHEP** **0812**, 040 (2008), [arXiv:0810.4077 \[hep-ph\]](#).
 - [205] A. J. Buras, in *Probing the standard model of particle interactions*, edited by R. Gupta, A. Morel, E. de Rafael, and F. David (North Holland, Amsterdam, 1999) pp. 281–539, [arXiv:hep-ph/9806471](#).
 - [206] V. M. Braun, S. Collins, M. Göckeler, P. Pérez-Rubio, A. Schäfer, R. W. Schiel, and A. Sternbeck (QCDSF Collaboration), **Phys. Rev.** **D92**, 014504 (2015), [arXiv:1503.03656 \[hep-lat\]](#).
 - [207] V. M. Braun *et al.* (QCDSF and UKQCD Collaborations), **Phys. Rev.** **D74**, 074501 (2006), [arXiv:hep-lat/0606012](#).
 - [208] P. A. Boyle, M. A. Donnellan, J. M. Flynn, A. Jüttner, J. Noaki, C. T. Sachrajda, and R. J. Tweedie (UKQCD Collaboration), **Phys. Lett.** **B641**, 67 (2006), [arXiv:hep-lat/0607018](#).
 - [209] R. Arthur *et al.* (RBC and UKQCD Collaborations), **Phys. Rev.** **D83**, 074505 (2011), [arXiv:1011.5906 \[hep-lat\]](#).
 - [210] G. Bell, M. Beneke, T. Huber, and X.-Q. Li, **Nucl. Phys.** **B843**, 143 (2011), [arXiv:1007.3758 \[hep-ph\]](#).
 - [211] S. Aoki *et al.* (Flavor Lattice Averaging Group), **Eur. Phys. J.** **C74**, 2890 (2014), [arXiv:1310.8555 \[hep-lat\]](#).
 - [212] V. M. Braun, D. Y. Ivanov, and G. P. Korchemsky, **Phys. Rev.** **D69**, 034014 (2004), [arXiv:hep-ph/0309330](#).
 - [213] S. J. Lee and M. Neubert, **Phys. Rev.** **D72**, 094028 (2005), [arXiv:hep-ph/0509350](#).
 - [214] P. Ball and R. Zwicky, **JHEP** **0604**, 046 (2006), [arXiv:hep-ph/0603232](#).